TU
WIEN

DISSERTATION

A Quantitative Test of Time-Dependent Density Functional Theory:

Two-electron systems in external laser fields

ausgeführt zum Zwecke der Erlangung des akademischen Grades
eines Doktors der technischen Wissenschaften

unter der Leitung von
O.Univ.-Prof. Dipl.-Phys. Dr. Joachim Burgdörfer
Institut für Theoretische Physik (136)

eingereicht an der Technischen Universität Wien,
Fakultät für Physik

von
Dipl.-Ing. Nina Rohringer
Matrikelnummer: 9525772
Grenzstr. 141/2
2231 Straßhof

Wien, am 13.01.05
Ort, Datum

Nina Rohringer
Unterschrift

Abstract

In this thesis a quantitative test of time-dependent density functional theory (TDDFT) for a two-electron system in a parabolic potential, driven by an external linear polarized laser field is performed. The full Hamiltonian of the interacting two-electron system is separable in center of mass and relative coordinates. The Schrödinger equation reduces to a stationary problem in the relative coordinate containing the Coulomb force, whereas the time-dependence of the system is shifted completely to the center of mass motion. The time-dependent electron density, the dipole moment and time-dependent occupation numbers of this separable problem constitute the reference physical quantities to be compared to the approximate TDDFT solution. The TDDFT solution is obtained by employing the time-dependent, self-interaction corrected adiabatic local-spin-density-approximation (ALSDA-SIC) . The system is discretized on a non-equidistant grid by applying a generalized pseudo-spectral method. The time-propagation of the TDDFT system is efficiently solved by a split-operator technique. As initial state of the system we study different choices: the spin-singlet ground state, the triplet ground state and arbitrary coherent superpositions of singlet states. For the first two choices the so-called harmonic potential theorem (HPT) applies, stating that the initial densities are rigidly shifted in time according to the classical solution of the center of mass coordinate, i.e. the density does not suffer distortions. Whereas for the spin-singlet ground state HPT in ALSDA-SIC is satisfied and the dipole moments. of exact and TDDFT calculation show excellent agreement, problems arise for propagation of the triplet ground state. In this case the error of the dipole moment increases after the switch-off of the laser pulse and the shape of the density is distorted. In the case of a superposition of states as initial state ALSDA-SIC fails, the exact dipole moment can not be reproduced by the TDDFT calculation.

Based on the harmonic two-electron system the problem of calculating many-particle observables within TDDFT is approached. As a first step in this direction state-to-state transition probabilities (occupation probabilities) in TDDFT are defined by the projection of the time-dependent Kohn-Sham Slater determinant onto either Kohn-Sham configuration state functions or exact eigenstates of the system. The overall shape of TDDFT occupation numbers compared to exact ones is in accordance for systems satisfying the HPT. TDDFT transition probabilities have, however, no asymptotic well defined limit, i.e. after the swith-off of the laser pulse TDDFT occupation

probabilities show oscillations ("spurious cross channel correlations" known from time-dependent Hartree-Fock). For weakly correlated systems, however, average over the oscillations give final occupations in good agreement with exact calculations. For one-dimensional systems an exact Kohn-Sham scheme is realized. For arbitrary initial states in the absence of an external laser field occupation probabilities of TDDFT with the exact exchange-correlation potential are calculated. It is not possible to extract occupation probabilities by the simple projection approach for arbitrary initial states.

Due to the deficiencies of the simple TDDFT projection mechanism to define state-to-state transition probabilities different combinations of TDDFT with other many-body theories are proposed and examined. In spirit of many-body perturbation theory a time-dependent perturbation approach to transition amplitudes is formulated. The time-dependent Kohn-Sham system serves as the unperturbed system. The first-order correction to the TDDFT transition amplitude turns out to be divergent. Resummation of this divergent series can be circumvented by means of a variational approach. Improvements of TDDFT results can, however, not be achieved.

As an alternative a functional integral approach is tested. The many-particle propagator can by means of an operator-identity be rewritten as a functional integral over one-particle propagators. The functional integral is approximated by the stationary-phase method, resulting in a set of Kohn-Sham like equations. The effective potentials in those equations are functionals of a generalized density depending on propagated initial and final state. Only in some non-generic cases this method can improve on TDDFT results.

A new functional to calculate state-to-state transition probabilities is proposed which directly depends on the time-dependent density. This new approach does not show the shortcomings of the projection approach which only depends implicitly on the density. First promising results of the this density functional applied to one-dimensional Kohn-Sham models are presented.

Zusammenfassung

In dieser Arbeit wird ein quantitativer Test der zeitabhängigen Dichtefunktionaltheorie (TDDFT) präsentiert. Das System, das unseren Untersuchungen zugrunde liegt, ist ein parabolischer Zwei-Elektron Quantenpunkt, der durch ein linear polarisiertes äußeres Feld getrieben wird. Der Hamilton-Operator dieses wechselwirkenden Zwei-Elektron Systems ist in Massenmittelpunkts- und Relativkoordinaten separierbar. Die Schrödinger Gleichung zerfällt in ein stationäres Eigenwertproblem in der Relativkoordinate, die Coulomb-Wechselwirkung beinhaltend, und in ein zeitabhängiges Problem in der Massenmittelpunktskoordinate. Zum Vergleich der exakten mit der TDDFT Lösung dienen physikalische Größen, wie die zeitabhängige Dichte, das Dipol-Moment und Besetzungswahrscheinlichkeiten. Die TDDFT Rechnung wird durch die adiabatische lokale Spin-Dichtefunktionaltheorie realisiert, wobei eine Korrektur der Selbstwechselwirkung berücksichtigt wird (ALSDA-SIC). Das System ist auf einem nicht-äquidistanten Gitter diskretisiert, wobei eine generalisierte pseudospektrale Methode verwendet wird. Die Zeitpropagation erfolgt durch eine effiziente Split-Operator Methode. Verschiedene Anfangszustände werden betrachtet. Neben dem Spin-Singlet und Spin-Triplet Grundzustand werden auch beliebige kohärente Überlagerungen von Eigenzuständen studiert. Wählt man einen Eigenzustand als Anfangszustand, gilt das sogenannte Theorem des Harmonischen Potentials (HPT), das besagt, dass die ursprüngliche Dichte durch das äußere Feld ohne Verformung nach der klassischen Bewegungsgleichung des Massenmittelpunkts verschoben wird. Während im Falle des Singlet-Grundzustandes die Übereinstimmung von exakter und TDDFT Lösung ausgezeichnet ist, treten für den Triplet-Grundzustand Probleme auf. Nach Abklingen des äußeren Feldes erhöht sich der Fehler im Dipol-Moment und die Dichte weist Verformungen auf. Trifft die Wahl des Anfangszustandes auf eine beliebige kohärente Überlagerung, so scheitert ALSDA-SIC, selbst das Dipol-Moment kann mit ALSDA-SIC nicht reproduziert werden.

Ein Hauptbestandteil dieser Arbeit ist die Berechnung von Mehrteilchen-Erwartungswerten mit TDDFT. Ein erster Schritt in diese Richtung erfolgt durch die Definition von Übergangswahrscheinlichkeiten (Besetzungswahrscheinlichkeiten) zwischen einzelnen Zuständen in Form von Projektion der zeitabhängigen Kohn-Sham Slater-Determinante auf stationäre Kohn-Sham Zustände einer bestimmten Konfiguration. Für Systeme, die dem HPT unterliegen, stimmen derartige Besetzungswahrscheinlichkeiten im groben Verlauf

sehr gut mit exakten Wahrscheinlichkeiten überein. Derartig berechnete TDDFT-Übergangswahrscheinlichkeiten haben aber keinen wohldefinierten zeitlich asymptotischen Grenzwert, sie weisen selbst nach Abklingen des Laserpulses Oszillationen auf. Diese Oszillationen bleiben auch bei Projektion der Kohn-Sham Slater-Determinante auf exakte Eigenzustände bestehen. Der Mittelwert dieser Oszillationen stimmt für schwach korrelierte Systeme aber sehr gut mit exakten Übergangswahrscheinlichkeiten überein.

Für eindimensionale Systeme wurde ein "exaktes" Kohn-Sham System realisiert. Kohärente Überlagerungen wurden so im exakten Austausch-Korrelations Potential propagiert. Selbst für diese "exakte" Kohn-Sham Rechnung können jedoch keine Besetzungswahrscheinlichkeiten durch Projektion eruiert werden.

Um diese Mängel von TDDFT bezüglich der Berechnung von Übergangswahrscheinlichkeiten zu beheben, werden Kombinationen von TDDFT mit verschiedenen anderen Methoden vorgeschlagen und getestet. Eine zeitabhängige Störungstheorie im Sinne von Møller-Plesset wird vorgeschlagen, in dem das zeitabhängige Kohn-Sham System als ungestörtes System fungiert. Es stellt sich jedoch heraus, dass die Korrektur erster Ordnung zum Übergangsmatrixelement divergiert. Resummierung der divergenten Störungsreihe kann durch ein Variationsverfahren umgangen werden, es ergeben sich aber keine Verbesserungen zur TDDFT Lösung.

Eine mögliche Alternative stellen Pfadintegralmethoden der Vielteilchensysteme dar. Mit Hilfe einer Operatoridentität kann der quantenmechanische Vielteilchen-Zeitentwicklungsoperator als ein Funktionalintegral über Einteilchen-Propagatoren geschrieben werden. Lösung dieses Pfadintegrals durch die Methode der stationären Phase resultiert in einem Set von selbstkonsistenten Kohn-Sham ähnlichen Gleichungen. Das effektive Potential in diesen Gleichungen ist ein Funktional eines verallgemeinerten Dichteoperators, der von vorwärtspropagiertem Anfangs- und rückwärtspropagiertem Endzustand abhängt. Nur für spezielle Bedingungen kann eine selbstkonsistente Lösung gefunden werden, Verbesserungen der TDDFT Übergangswahrscheinlichkeit können jedoch nicht erzielt werden.

Ein neues Dichtefunktional zur Berechnung von Übergangswahrscheinlichkeiten wird vorgeschlagen, das direkt von der zeitabhängigen Dichte abhängt. Dieses Funktional ist von den Mängeln der Projektionsmethode befreit. Erste vielversprechende Resultate durch Anwendung auf eindimensionale "exakte" Kohn-Sham Systeme werden präsentiert.

Chapter 1

Introduction

In the last decades the progress in experimental techniques made it possible to reach electric laser fields exceeding the Coulomb field of the nucleus. This electric field regime is highly non-perturbative, so that traditional perturbative methods to calculate observables such as transition or ionization probabilities fail. Many laser-atom interactions are explained in the so-called single active electron approximation [1]. In laser-induced processes like higher harmonics generation or double ionization of Helium [2], however, electron correlation often plays a crucial role [3, 4]. Time-dependent density functional theory (TDDFT) [5] is often seen as an alternative to describe correlation effects and simultaneously account for the matter-field interaction non-perturbatively. Recent studies of double ionization yields within state of the art TDDFT approximations [6] failed to reproduce characteristic features of the ion yield, underlining the problems of present-day approximations of TDDFT.

There are two independent sources of error in TDDFT approximations. One crucial ingredient is the approximation of the time-dependent exchange-correlation potential which, if an exact expression was known, would determine the exact time-dependent electron density of the system. The second critical item is the calculation of two-body (or n-body) observables from the density, a problem which is decoupled from the approximation of exchange-correlation potentials. Questions how to properly define state-to-state transition amplitudes within TDDFT seem to have been hardly ever raised, let alone answered.

In this work we present a critical case-study with the goal to shed light onto the difficulties involved in calculating many-body observables within TDDFT. Our rather simple model consists of two interacting electrons in a harmonic potential driven by a linear polarized laser field. The exact quantum mechanical solution of this problem is known.

Related systems served already in the past as benchmark systems to test the quality of diverse approximation techniques. The two-electron quantum dot was studied in its stationary form [39, 41, 40] to test the quality of different exchange correlation potentials of ground-state density functional theory. Recently a system was studied, where the harmonic well suffers time-dependent oscillations in the confining strength [48]. Focus of this work was the comparison of the exact time-dependent exchange-correlation potential (which was calculated backwards from the exact density) to usual present-day approximations. Other works relying on the harmonic system of time-dependent confining strength checked on the validity of the virial theorem within TDDFT [50, 51] and focused on memory effects [51], i.e. showing that the exact exchange-correlation potential is generally strongly nonlocal in time.

The laser-driven two electron quantum dot obeys the so-called harmonic potential theorem (HPT) [106], stating that only rigid shift motion of the density, i.e. no distortion of the shape, is supported by the Hamiltonian when the propagation starts from a stationary state. This exact property of a time-dependent many-body system has to be maintained also in the TDDFT system which results in necessary and sufficient conditions of the exchange-correlation potential upon transformation into a moving reference frame. The adiabatic local spin-density approximation (ALSDA) satisfies this condition. In this work we will directly test if the HPT is satisfied in the self-interaction corrected ALSDA (ALSDA-SIC). Propagation from the singlet and the triplet ground state will be performed and the results are compared to the exact solution.

To allow for a more general dynamics of the density we also study propagation from a coherent superposition of eigenstates. These systems are not subject to the HPT and therefore do not support the rigid density transport, but also allow for distortions of the density.

The main questions we want to address in this thesis and which are studied by means of our two-electron model are the following: What kind of observables can be legitimately calculated from TDDFT? Is it possible to calculate cross-sections or state-to-state transition amplitudes within TDDFT? Must TDDFT calculations be limited to the prediction of single-particle operators? If it should be the case, can one find suitable modifications allowing access to other quantities?

The proper definition of transition amplitudes within mean-field approaches is a well known problem since the early days of time-dependent Hartree Fock (TDHF). The intuitive way to define transition amplitudes would be the following. Choose an initial state and propagate it self-consistently within TDDFT (or TDHF). The transition amplitude is defined by projection of

the propagated wavefunction onto appropriate channel (final) states. One deficiency of such a definition is, that even in the limit of times long after the interaction period, oscillations in the obtained transition amplitudes are observed. This so-called "spurious cross-channel correlation" [58] originates from the restriction of the wavefunction to a single Slater determinant. The cross-channel correlations will be studied for singlet and triplet ground state propagation as well as for arbitrary initial states. In the latter case we will introduce a one-dimensional model system for which the exact exchange-correlation potential can be constructed. For arbitrary initial states the simple projection approach to define state-to-state transition amplitudes within TDDFT fails.

Due to the deficiencies of the projection approach we introduce combinations of TDDFT with other many-body approaches. Several authors [60, 63, 67, 68] proposed a functional integral approach to solve the problem of defining transition amplitudes in mean-field theories. This method is based on a functional integral formulation of the many-body S-matrix and involves the stationary phase approximation of this functional integral. Initial and final states in this approach are fixed and one tries to calculate a self-consistent mean-field which connects initial and final states. The approximate dynamics will therefore depend on the observable to be calculated, namely on the nature of measurement to be performed at a given time. The time-dependent self-consistent Kohn-Sham potential of TDDFT or the Hartree potential of TDHF should provide a good starting point for the iterative scheme. We test this method in order to calculate state-to-state transition amplitudes, but only in a few, non-generic cases convergence of the self-consistent solution can be achieved. Another method we explore is time-dependent perturbation theory. To improve on TDDFT transition probabilities a time-dependent perturbative approach in spirit of Møller-Plesset [122, 123] will be tested, which, however, turns out to be divergent. Resummation of this divergent series can be circumvented by means of a variational approach. The connection of the variational approach with perturbation theory will be established. The variational approach was initially introduced in collision theory for purely formal reasons [69] and was later applied to improve on TDHF transition amplitudes [73, 74]. Application of this variational approach to TDDFT does, however, not yield the desired improvements.

In contrast to the implicit density functionals involving the time-dependent Kohn-Sham orbitals we propose an alternative approach to calculate state-to-state transition probabilities directly from the time-dependent density. The new method will be tested on the one-dimensional two-electron quantum dot.

This thesis is organized as follows: In chapter 2 the model system is introduced and the exact solution is presented. The TDDFT method and the exchange-correlation potentials used in this work are presented in chapter 3. In chapters 4 and 5 the quality of ground-state DFT of the singlet- and triplet ground state is assessed. Existing approximations to the pair-correlation functions in DFT are compared to exact results. In chapter 7 one-particle observables such as dipole-moment and expectation values of the momentum-operator are calculated and discussed in the light of the HPT. In chapter 8 the transition probabilities within TDDFT are defined and the results for the singlet ground state- propagation are presented and analyzed. Chapter 9 exposes the problems related to the propagation of the triplet ground state within TDDFT. A time-dependent configuration interaction method which finds application in the case of the exact propagation of a coherent superposition of states is explained in chapter 10. The failure of ALSDA-SIC to propagate a coherent-superposition of states is documented in chapter 11. An implementation of an "exact" Kohn-Sham scheme for one-dimensional model systems is highlighted in chapter 12. The functional integral approach is examined in chapter 13. Combinations of TDDFT with perturbation theory are presented and examined in chapter 14. Chapter 15 introduces a variational approach to improve on transition matrix elements of the TDDFT projection approach. A functional to calculate state-to-state transition probabilities which explicitly depends on the time-dependent density is proposed and tested in chapter 16. A brief summary is given in the conclusions. The appendix gives detailed information about the discretization techniques applied in this work (appendix A), analytical results to expand spherical harmonics of the center of mass and relative angular coordinates within a series of spherical harmonics of one-particle angular coordinates (appendix B), details to calculate matrix-elements in the configuration interaction approach (appendix C), a configuration interaction analysis of the eigenstates involved in our calculations (appendix D) and analytic results to relate the Cartesian to the spherical eigenfunctions of the harmonic oscillator (appendix E). Atomic units $\hbar = m = e = 1$ are used throughout.

11

Chapter 2

Model systems

Three-dimensional harmonic two-electron quantum dot

In this thesis we study different two-electron models. Our major study relies on a three-dimensional harmonically confined two electron system which is driven by an external time-dependent electric field. The total time-dependent Hamiltonian of this three-dimensional two-electron quantum dot is given by

$$\hat{H}(t) = -\frac{1}{2}\left(\vec{p}_1^{\,2} + \vec{p}_2^{\,2}\right) + \frac{\omega^2}{2}\left(\vec{r}_1^{\,2} + \vec{r}_2^{\,2}\right) + \frac{1}{|\vec{r}_1 - \vec{r}_2|} - (\vec{r}_1 + \vec{r}_2) \cdot \vec{E}(t) , \quad (2.1)$$

where $\vec{r}_i$ and $\vec{p}_i$ are the coordinates and momenta of electron i ($i = 1, 2$). The electric field is denoted with $\vec{E}(t)$. The electrons are interacting via Coulomb force. The confining strength ω can be varied and therefore different correlation regimes can be explored. For $\omega \ll 1$ the Coulomb interaction $\frac{1}{|\vec{r}_1 - \vec{r}_2|}$ dominates and the system is strongly correlated. In the case of $\omega \simeq 1$ we are in the regime of weak to intermediate correlation.

One-dimensional two-electron model systems

In relation with the propagation of an arbitrary coherent superposition of states we are also studying one-dimensional model-systems. Compared to the three-dimensional case for those systems it is much simpler to construct the "exact" time-dependent exchange-correlation potential. In chapter 12 we will consider the field-free propagation of a one-dimensional two-electron quantum dot given by the Hamiltonian

$$\hat{H} = \sum_{i=1,2}\left(-\frac{1}{2}\frac{\partial^2}{\partial x_i^2} + \frac{\omega^2}{2}x_i^2\right) + \frac{1}{\sqrt{(x_1 - x_2)^2 + b^2}} \quad (2.2)$$

and a one-dimensional model of the helium atom

$$\hat{H} = \sum_{i=1,2} \left(-\frac{1}{2}\frac{\partial^2}{\partial x_i^2} - \frac{2}{\sqrt{x_i^2 + b^2}} \right) + \frac{1}{\sqrt{(x_1 - x_2)^2 + b^2}} \ . \tag{2.3}$$

b is a parameter commonly introduced to allow the electrons to bypass each other without passing through a singularity. We set the parameter $b = 0.7408$ in order to get a ground state energy for the model helium atom that is close to the ground state energy of the three-dimensional helium atom. Those one-dimensional systems were used in the past to study the double-ionization of helium [152] and to test a multi-configurational time-dependent Hartree-Fock method [153].

2.1 Exact Solution of the parabolic 2-electron quantum dot in external laser field

In this section present the exact solution of the Schrödinger equation

$$i\frac{\partial}{\partial t}\Psi(\vec{r_1},\vec{r_2},t) = \left\{ \sum_{i=1,2} \left(-\frac{1}{2}\vec{\nabla}_i^2 + \frac{\omega^2}{2}\vec{r_i}^2 - \vec{r_i}\cdot\vec{E}(t) \right) + \frac{1}{|\vec{r_1} - \vec{r_2}|} \right\} \Psi(\vec{r_1},\vec{r_2},t)$$
$$\tag{2.4}$$

of the three-dimensional harmonic two-electron quantum dot. The polarization of the laser pulse is chosen along the z-axes, so that $\vec{E}(t) = \vec{e}_z E(t)$. The pulse shape is chosen as sine squared with total pulse duration τ and the field oscillates with the frequency ω_p, so that the amplitude $E(t)$ is

$$E(t) = A_0 \sin(\omega_p t) \sin^2\left(\frac{\pi t}{\tau}\right) \tag{2.5}$$

Introducing center of mass (c.o.m.) coordinates $\vec{R} = (\vec{r_1} + \vec{r_2})/2$ and relative (internal) coordinates $\vec{r} = \vec{r_1} - \vec{r_2}$ the Hamiltonian of eq. (2.4) separates as

$$\hat{H} = \underbrace{\left(\frac{1}{2m_r}\vec{p}^2 + \frac{m_r\omega^2}{2}\vec{r}^2 + \frac{1}{|r|} \right)}_{\hat{H}_{rel}} + \underbrace{\left(\frac{1}{2M}\vec{P}^2 + \frac{M\omega^2}{2}\vec{R}^2 - 2\vec{R}\cdot\vec{E}(t) \right)}_{\hat{H}_{cm}(t)} \tag{2.6}$$

where $m = \frac{1}{2}$ and $M = 2$ denote the reduced masses. The wavefunction $\Psi(\vec{r_1},\vec{r_2},t)$ can therefore be separated in c.o.m. and relative coordinates

$$\Psi = \phi(\vec{r},t)\Phi(\vec{R},t)\chi(s_1,s_2) \ , \tag{2.7}$$

where $\chi(s_1, s_2)$ denotes the part of the wavefunction related to the spin degree of freedom. In this work singlet and triplet states will be considered. In the case of the spin-singlet state the spin-part of the wavefunction, χ, is antisymmetric against particle exchange, therefore the orbital part of the wavefunction $\phi(\vec{r}, t)$ has to be symmetric against inversion $\vec{r} \rightarrow -\vec{r}$ (the c.o.m. coordinate $\vec{R}$ is symmetric in particle exchange, therefore also $\Phi(\vec{R}, t)$). For spin-triplet states with symmetric spin-part of the wavefunction we have to impose $\phi(-\vec{r}, t) = -\phi(\vec{r}, t)$.

The internal motion of the electrons is governed by a time-independent Hamiltonian. The time-dependent external potential only affects the c.o.m. part. The Schrödinger equation for the relative coordinates therefore reduces to a stationary problem (with Dirichlet boundary conditions at infinity)

$$\hat{H}_{rel}\phi(\vec{r}) = \left[\frac{1}{2m_r}\vec{p}^2 + \frac{m_r\omega^2}{2}\vec{r}^2 + \frac{1}{|r|}\right]\phi(\vec{r}) = E_{rel}\phi(\vec{r}). \qquad (2.8)$$

Since the time-dependence of ϕ only consists of an overall phase-factor ($\phi(\vec{r}, t) = \phi(\vec{r})e^{-iE_{rel}t}$), it will be omitted in the following. We separate eq. (2.8) in spherical coordinates, $\phi(\vec{r}) = \frac{\varphi_{l,k}(r)}{r}Y_l^m(\Omega_r)$. The radial equation becomes

$$\left[-\frac{1}{2m_r}\frac{d^2}{dr^2} + \frac{l(l+1)}{2m_r r^2} + \frac{m_r\omega^2}{2}r^2 + \frac{1}{r}\right]\varphi_{l,k}(r) = \epsilon_{l,k}\varphi_{l,k}(r) . \qquad (2.9)$$

According to the symmetry relations of the spherical harmonics $Y_l^m(-\Omega) = (-1)^l Y_l^m(\Omega)$ solutions $\varphi_{l,k}(r)$ with even angular momentum quantum number l belong to the spin singlet state, solutions with odd angular momentum l are triplet states. We introduce the principal quantum number $n := 2(k-1) + l$, so that in the limit of vanishing Coulomb potential the energy reduces to the harmonic oscillator energy $\epsilon_{k,l} = \omega(n(k, l) + 3/2)$. The singlet-ground state is therefore characterized by the quantum numbers $n = 0$ and $l = 0$, the triplet-ground state by $n = 1$ and $l = 1$.

A solution of eq. (2.9) by standard Frobenius power series method is not possible [38], since the Frobenius ansatz leads to an irreducible three-term recursion formula. Nevertheless eq. (2.8) can be analytically solved for a discrete set of oscillator frequencies ω [39]. We decided to solve eq. (2.9) numerically, to generate solutions for arbitrary ω. To this end we apply a generalized pseudo-spectral method [85],[86],[87]. This method employs a non-equidistant Gauss-Legendre grid. The grid is denser at the origin to reliably represent the Coulomb singularity at the origin. The method is explained in detail in appendix A.

The Schrödinger equation of the c.o.m. part reads

$$\hat{H}_{cm}(t)\Phi(\vec{R},t) = \left[\frac{1}{2M}\vec{P}^2 + \frac{M\omega^2}{2}\vec{R}^2 - 2\vec{R}\cdot\vec{E}(t)\right]\Phi(\vec{R},t) = i\frac{\partial}{\partial t}\Phi(\vec{R},t)$$

(2.10)

and includes the external driving potential.

In this work we will study different initial states. For the spin-singlet and triplet initial state, the c.o.m. part of the wavefunction is identical and $\Phi(\vec{R},0)$ at $t=0$ is fixed as the ground state of the harmonic potential and reads

$$\Phi(\vec{R},0) = \left(\frac{\beta}{\sqrt{\pi}}\right)^{3/2} e^{-\frac{\beta^2\vec{R}^2}{2}},$$

(2.11)

with $\beta = \sqrt{M\omega}$. We will also study the propagation of a coherent superposition of c.o.m. eigenstates.

Since the laser pulse is polarized in z-direction, the time-dependent part of the c.o.m. problem is only reflected in the z-coordinate. We therefore separate the wavefunction $\Phi(\vec{R},t)$ into the product $\Phi(\vec{R},t) = \Phi_1(X,Y)\cdot\Phi(Z,t)$. The time dependent problem therefore reduces to solve the one-dimensional harmonic oscillator driven by an external force $2E(t)$. The time-evolution operator therefore is formally given by

$$U(t,0) = \exp\{lkjlk\}$$

(2.12)

The Feynman propagator for the forced oscillator [53] is given by

$$K(Z_1,0,Z_2,t) = \frac{\beta}{\sqrt{2\pi i\sin(\omega t)}} e^{iS_{cl}},$$

(2.13)

where S_{cl} denotes the classical action of the forced oscillator

$$S_{cl} = \frac{\beta^2}{2\sin(\omega t)}\left[(Z_1^2 + Z_2^2)\cos(\omega t) - 2Z_1Z_2 + \frac{4Z_2}{\beta^2}\int_0^t E(t')\sin(\omega t')dt'\right.$$

$$+\frac{4Z_1}{\beta^2}\int_0^t E(t')\sin\left(\omega(t-t')\right)dt'$$

$$\left.-\frac{8}{\beta^4}\int_0^t\int_0^{t'} E(t')E(s)\sin\left(\omega(t-t')\right)\sin(\omega s)ds\,dt'\right].$$

(2.14)

The time-dependent part $\Phi(Z,t)$ of the wavefunction of the c.o.m. system at time $t>0$ is

$$\Phi(Z,t) = \int_{-\infty}^{\infty} K(Z_1,0,Z,t)\,\Phi(Z_1,t=0)\,dZ_1.$$

(2.15)

For the triplet and singlet ground state the wave-function is therefore

$$\Phi(Z,t) = \left(\frac{\beta}{\sqrt{\pi}}\right)^{1/2}\int_{-\infty}^{\infty} K(Z_1,0,Z,t)\,e^{-\frac{\beta^2 Z_1^2}{2}}\,dZ_1.$$

(2.16)

15

For special choices of the pulse shape $E(t)$ the Fourier-like integrals in eq. (2.14) can be calculated analytically. The calculation of the propagated ground-state eq. (2.16) then results in solving Gaussian integrals, which have analytical solutions. For arbitrary pulse shape $E(t)$ the numerical solution of eq. (2.16) for several times t is time-consuming. We therefore apply a numerically very efficient split-operator technique to solve the Schrödinger equation of the Z-component.

Chapter 3

Time-dependent density functional theory

3.1 Brief review of the extended Runge-Gross theorem

The basics underlying the time-dependent density functional theory (TDDFT) is the Runge-Gross theorem [5], which is the extension of the Hohenberg-Kohn theorem [11] of ground state density functional theory to the time-dependent case. It states that for a fixed initial many-body wavefunction $|\Psi_0\rangle$ and a given two-particle interaction there exists a one-to-one mapping between the time-dependent external one-particle potential $V_{ext}(t)$ and the time-dependent density $n(t)$. As in the ground state density functional theory [12] the practical use consists in constructing a non-interacting many-particle system of the same density as the interacting system, giving rise to the so-called time-dependent Kohn-Sham equations. The non-interacting Kohn-Sham system is determined by a local potential V_{KS} (basically the exchange-correlation potential) that incorporates all the exchange-correlation effects of the fully interacting system and is obtained by the density-derivative of the action [9]. The Runge-Gross theorem applies to systems evolving from the same initial state $|\Psi_0\rangle$. The unique local potential V_{KS} in this case is a unique functional of the time-dependent density $n(t)$ and the initial state $|\Psi_0\rangle$. In the case that the system evolves from a many-particle ground state $|\Psi_0\rangle$, the initial state $|\Psi_0\rangle$ is determined by the initial ground state density n_0 according to the Hohenberg-Kohn theorem. In this special case, the time-dependent local potential V_{KS} only has functional dependence on the density. For initial states other than the ground state, the Runge-Gross theorem applies to systems evolving from the same state. In particular, the interacting

many-particle system and the non-interacting Kohn-Sham system have to evolve from the same initial state. Van Leeuwen [10] extended the Runge-Gross system to different initial states. The interacting many-particle system (reference system) evolves from $|\Psi_0\rangle$ in an external potential $V_{ext}(t)$ producing the time-dependent density $n(t)$. Having a many-particle system of different particle-interaction (this includes also the case of non-interacting particles) with initial state $|\Phi_0\rangle \neq |\Psi_0\rangle$ but the same density $n(0)$ and initial current $\partial_t n(t)|_{t=0}$ as the interacting many-particle system, the density $n(t)$ of the reference system can always be reproduced by an external, local potential $\tilde{V}_{ext}(t)$. For fixed particle-interactions of both systems, the external potential $\tilde{V}_{ext}(t)$ is uniquely (up to a purely time-dependent constant) determined by the density $n(t)$ and both initial states $|\Psi_0\rangle$ and $|\Phi_0\rangle$.

For the non-interacting time-dependent Kohn-Sham system this implies that the exchange-correlation potential V_{xc} is a functional of the density $n(t)$ and both initial states $|\Psi_0\rangle$ and $|\Phi_0\rangle$. The Kohn-Sham system can be realized by many different initial states $|\Phi_0\rangle$, all giving rise to mutually different exchange-correlation potentials and time-dependent Kohn-Sham orbitals (extended Runge-Gross theorem).

Little is known about the initial-state dependence of the exchange-correlation potential [114, 115, 116]. It was shown that the whole initial-state dependence can be traced back to a history-dependence of the system (memory-effects) [115]. Only a few approximations to exchange-correlation potentials containing history dependence exist and suffer of different deficiencies. They are either restricted to the linear-response regime [117] and violating the harmonic potential theorem (to be introduced in chapter 6), replacing TDDFT by time-dependent current density functional theory [119, 120], or are numerically difficult and expensive to implement[118]. In our studies we therefore will rely on the Adiabatic Local Spin Density Approximation (ALSDA) which, however, disregards memory effects. It will be demonstrated that for the parabolic quantum-dot evolving from the ground state a self-interaction corrected version of ALSDA provides an excellent exchange-correlation potential. For an arbitrary initial state (coherent superposition of states) ALSDA fails to reproduce the correct density and memory effects will become important. In chapter 12 we study one-dimensional two-electron model-systems in singlet states propagating from a coherent superposition of ground and excited states. For this system it is possible to construct the exact exchange correlation potential, i.e. including all initial-state and history dependence. In this context we are also studying different realizations of the Kohn-Sham system. In the first case initial states of exact and Kohn-Sham system are identical. The second case applies to two different initial states, but reproducing the same initial density. We will show that for the problem

18

of extracting occupation probabilities from TDDFT Kohn-Sham orbitals the choice of the Kohn-Sham initial state is not critical.

In the following chapter we are introducing the Kohn-Sham equations within the Adiabatic Local Spin-Density Approximation with Self-Interaction Correction (ALSDA-SIC) which is used in the major part of this thesis.

3.2 Time-dependent Kohn-Sham equations

The time-dependent Kohn-Sham scheme of spin density functional theory involves solving self-consistently the Schrödinger like equations

$$i\frac{\partial}{\partial t}\Phi_{j,\sigma}(\vec{r},t) = \left[-\frac{1}{2}\vec{\nabla}^2 + V_\sigma[n_\downarrow, n_\uparrow](\vec{r},t)\right]\Phi_{j,\sigma}(\vec{r},t) \tag{3.1}$$

for the non-interacting single-particle orbitals $\Phi_{j,\sigma}$ of spin projection $\sigma =\uparrow$, $downarrow$ in the time-dependent Kohn-Sham potential $V_\sigma[n_\uparrow, n_\downarrow](\vec{r},t)$, which is a functional of the electron spin-densities

$$n_\sigma(\vec{r},t) = \sum_{j=1}^{N_\sigma} |\Phi_{j,\sigma}|^2 = \sum_{j=1}^{N_\sigma} n_{j,\sigma}, \tag{3.2}$$

where N_σ is the total number of electrons of spin projection σ and we defined orbital densities by $n_{j,\sigma} = |\Phi_{j,\sigma}|^2$. The total density of the system is $n(\vec{r},t) = n_\uparrow(\vec{r},t) + n_\downarrow(\vec{r},t)$. The Kohn-Sham potential is decomposed into the external potential $V_{ext}(\vec{r},t)$, the Hartree-potential and the exchange-correlation potential V_{xc}

$$V_\sigma[n_\uparrow, n_\downarrow](\vec{r},t) = V_{ext}(\vec{r},t) + \int \frac{n(\vec{r'},t)}{|r-r'|}d\vec{r'} + V_{xc,\sigma}[n_\downarrow, n_\uparrow](\vec{r},t) . \tag{3.3}$$

In our case the external potential is

$$V_{ext}(\vec{r},t) = \frac{m\omega^2}{2}\vec{r}^2 - z\,E(t) . \tag{3.4}$$

The exchange correlation potential is, in principle, a universal functional of the densities and the initial states (for a given particle interaction it is independent of the external potential V_{ext}). Since the functional dependence of V_{xc} on $n_\downarrow$ and $n_\uparrow$ is not known, in practice it has to be approximated. The aim of our work is to quantitatively test one of the standard approximations by applying it to an exactly solvable problem. We employ the so-called adiabatic local spin density approximation (ALSDA), where the

exchange-correlation potential is approximated by the functional derivative of the exchange-correlation energy of the homogenous spin-polarized electron gas.

$$V_{xc,\sigma}[n_\downarrow, n_\uparrow](\vec{r}, t) = \left. \frac{\delta E_{xc}^{LSDA}[n_\downarrow, n_\uparrow]}{\delta n_\sigma} \right|_{n_\uparrow(\vec{r},t), n_\downarrow(\vec{r},t)} \tag{3.5}$$

The ALSDA exchange correlation potential is local in space and time and does not include memory effects. The LSDA energy functional consists of the exchange energy of the homogenous electron gas plus a correlation term, for which we chose the Vosko Wilk Nusair(VWN) correlation energy [151]

$$E_{xc}^{LSDA}[n_\downarrow, n_\uparrow] = -\frac{3}{4}\left(\frac{3}{\pi}\right)^{\frac{1}{3}} \int d\vec{r}\, (n_\downarrow^{4/3} + n_\uparrow^{4/3}) + \int d\vec{r}\, n\, \epsilon_{vwn}[n_\downarrow, n_\uparrow] \, . \tag{3.6}$$

One deficiency of this exchange correlation potential is that it does not have the proper long range (Coulomb tail) behavior, since it includes self-interaction. The next step of improvement is to correct for the self-interaction of the Coulomb potential and the exchange correlation energy of each single orbital [88]. The self-energy corrected (SIC) exchange correlation energy reads

$$E_{xc}^{SIC}[n_\downarrow, n_\uparrow] = E_{xc}^{LSDA}[n_\downarrow, n_\uparrow] - \sum_{\sigma=\downarrow,\uparrow}\sum_{j=1}^{N_\sigma} \left(E_{xc}^{LSDA}[n_{j,\sigma}, 0] + J[n_{j,\sigma}] \right) \, , \tag{3.7}$$

with the Hartree energy

$$J[n] = \frac{1}{2} \int d\vec{r} \int d\vec{r'}\, \frac{n(\vec{r'})n(\vec{r})}{|r - r'|} \, . \tag{3.8}$$

The exchange-correlation potential $V_{xc,\sigma}$ in the Kohn-Sham scheme is usually defined by a functional derivative of the expression of the exchange-correlation energy with respect to the spin-densities n_σ. In the case of eq. (3.7) E_{xc}^{SIC} is also depending on the orbital densities $n_{j,\sigma}$, which poses problems to determine an exchange-correlation potential $V_{xc,\sigma}$ in the usual sense. A solution to this problem was first proposed by Perdew and coworkers [88] in defining an orbital dependent self-energy corrected exchange correlation potential through

$$V_{xc,\sigma,j}^{SIC}[n_\downarrow, n_\uparrow] = \frac{\delta E_{xc}^{LSDA}[n_\downarrow, n_\uparrow]}{\delta n_\sigma} - \int \frac{n_{\sigma,j}(\vec{r'}, t)}{|r - r'|} d\vec{r'} - \frac{\delta E_{xc}^{LSDA}[n_{\sigma,j}, 0]}{\delta n_{\sigma,j}} \, . \tag{3.9}$$

Orbital dependent effective potentials, however, imply that the orbitals are no longer orthogonal to each other and the conventional Kohn-Sham procedure is not applicable. To circumvent this problem often a different approach

20

is used, the optimized effective potential (OEP) method [89] which yields an integral-equation for an orbital independent exchange correlation potential. Usually an approximated solution to this integral equation is used, proposed by Krieger, Li and Iafrate (KLI-OEP) [90, 91, 97, 98]. The OEP method was also generalized for the time-dependent case [103], for which no adiabatic approximation has to be made. The resulting system of coupled differential equations including memory integrals is too complex to solve even for one-dimensional systems. Like the static OEP it rather serves as a tool to construct approximations of the time-dependent exchange-correlation potential starting from an appropriate approximation of the exchange-correlation action integral. For currently used adiabatic approximations and the Hartree-Fock functional of the action-integral, however, memory integrals in the time-dependent OEP approach vanish. In the case of the exchange correlation energy of eq. (3.7) it was shown [100], that time-dependent OEP and the adiabatic approximation in the time-independent KLI-OEP approach yield the same orbital independent exchange correlation potential.

In our two-electron problem always different spin-projection can be assigned to the electrons. Therefore only one spin-orbital per spin projection is occupied ($N_\sigma = 1$ and $n_\sigma = n_{1,\sigma}$ for $\sigma = \uparrow, \downarrow$). In this special case the exchange-correlation potential of eq. (3.9) only depends on the spin-densities n_σ and we do not face the problem of non-orthogonal orbitals. The KLI-OEP formalism based on the self-interaction corrected exchange correlation functional eq. (3.7) reduces to eq. (3.9) for one occupied spin-orbital.

In this thesis we consider different choices of initial states for eq. (3.1). In the simplest case the initial state $\Phi_{\sigma,i}(t = 0)$ is fixed as the self-consistently calculated ground state satisfying the Kohn-Sham equation

$$\hat{H}_0 \Phi_{\sigma,i} = \left[\frac{1}{2m}\frac{d^2}{dr^2} + \frac{\hat{L}^2}{2mr^2} + V_{ext}(\vec{r}, 0) + V_H(\vec{r}, 0) + V_{xc,\sigma}^{SIC}(\vec{r}, 0) \right] \Phi_{\sigma,i} = \epsilon_{\sigma,i}\Phi_{\sigma,i} \ ,$$

(3.10)

where $V_H(\vec{r}, t)$ denotes the Hartree potential $V_H(\vec{r}, t) = \int d\vec{r'} \frac{n(\vec{r'})}{|\vec{r}-\vec{r'}|}$. In the case of two particles, the ground state is achieved by occupying the lowest spherical symmetric spin-orbital of each spin-projection (singlet-state), we therefore make the spherical symmetric ansatz

$$\Phi_{\uparrow,1} = \Phi_{\downarrow,1} = \Phi_0(\vec{r}) \ .$$

(3.11)

Solving eq. (3.10) with the ansatz of eq. (3.11) self-consistently, we get a converged exchange correlation potential $V_{xc}^{SIC}(\vec{r}, 0)$ for the occupied ground state, the converged ground state orbitals and (vacant,virtual) higher excited Kohn-Sham spin-orbitals with angular momentum $l = 0$. To get excited

Kohn-Sham spin-orbitals $\Phi_{k,l}(\vec{r}) = \frac{\phi_{k,l}(r)}{r} Y_l^m(\Omega)$ with $l > 0$, we solve the eigenvalue problem of eq. (3.10) for $\Phi_{k,l}$ with the self-consistently calculated correlation potential V_{xc}^{SIC} of the ground state occupation. The resulting Kohn-Sham spin-orbitals

$$\Phi_{n,l,m}(\vec{r}) = \frac{\phi_{n,l}(r)}{r} Y_l^m(\Omega) \tag{3.12}$$

constitute an orthonormal basis set. We introduce the principal quantum number $n := 2(k-1) + l$ of the Kohn-Sham orbitals. For vanishing Coulomb force the energy of the orbitals of quantum numbers n, l would then reduce to the harmonic oscillator energy $E_{n,l} = \omega(n + 3/2)$.

In this work the initial state is not restricted to the ground state and we also consider arbitrary initial states composed of not necessarily identical spin-orbitals $\Phi_{\sigma,i}$. The initial state and the resulting time-dependent Kohn-Sham orbitals $\Phi_{\sigma,i}(\vec{r}, t)$ are expanded in terms of the basis given by eq. (3.12)

$$\Phi_{\sigma,i}(\vec{r}, t) = \sum_{n,l} c_{n,l}(t) \frac{\phi_{n,l}(r)}{r} Y_l^0(\Omega) \tag{3.13}$$

which allows for an efficient Suzuki-Trotter like split-operator propagation of the initial state [144, 145]. For an overview of possible different propagation schemes for time-dependent Kohn-Sham equations and detailed comparison of different methods see the recently published work [146]. Since our problem is cylindrically symmetric only angular momentum projection quantum numbers $m = 0$ will appear in the expansion. Defining

$$\hat{V}_\sigma(\vec{r}, t) = -ezE(t) + V_{xc,\sigma}^{SIC}(\vec{r}, t) - V_{xc,\sigma}^{SIC}(\vec{r}, 0) + V_H(\vec{r}, t) - V_H(\vec{r}, 0) \tag{3.14}$$

the propagated Kohn-Sham orbital wavefunctions are given by

$$\Phi_{\sigma,i}(\vec{r}, t + \Delta t) \simeq e^{-i\frac{\Delta t \hat{H}_0}{2\hbar}} e^{-i\hat{V}_\sigma(\vec{r}, t+\Delta t/2)\Delta t/\hbar} e^{-i\frac{\Delta t \hat{H}_0}{2\hbar}} \Phi_{\sigma,i}(\vec{r}, t) + O(\Delta t^3) . \tag{3.15}$$

The problem one encounters is that the potentials $\hat{V}_\sigma(\vec{r}, t + \Delta t/2)$ has to be evaluated at time $t + \Delta t/2$, whereas the wave-function and therefore $V_{xc,\sigma}^{SIC}$ are only known at time t. The simplest solution to this problem would be to evaluate the potential $V_{xc,\sigma}^{SIC}$ at time t, whereas the known external field E is taken at the midpoint $t + \Delta t/2$. The error will be generally increased to be of the order of Δt^2. A computationally expensive method to determine the self-consistent potential at $t + \Delta t/2$ would be a predictor-corrector method or as an alternative to extrapolate $V_{xc,\sigma}^{SIC}$ from time t to $t + \Delta t/2$. Details of those improved methods can be found in references [146] and [147]. A

computationally cheap and efficient method, put on theoretical grounds in reference [147], is to evaluate the exchange-correlation potential $V_{xc,\sigma}^{SIC}$ at time t, but instead of determining the potential with the density $n(t)$, the functional $V_{xc,\sigma}^{SIC}$ is evaluated with the half-way propagated density resulting from the first part of the split-operator propagation $e^{-i\frac{\Delta t \hat{H}_0}{2\hbar}}$. An estimate [147] shows that this method reduces the error to the order of $O(\Delta t^3)$. In chapter 7 we show that this method reduces the absolute error by a factor of 10 compared to the simple method of evaluating $V_{xc,\sigma}^{SIC}$ with $n(t)$.

Numerical calculations are performed on a grid using a generalized Gauss-Legendre pseudo-spectral method [85],[86],[87]. In this approximation the wavefunction is represented on a non-uniform grid of the radial and angular coordinates, allowing for higher grid-point density for the dominant part of the wavefunctions. In principle also an equidistant grid would be appropriate for the harmonically confined system, so that in some sense we overshoot the mark. We are, however, seeking to apply this method to the case of more realistic systems, like helium, involving Coulomb potentials. For these systems it will be indispensable to have a high grid-point density at the origin to represent the Coulomb singularity. The non-equidistant grid with fewer grid-points at large distances from the origin allows to explore the Coulombic tail of the potential, keeping the total number of grid-points at manageable size.

Chapter 4

The singlet ground state

The exactly soluble parabolic two-electron quantum dot already served in the past as a benchmark system to test ground state DFT. Detailed quantitative studies were performed [40, 41] in order to test different exchange correlation potentials for the singlet ground state density and energy. With the knowledge of the exact ground state density of a two-electron singlet ground state it is also possible to calculate the corresponding exact exchange-correlation potential. This exact exchange correlation potential was compared with one-particle approximations (LDA exchange only, LDA Wigner, LDA Ceperley-Alder, LDA SIC and also non-local general gradient approximations, Hartree Fock)[40, 41]. In reference [41] also a detailed study of the ground state in dependence of the correlation strength (oscillator frequency ω) was presented. All those studies show that self-interaction corrected LDA is in good agreement with the exact solution. Generalized gradient approximations are of minor importance. This observation motivates the choice of our exchange correlation potential used (LSDA SIC). Since the above mentioned works extensively studied the quality of DFT calculated ground state densities and energies upon different choices of exchange correlation potentials, we will not represent detailed studies on this subject. Some comparisons of DFT and exact densities in different correlation regimes are nevertheless presented to demonstrate the quality of the exchange-correlation potentials used for ground state and forthcoming time-dependent calculations.

Other studies calculated the exchange correlation hole of the ground state of the two-electron quantum dot [42, 43, 44]. Comparison of exact exchange-correlation holes to that calculated within DFT approximations were so far not presented. A comparison of these functions will be presented in the following chapter.

24

4.1 The singlet ground state density

The singlet ground state density of a two-electron parabolic quantum dot is defined as

$$n(\vec{r}_1) = n(r_1) = 2 \int d\vec{r}_2 \, |\Psi(\vec{r}_1, \vec{r}_2)|^2 , \qquad (4.1)$$

where Ψ denotes the ground state of Hamiltonian eq. (2.4) without external field $E(t)$. The singlet ground state density is spherically symmetric. Due to the separability of the problem and the special Gaussian like form of the center of mass ground state function eq. (2.11) it is possible to reduce eq. (4.1) to one single integral. After performing some analytical manipulations one arrives at

$$n(r_1) = \frac{8}{r_1} \frac{\beta}{\sqrt{\pi}} e^{-\beta^2 r_1^2} \int_0^\infty r \phi^2(r) \, e^{-\beta^2 r^2/4} \sinh(\beta^2 r_1 r) dr , \qquad (4.2)$$

where $\phi(r) = \frac{\varphi_{0,0}(r)}{r} \frac{1}{\sqrt{4\pi}}$ denotes the ground state of the internal Hamiltonian of eq. (2.8) and accordingly $\varphi_{0,0}$ is the ground state of the radial Schrödinger equation (eq. (2.9)). The density can therefore be calculated by a single numerical integral. Figures 4.1 to 4.3 show a comparison of the exact density and the self-consistently calculated DFT density using LSDA-SIC in different correlation regimes. For $\omega = 1$ (figure 4.1) the exact density is very well produced, plotting $r^2 n(r)$ almost no difference between exact and DFT density can be seen. The situation gets worse if one considers smaller oscillator strength. At $\omega = 0.01$ the exact density shows a pronounced minimum at the origin, which is due to electron correlation (see figure 4.2). DFT in the LDA-SIC is not able to reproduce the minimum. For the even stronger correlated system at $\omega = 0.0023$ (figure 4.3) the DFT with LSDA-SIC manages to produce a minimum at the origin. Nevertheless the DFT density is in very poor agreement with the exact result. Other local density functionals tried did not give relevant improvements.

4.2 Definition of the pair correlation hole

Internal particle distribution functions are determined via the diagonal elements of the reduced density matrix [19]. For the special case of a two-electron system the reduced second-order density matrix equals the absolute square of the wavefunction $\rho_2(\vec{r}_1, \vec{r}_2) = |\Psi(\vec{r}_1, \vec{r}_2)|^2$. The pair correlation function $h(\vec{r}_1, \vec{r}_2)$ is defined as [14]

$$\rho_2(\vec{r}_1, \vec{r}_2) = \frac{1}{2} n(\vec{r}_1) n(\vec{r}_2)[1 + h(\vec{r}_1, \vec{r}_2)] , \qquad (4.3)$$
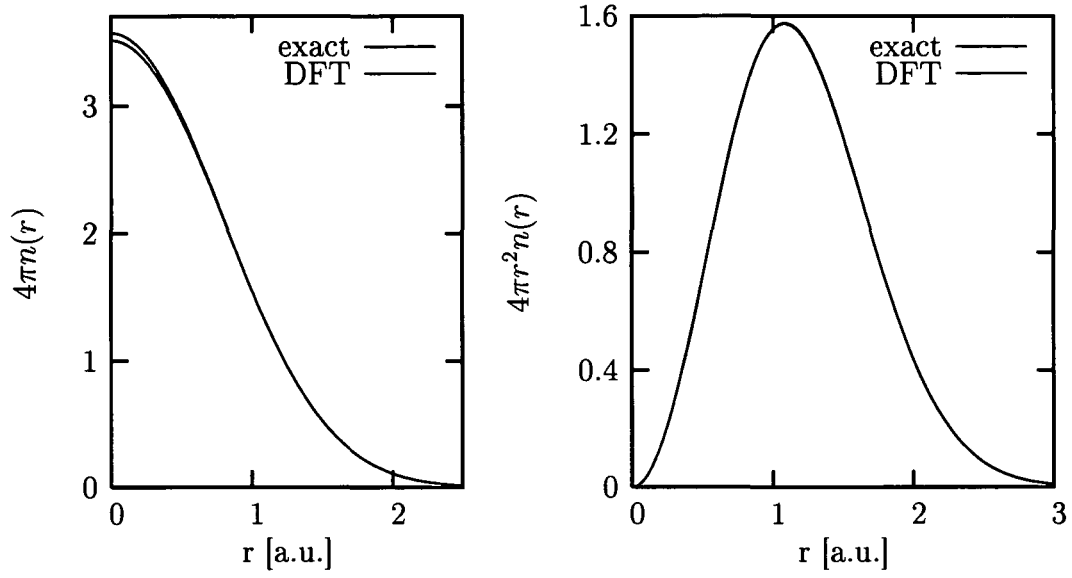
Figure 4.1: Singlet ground state densities $n(r)$ and $r^2 n(r)$ of the 2-electron parabolic quantum dot for $\omega = 1$: Shown is a comparison of the exact density (red) and the self-consistent DFT density (green) using LSDA-SIC with correlation potential of Vosko, Wilk and Nusair [151].
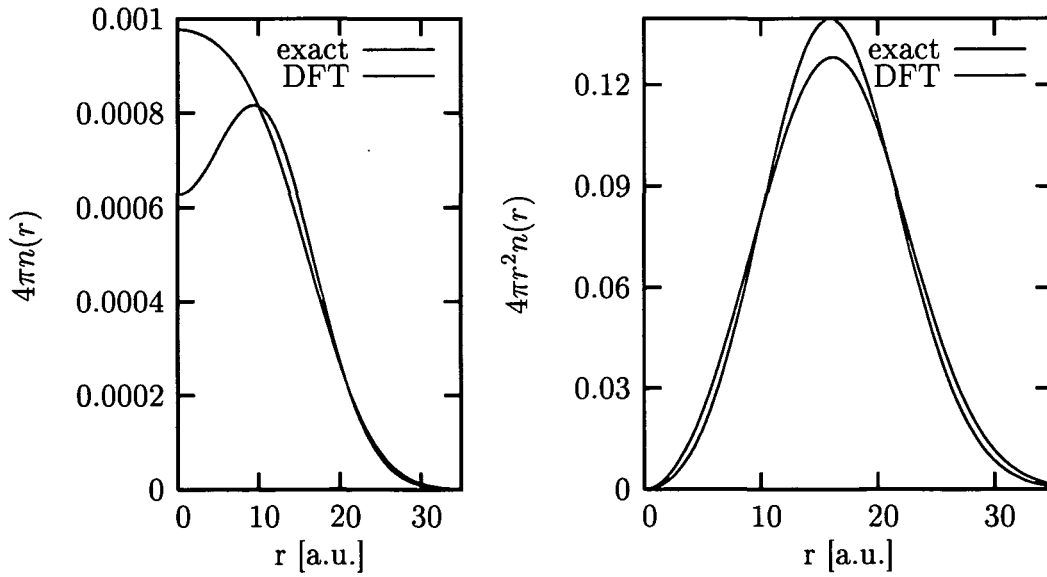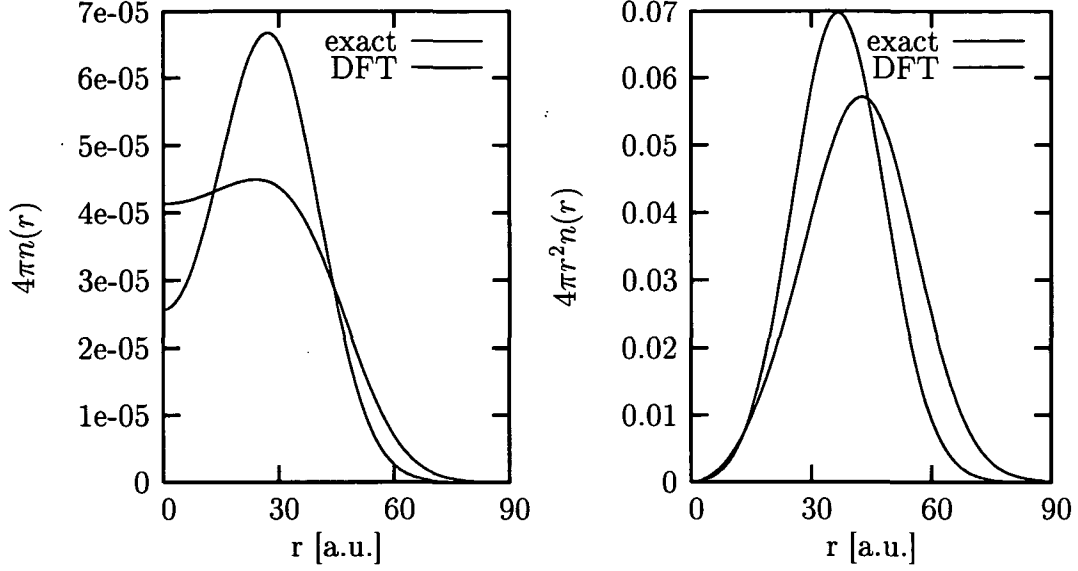

Figure 4.2: Comparison of exact (red) and DFT (green) singlet ground state densities $n(r)$ and $r^2 n(r)$ of the 2-electron parabolic quantum dot for $\omega = 0.01$

Figure 4.3: Comparison of exact (red) and DFT (green) singlet ground state densities $n(r)$ and $r^2 n(r)$ of the 2-electron parabolic quantum dot for $\omega = 0.0023$

and describes the non-factorizable part of the reduced two-particle density matrix. We therefore get

$$h(\vec{r}_1, \vec{r}_2) = \frac{2|\Psi(\vec{r}_1, \vec{r}_2)|^2}{n(\vec{r}_1)n(\vec{r}_2)} - 1 =: g(\vec{r}_1, \vec{r}_2) - 1 \ . \qquad (4.4)$$

In eq. (4.4) we defined the pair-correlation function $g(\vec{r}_1, \vec{r}_2)$ which is often used and has the interpretation of a conditional probability. The quantity $g(\vec{r}_1, \vec{r}_2)n(\vec{r}_2)d\vec{r}_2$ gives the expected number of electrons in the volume $d\vec{r}_2$ around $\vec{r}_2$, given that there is an electron at the reference position $\vec{r}_1$. One defines the pair-correlation hole or exchange-correlation hole (or Fermi-correlation hole) as

$$\rho_{xc}(\vec{r}_1, \vec{r}_2) = n(\vec{r}_2)h(\vec{r}_1, \vec{r}_2) = \frac{2|\Psi(\vec{r}_1, \vec{r}_2)|}{n(\vec{r}_1)} - n(\vec{r}_2) \ . \qquad (4.5)$$

The pair correlation function $h(\vec{r}_1, \vec{r}_2)$ has to satisfy the following sum rule

$$\int n(\vec{r}_2)h(\vec{r}_1, \vec{r}_2)d\vec{r}_2 = -1 \quad \forall \vec{r}_1 \ , \qquad (4.6)$$

which follows directly from

$$n(\vec{r}_1) = 2 \int \rho_2(\vec{r}_1, \vec{r}_2)d\vec{r}_2 \ . \qquad (4.7)$$

27

The sum rule of eq. (4.6) is one of the few exact properties known for the correlation function and constitutes a stringent test on approximations. Eq. (4.6) can also be interpreted as the normalization condition of a charge distribution with total charge -1. This charge-distribution depends on the reference point $\vec{r}_1$. Attention should be drawn to the fact, that in contrast to $h(\vec{r}_1, \vec{r}_2)$ the exchange-correlation hole $\rho_{xc}(\vec{r}_1, \vec{r}_2)$ is not symmetric in exchange of $\vec{r}_1$ and $\vec{r}_2$.

The Hartree Fock two-particle density matrix for a closed shell is $\rho_2^{HF}(\vec{r}_1, \vec{r}_2) = n(\vec{r}_1)n(\vec{r}_2)/4$ and therefore factorizable. The pair-correlation function is simply $h(\vec{r}_1, \vec{r}_2) = -\frac{1}{2}$. In analogy to the exchange part of the total energy one defines an exchange hole (Fermi hole) which is given as the Hartree-Fock solution of the pair correlation hole as

$$\rho_x(\vec{r}_1, \vec{r}_2) = -\frac{n(\vec{r}_2)}{2} . \qquad (4.8)$$

The density $n(\vec{r}_2)$ in eq. (4.8) denotes the exact density (in Hartree-Fock the density does not necessarily equal the exact density), only the functional form of the exchange (Fermi) hole is taken from Hartree-Fock theory. The exchange hole $\rho_x(\vec{r}_1, \vec{r}_2)$ is independent of the reference point $\vec{r}_1$. The difference between the Hartree-Fock exchange hole and the total pair-correlation hole is then defined as the correlation (Coulomb) hole

$$\rho_c(\vec{r}_1, \vec{r}_2) := \rho_{xc}(\vec{r}_1, \vec{r}_2) - \rho_x(\vec{r}_1, \vec{r}_2) . \qquad (4.9)$$

4.3 The pair correlation hole in DFT

The pair correlation function defined in eq. (4.4) is, as every other quantity in spin DFT, a functional of the spin densities. It is of crucial importance in DFT since the exchange-correlation energy can be calculated via the coupling constant integral of the pair-correlation function. Therefore it is mostly the coupling constant integrated pair-correlation function which is studied in literature. Reference [27] gives a pedagogical overview of this subject. The coupling constant average of the pair correlation function is defined as

$$\bar{g}(\vec{r}_1, \vec{r}_2) := \int_0^1 d\lambda g^\lambda(\vec{r}_1, \vec{r}_2) , \qquad (4.10)$$

where g^λ is the pair correlation function of the system with electron-electron interaction $\lambda/|\vec{r}_1 - \vec{r}_2|$ under the constraint that the electron density is fixed at the physical full coupling strength $\lambda = e^2 = 1$ (in a.u.). The exchange

correlation energy is then given by

$$E_{xc} = \frac{1}{2} \int d\vec{r}_1 \int d\vec{r}_2 \frac{n(\vec{r}_1)n(\vec{r}_2)}{|\vec{r}_1 - \vec{r}_2|} [\bar{g}(\vec{r}_1, \vec{r}_2) - 1] . \qquad (4.11)$$

One often defines a Kohn-Sham exchange correlation hole

$$\rho_{xc}^{KS}(\vec{r}_1, \vec{r}_2) := n(\vec{r}_2)[\bar{g}(\vec{r}_1, \vec{r}_2) - 1] , \qquad (4.12)$$

where in contrast to the exchange-correlation hole ρ_{xc} defined in eq. (4.5) in eq. 4.12 at the right hand-side the coupling constant integrated pair-correlation function $\bar{g}$ enters. Since the density is kept fixed at the physical coupling strength $\lambda = 1$ during the variation of λ, the Kohn-Sham exchange correlation hole ρ_{xc}^{KS} equals the coupling constant averaged value of the exchange-correlation hole ρ_{xc}

$$\rho_{xc}^{KS}(\vec{r}_1, \vec{r}_2) = \bar{\rho}_{xc}(\vec{r}_1, \vec{r}_2) = \int_0^1 d\lambda \rho_{xc}^{\lambda}(\vec{r}_1, \vec{r}_2) . \qquad (4.13)$$

The exchange correlation energy can be interpreted as a resulting interaction of the density with its hole charge-distribution

$$E_{xc} = \frac{1}{2} \int d^3r_1 \int d^3r_2 \frac{n(\vec{r}_1)\rho_{xc}^{KS}(\vec{r}_1, \vec{r}_2)}{|\vec{r}_1 - \vec{r}_2|} . \qquad (4.14)$$

Following the spirit of LDA, approximations of pair-correlation functions generally rely on the homogeneous electron gas. The construction of approximations of the hole-functions is difficult, since not even for the homogeneous electron gas they are accurately known [88]. In developing approximations to the exchange-correlation holes one differentiates between electron pairs of different or alike spin projection. Because of the Pauli exclusion principle, electrons with parallel spins would avoid each other even if they were non-interacting. This leads to the concept of the Fermi (exchange) hole. Electrons with antiparallel spins do not feel Pauli's exclusion principle and are only kept apart through the Coulomb interaction (Coulomb or correlation hole). In the latter case the behavior of many-body wavefunctions at small interparticle distances is governed by the Coulomb interaction. This gives rise to the so called called cusp conditions [15, 16, 17, 18], an ingredient for the construction of most approximations to Coulomb hole functions.

In general Fermi and Coulomb hole depend on the Spin-polarization $\xi = (n_\uparrow - n_\downarrow)/n$ of the system. Interpolations of the correlation functions between the totally spin-polarized $\xi = \pm 1$ and totally unpolarized $\xi = 0$ homogeneous gas are given in [151] and originally in reference [25]. Accurate studies

of the homogeneous electron gas also resolve the correlation functions with respect to spin-projection, defining hole functions of alike $\rho_c^{\uparrow\uparrow}(\vec{r_1}, r)$, $\rho_c^{\downarrow\downarrow}(\vec{r_1}, r)$ or different spin-projection $\rho_c^{\downarrow\downarrow}(\vec{r_1}, r)$ and $\rho_c^{\downarrow\uparrow}(\vec{r_1}, r)$. The spin-resolved hole function $\rho_c^{\downarrow\uparrow}(\vec{r_1}, r)$ is then related to the probability of finding an electron of spin-projection $\uparrow$ at distance r from $\vec{r_1}$, provided that there is an electron of spin $\downarrow$ at the reference point $\vec{r_1}$.

Most of the analytical models for the pair-correlation function are deduced
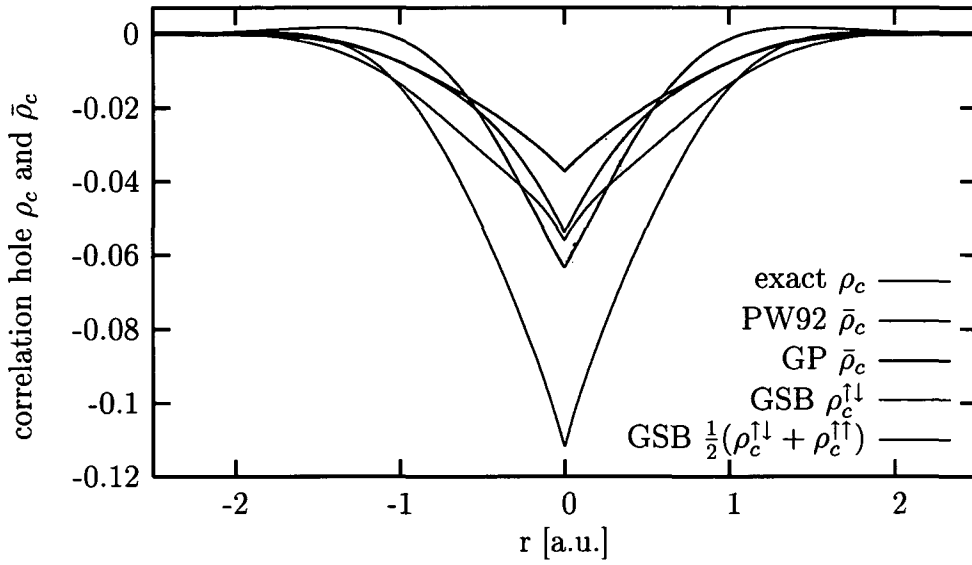
Figure 4.4: Correlation hole $\rho_c(0, \vec{r})$ at reference point $r_1 = 0$ for the singlet ground state of the quantum dot with frequency $\omega = 1$: Shown are the exact correlation hole corresponding to eq. (4.9) (red line), parameterizations of the coupling-constant integrated $\bar{\rho}_c$ of Perdew-Wang [26] (green, PW) and of Gori-Giorgi Perdew [30] (blue, GP) and the parameterization of correlation hole at full coupling strength ρ_c of Gori-Giorgi Sacchetti and Bachelet [29], where $\rho_c^{\uparrow\downarrow}$ (cyan, GSB) and $\frac{1}{2}(\rho_c^{\uparrow\downarrow} + \rho_c^{\uparrow\uparrow})$ (magenta, GSB).

for the coupling constant averaged functions [26, 30]. We are interested in the pair-correlation function at full coupling-constant strength, in view of the calculation of two-particle observables. A scaling relation of hole functions between integrated and full coupling strength is known for the homogeneous

electron gas [26]

$$g_c(k_F \cdot r; r_s) = \left(1 + r_s \frac{\partial}{\partial r_s}\right) \bar{g}_c(k_F \cdot r; r_s) , \qquad (4.15)$$

where $k_F = (3\pi^2 n)^{1/3}$ and $r_s = (4\pi n/3)^{-1/3}$ are deduced quantities of the homogeneous density n, r denotes the distance from the reference point. The correlation function of the homogeneous electron gas is translational invariant with respect to the reference point and spherically symmetric around the reference point. Relation eq. (4.15) would, in principle, make it possible to deduce the hole function at full coupling strength from a given approximation for an integrated pair-correlation function. In practice, however, this is quite difficult and introduces errors. Most parameterizations of the correlation functions of the homogeneous electron gas (of Perdew type [24, 25, 26, 29, 30]) are built from the short- (cusp-condition) and non-oscillatory long-range behavior of the correlation function. An interpolation between those two limits is built under various constraints as the sum rule of eq. (4.6), the energy sum rule (related to eq. (4.14)) and forcing cancellation of singularities at $r \to 0$ resulting from the long-range behavior of the correlation function. Those constraints change slightly for the correlation hole at full coupling strength. Cancellation of the singularities at $r \to 0$ is no longer satisfied, if one applies eq. (4.15) on a parameterized $\bar{g}_c$ and one gets qualitatively wrong results. Analytical representations of pair-correlation functions at full coupling strength are rare [29].

Figures 4.4 and 4.5 show a comparison of the correlation hole and different approximations relying on the homogeneous electron gas at two different reference points (for details see figure captions). We choose the weakly correlated system at $\omega = 1$, since for higher correlated systems in the local density approximation not even the densities can be reliably reproduced. The approximative parameterizations of the pair-correlation hole have been worked out with the exact density. The reference point in figure 4.4 is chosen as the origin of the quantum dot. Around this special point the correlation hole shows spherical symmetry. The best agreement with the exact result gives the parameterization of Perdew and Wang (PW02) [26], which is surprising, since it is a parameterization of the coupling-constant integrated correlation hole. The construction of the different correlation functions [26, 29, 30] examined in our analysis is quite similar. Per se they do not differ much in the considered density range. In contrast to parameterizations of the coupling-constant integrated correlation function [26] (PW) and [30] (GP), the correlation function at full coupling strength of Gori-Giorgi Sacchetti and Bachelet [29] (GSB) is spin-resolved, i.e. gives different parameterizations for $g_c^{\uparrow\uparrow}$ and $g_c^{\uparrow\downarrow}$. Since we are considering a 2-electron system in a singlet state,
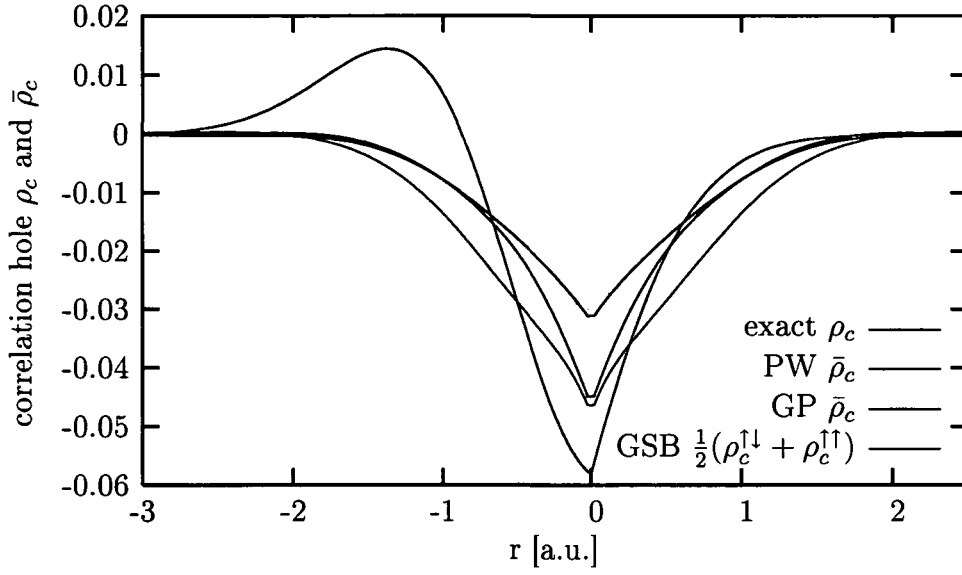
Figure 4.5: Coulomb correlation hole $\rho_c(\vec{r}_1, \vec{r}_1 - \vec{r})$ at reference point $r_1 = 0.512$, where $\vec{r}_2 = \vec{r}_1 - \vec{r}$ is varied collinearly to $\vec{r}_1$. Shown are the exact correlation hole of eq. (4.9) (red line), parameterizations of the coupling-constant integrated $\bar{\rho}_c$ of Perdew-Wang [26] (green, PW) and of Gori-Giorgi Perdew [30] (blue, GP) and the parameterization of correlation hole at full coupling strength ρ_c of Gori-Giorgi Sacchetti and Bachelet [29] $\frac{1}{2}(\rho_c^{\uparrow\downarrow} + \rho_c^{\uparrow\uparrow})$ (magenta, GSB).

the correlation function of opposite spins $\rho_c^{\uparrow\downarrow}$ should be the proper one. However, figure 4.4 rather suggests that the averaged form $\frac{1}{2}(\rho_c^{\uparrow\uparrow} + \rho_c^{\uparrow\downarrow})$ gives the right order of magnitude. This is not consistent and reveals the problems in applying results of the homogeneous electron gas to highly inhomogeneous systems.

Figure 4.5 shows results for a reference point other than the origin (at distance $r_1 = 0.512$ from the origin). The exact pair-correlation hole is no longer spherically symmetric around the reference point, a behavior which no approximation relying on the homogeneous electron gas can reproduce. The pair correlation functions of the homogeneous electron gas only depend on the local density of the reference point and on the distance between reference and observation point. Therefore the approximated correlation holes only differ slightly for the two reference points.

We also performed studies of the pair-correlation hole with self-interaction correction (SIC) [88]. In contrast to reference [88] we treat exchange exactly. This alters the expression for the self-interaction corrected correlation hole:

$$\rho^{SIC}(\vec{r}_1, r = |\vec{r}_1 - \vec{r}_2|) = \rho_c(n_\uparrow(\vec{r}_1), n_\downarrow(\vec{r}_1); r) - \sum_{\sigma=1,2;\alpha=1}^{N_\sigma} \frac{n_{\sigma,\alpha}(\vec{r}_1)}{n(\vec{r}_1)} \rho_c(n_{\sigma,\alpha}(\vec{r}_1), 0; r) ,$$

(4.16)

where $\rho_c(n_\uparrow(\vec{r}_1), n_\downarrow(\vec{r}_1); r)$ stands for an approximate parameterization of the correlation hole of the homogeneous electron gas. In our treatment the density dependent term, which usually breaks spherical symmetry in SIC does not appear. In the original SIC approach [88] this term comes from the correction of Coulombic self-interaction, which is already taken care of in the exact exchange approach. Figure 4.6 shows the self-interaction corrected exchange hole of the spin-resolved parameterization of Gori-Goirgi, Sacchetti and Bachelet (GSB) [29] and the self-interaction corrected coupling-constant integrated parameterization of Perdew and Wang (PW) [26] in comparison to the exact result. The self-interaction corrected parameterization PW is in good agreement with the exact correlation hole. The self-interaction term of the orbital densities was evaluated for total spin-polarization $\xi = 1$. In the GSB approach the self-interaction part was evaluated by taking the correlation hole of alike spins $\rho_c^{\uparrow\uparrow}$, whereas the basic term of the total density was taken as $\frac{1}{2}(\rho_c^{\uparrow\uparrow} + \rho_c^{\uparrow\downarrow})$. In the case of the reference point at distance $r_1 = 0.512$ from the origin (see figure 4.7) the self-interaction correction only leads to a slight improvement and can not compensate for the deficiencies of the parameterizations of the homogeneous electron gas.

Besides the correlation functions based on the homogeneous electron gas there exists another type of functionals based on Hartree-Fock second-order reduced density matrices, functions of the Colle-Salvetti type [31]. Lee, Yang
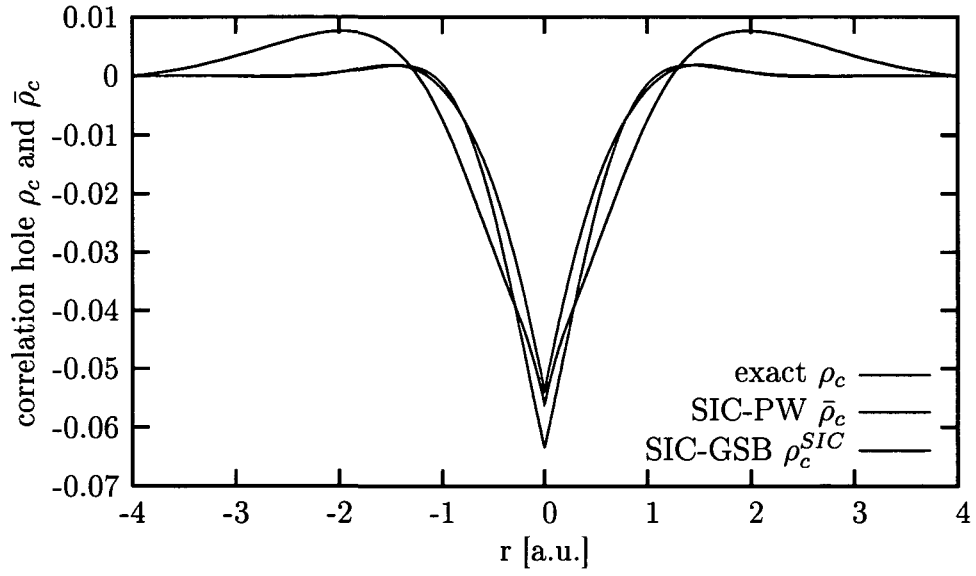
Figure 4.6: Coulomb correlation hole $\rho_c(0, \vec{r})$ at reference point $r_1 = 0$ for the singlet ground state of the quantum dot with frequency $\omega = 1$: Shown are the exact correlation hole corresponding to eq. (4.9) (red line), parameterizations of the coupling-constant integrated $\bar{\rho}_c$ of Perdew-Wang [26] (green, PW) and self-interaction corrected correlation hole at full coupling strength ρ_c of Gori-Giorgi Sacchetti and Bachelet [29] (blue, SIC-GSB).

and Parr transformed the empirical Colle-Salvetti correlation energy formula into a nowadays extensively used Kohn-Sham energy functional [32] (LYP). A detailed study of Colle-Salvetti type correlation functions, optimized to give the exact correlation energy of helium, was performed for helium [35] and it was argued that results obtained based on it were inaccurate and not well founded. Most of the known exact constraints of pair correlation functions are violated. Recently a improved functional was proposed [33] and tested for the two-electron parabolic quantum dot and helium [34]. Those functionals possess a variety of free parameters to tune. Gradients of the density are included in the functional, resulting in correlation functions which go beyond the spherical symmetry around the reference point. Whereas an additional self-interaction correction of the energy functional gives good correlation-energy estimates, really convincing results for correlation holes could not be achieved.

The considered correlation holes all gave reasonable correlation energies, a few percents off the exact solution. The correlation energy is determined by the spherically averaged coupling-constant integrated correlation hole. Most of the errors of available functionals and parameterizations are therefore averaged out in considering energies. If one is interested in two-particle observables, existing approximations of the correlation function are not reliable and would introduce considerable deviations from exact properties.
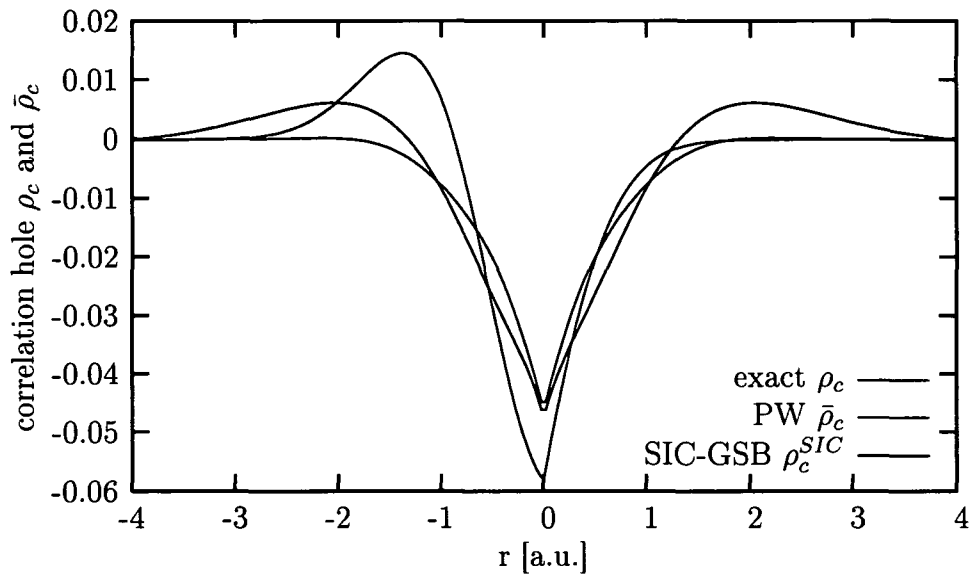
Figure 4.7: Coulomb hole $\rho_c(0, \vec{r})$ at reference point $r_1 = 0.512$ for the singlet ground state of the quantum dot with frequency $\omega = 1$: Shown are the exact correlation hole corresponding to eq. (4.9) (red line), parameterizations of the coupling-constant integrated $\bar{\rho}_c$ of Perdew-Wang [26] (green, PW) and self-interaction corrected correlation hole at full coupling strength ρ_c of Gori-Giorgi Sacchetti and Bachelet [29] (blue, SIC-GSB).

Chapter 5

The triplet ground state

5.1 The exact triplet ground state density

The triplet ground state of the harmonic dot has relative angular momentum quantum number $l = 1$, since the internal part of the wavefunction has to be antisymmetric with respect to the inversion of the interparticle vector $\vec{r} = \vec{r}_1 - \vec{r}_2$. The symmetry relations of the spherical harmonics with respect to space-inversion $Y_l^m(-\Omega) = (-1)^l Y_l^m(\Omega)$ therefore allow only for odd angular momentum quantum numbers for spin triplet systems. The c.o.m. part of the wavefunction for triplet and singlet ground state is identical ($L = 0$, $N = 0$). Before touching upon the problem of how to treat the spin triplet ground state within density functional theory, we construct the exact triplet ground state density. The exact triplet ground state wavefunction is given by

$$\Psi(\vec{r}, \vec{R}) = \left(\frac{\beta}{\sqrt{\pi}} \right)^{3/2} e^{-\frac{\beta^2 \vec{R}^2}{2}} \frac{\varphi_{1,0}(r)}{r} Y_1^0(\Omega_r) \tag{5.1}$$

according to eq. (2.9) and eq. (2.11). The function $\varphi_{1,0}(r)$ satisfying the radial equation of the internal degree of freedom with $l = 1$ is generally only given on a numerical grid. To simplify the notation we skip the indices in $\varphi_{1,0}$ in the following. The total electron density is given by the integral

$$n(\vec{r}_1) = 2 \int d\vec{r}_2 \left| \Psi \left(\vec{r} = \vec{r}_1 - \vec{r}_2, \vec{R} = \frac{(\vec{r}_1 + \vec{r}_2)}{2} \right) \right|^2 =$$

$$= 2 \left(\frac{\beta}{\sqrt{\pi}} \right)^3 \int d\vec{r}_2 \left(\frac{\varphi(|\vec{r}_1 - \vec{r}_2|)}{|\vec{r}_1 - \vec{r}_2|} Y_1^0(\Omega_r) \right)^2 e^{-\beta^2 (\vec{r}_1 + \vec{r}_2)^2 / 4} . \tag{5.2}$$
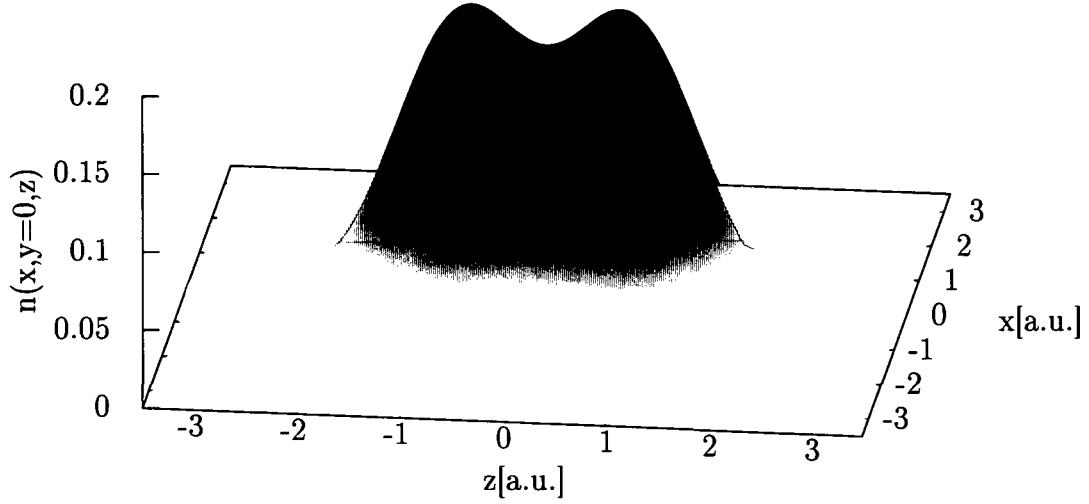
Figure 5.1: Triplet ground state density in the $y = 0$ plane for $\omega = 1$

With the use of appendix B.1 and some straight-forward calculations one arrives at

$$n(\vec{r_1}) = 4\frac{\beta^3}{\sqrt{\pi}} e^{-\beta^2 r_1^2/4} \left\{ \int_0^\infty r_2^2 F_0^1(r_1, r_2) dr_2 + \frac{1}{\sqrt{5\pi}} Y_2^0(\Omega_1) \cdot \right.$$

$$\left. \int_0^\infty r_2^2 e^{-\beta^2 r_2^2/4} \left[r_1^2 F_0^2(r_1, r_2) + r_2^2 F_2^2(r_1, r_2) - 2r_1 r_2 F_1^2(r_1, r_2) \right] dr_2 \right\} (5.3)$$

with

$$F_l^k(r_1, r_2) := \int_{-1}^1 d(\cos\theta) \frac{\varphi^2(\sqrt{r_1^2 + r_2^2 - 2r_1 r_2 \cos\theta})}{(r_1^2 + r_2^2 - 2r_1 r_2 \cos\theta)^k} e^{-\beta^2 r_1 r_2 \cos\theta/2} P_l(\cos\theta) \quad (5.4)$$

where $P_l(\cos\theta_r)$ denotes the Legendre Polynomial of degree l. The exact electron density therefore has a spherical harmonic component of $l = 2$ and is therefore no longer radially symmetric. Figure 5.1 shows the triplet ground state density in the $y = 0$ plane.

38

5.2 The DFT solution of the triplet ground state

In this section we construct the triplet ground state density within DFT. The triplet ground state, as the energetically lowest lying state of a given symmetry class, can be calculated by means of the Kohn Sham formalism [22]. The Kohn-Sham Hamiltonian is often of lower symmetry than the original full many-body Hamiltonian. This problem only comes into play if eigenstates of the system of total angular momentum greater than $L = 0$ are considered, as it is the case for the triplet ground state with total angular momentum $L = 1$.

For a general state of well defined total angular momentum L, the total electron density always has the form [108]

$$n(\vec{r}) = \sum_{l=0}^{L} n_{2l}(r) Y_{2l}^0(\Omega) \,. \tag{5.5}$$

Each approximation of the exchange correlation potential therefore should maintain the correct form of the density. An approximation which fulfills this requirement and is often applied (for practical purpose) is the spherical average of the exchange-correlation and Hartree potentials, yielding Kohn-Sham orbitals of good angular momentum quantum numbers. The errors of this approximation have been studied for a only small number of systems.

Janak and coworkers [112] studied the energy difference of spherical symmetrized and angular dependent Kohn-Sham potentials (LDA, no correlation included) of some atoms. The energy differences were negligible compared to the error of LDA. Surprisingly, the ground-state energies of the non-spherical average were slightly higher in energy (which was related to the coulomb self-interaction in LDA). In LDA spherical-average or total angular dependence of the Kohn-Sham potential gives essentially identical ground state energies. Using non-local functionals (generalized gradient approximations) it was shown for some atomic systems and diatomic molecules [113] that the non-spherical averaging gives generally better energy results.

Fertig and Kohn [108] constructed the exact exchange correlation potential for the triplet ground state of an two-electron harmonic dot with harmonic particle interaction. They could show that the unique exchange correlation potential has contributions of spherical harmonics of all even orders. Depending on the particle interaction, the approximation of spherically averaging the effective Kohn-Sham potential may introduce big discrepancies in the energies and densities. So far not examined is the influence of the spherical average on the density profile within existing approximations of the exchange correlation potential. In the following we are comparing densities of LSDA-SIC calculations of spherical and non-spherical average to the

exact densities.

In the case of the spherical averaged effective Kohn-Sham potentials, the two Kohn-Sham orbitals involved are chosen as the $0s : n_1 = 0, l_1 = 0$ and $1p : n_2 = 1, l_2 = 1$ (the lowest lying one-particle states producing a state of relative angular momentum $l = 1$). Corresponding to eq. (5.5) the density obtained via the spherical averaged Coulomb potential has only contributions of $l = 0$ and $l = 2$. In the case of the non-spherical averaging the $0s1p$ configuration is chosen as initial guess from which the self-consistency loop is started.

A decision one has to take in LSDA concerns the spin-polarization of the Kohn-Sham orbitals. The spin part of the triplet ground state can be either totally spin-polarized ($|\uparrow\uparrow\rangle$ or $|\downarrow\downarrow\rangle$) or of the symmetric spin-compensated form $\frac{1}{\sqrt{2}}(|\downarrow\uparrow\rangle + |\uparrow\downarrow\rangle)$. The exact exchange-correlation functional should take care of the choice and always give the same energy and density. Approximate functionals, however, give rise to two different results. In the following we are considering the spin compensated case in view of the harmonic potential theorem, which should be satisfied in the case of spin-compensated LSDA-SIC (see chapter 6). In the case of the spherical-averaging we therefore have to deal with two different spherical symmetric effective Kohn-Sham potentials. The two effective Kohn-Sham potentials obtained without spherical average show different angular dependence. Whereas the effective potential creating the $1p$ orbital is almost spherically symmetric, the effective potential giving rise to the initially $0s$-related orbital shows a pronounced spherical harmonic component of $l = 2$. A comparison of the exact and DFT triplet ground state densities shows that LSDA-SIC overestimates the spherical-symmetric component of the density (component with $l = 0$) at the origin (see figure 5.2). The $l = 0$ component of the density obtained by spherical average of the effective Kohn-Sham potential or by no averaging shows no significant difference. Comparing the $l = 2$ component of the exact (red line) and LSDA-SIC densities (see figure 5.3) a considerable difference of the components corresponding to spherical average (blue line) and no average (green line) can be seen. Both DFT approximations of the density underestimate the non-spherical part of the triplet ground state density, spherical average, however, gives a slightly better result. Compared to the exact value of $E = 4.5151$ the energy of the triplet ground state obtained by spherical average is $E = 4.3489$ and is slightly better than the energy obtained by no spherical average which is $E = 4.3271$. The violation of eq. (5.5) of the non-spherical averaged Kohn-Sham calculation is very small. The $l = 4$ component of the density is 2 orders of magnitude smaller than the $l = 2$ component. Similar to previous works [108] higher angular momentum components fall off rapidly. In figure 5.4 we show a comparison of the integrated density $n(z) := \int dx \int dy\, n(\vec{r})$ for
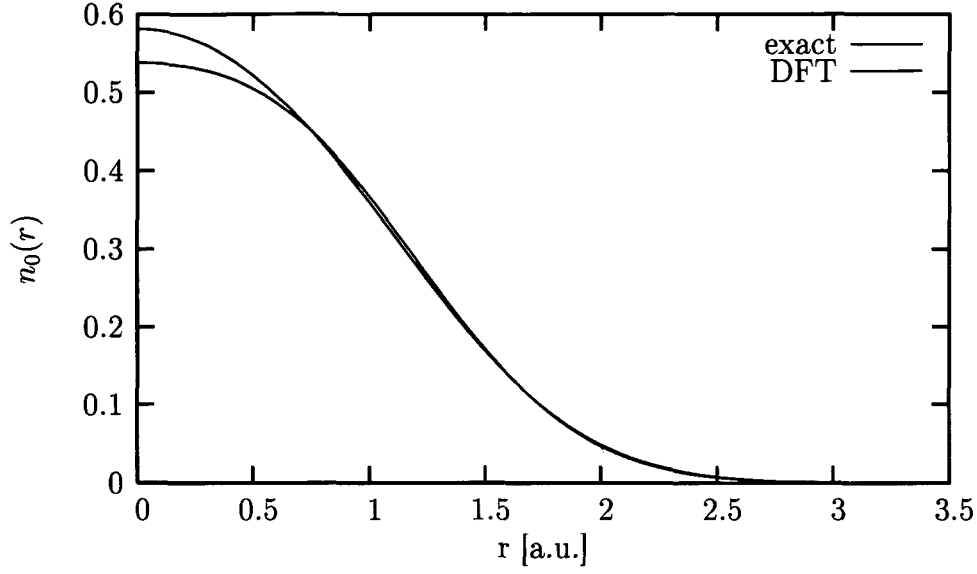
Figure 5.2: Comparison of density components of $l = 0$ of exact (red) and non-spherical average DFT (green) solution for the triplet ground state density of $\omega = 1$. The density component obtained by spherical averaging of the Kohn-Sham potential shows no significant difference compared to the non-spherical average.
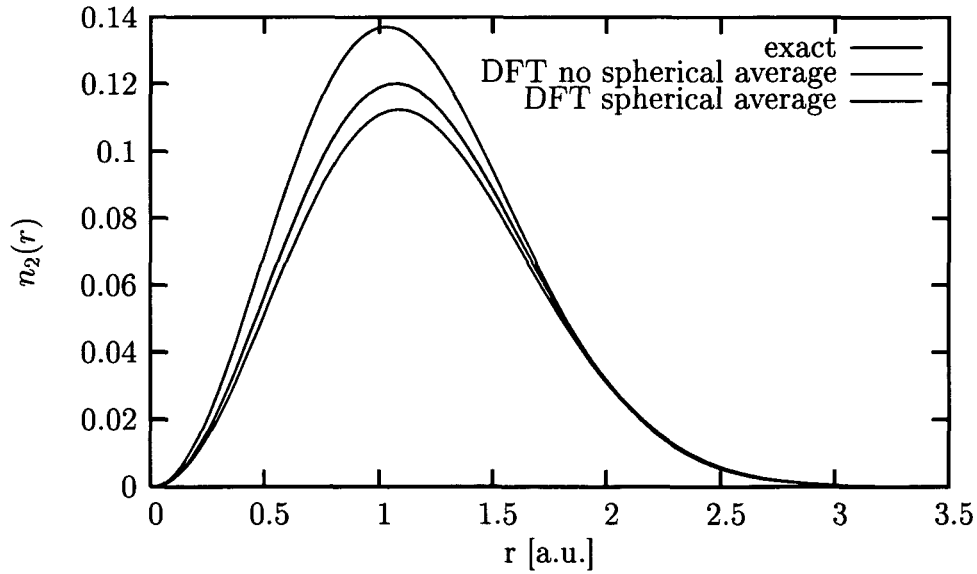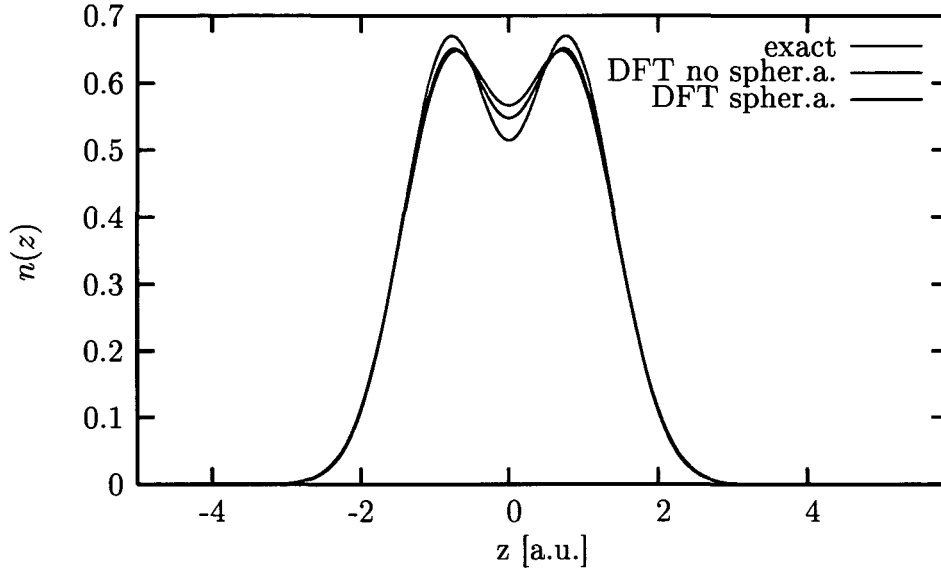

Figure 5.3: Comparison of density components of $l = 2$ of exact (red), non-spherical (green) and spherical average DFT (blue) solution for the triplet ground state density of $\omega = 1$.

41

Figure 5.4: Comparison of reduced density $n(z) = \int dx \int dy\, n(\vec{r})$ of exact (red) solution, DFT without spherical average (green) and DFT with spherical average (blue) for the triplet ground state density of $\omega = 1$.

exact and DFT results. Both DFT solutions (spherical average and no averaging) exhibit the double peak structure of the exact density. The spherical average shows a more pronounced local minimum and is, as already observed in the angular component analysis, in better agreement with the exact solution. Both different DFT densities will serve in chapter 9 as initial state for the time-dependent problem.

Chapter 6

Harmonic potential theorem

In this chapter we will introduce an exact condition of a many-body system in a parabolic potential, the so-called Harmonic Potential Theorem (HPT). This exact property of a time-dependent many-body system will give constraints on the TDDFT counterpart, in particular constraints on the exchange-correlation potential. We will study upto which extend those exact constraints are fulfilled for current approximations of exchange-correlation potentials. The HPT [106] is valid for a system of N-interacting particles in a harmonic potential of total Hamiltonian

$$H_0(\vec{r}_1, \vec{r}_2, ..., \vec{r}_N) = \sum_{i=1}^{N} \left(\frac{\vec{p}_i}{2} + \frac{1}{2}\vec{r}_i \cdot \mathbf{K} \cdot \vec{r}_i \right) + \frac{1}{2} \sum_{i \neq j} V(\vec{r}_i - \vec{r}_j) , \qquad (6.1)$$

where $\mathbf{K}$ denotes a generalized spring constant and is a symmetric, positive-definite tensor of rank three. $V(\vec{r}_i - \vec{r}_j)$ denotes an arbitrary particle interaction potential. The HPT states that the density $n(\vec{r}, t)$ of a system of interacting particles in a harmonic potential with Hamiltonian H_0 and subject to an additional uniform electric field $\vec{E}(t)$ is rigidly transported under the equation

$$n(\vec{r}, t) = n_0(\vec{r} - \vec{x}(t)) , \qquad (6.2)$$

provided that it evolves from an initially stationary state satisfying $H_0 \Psi_0 = E_0 \Psi_0$ at $t = 0$ with density $n_0(\vec{r})$. $\vec{x}(t)$ is the classical solution of

$$\ddot{\vec{x}}(t) = -\mathbf{K} \cdot \vec{x}(t) + \vec{E}(t) . \qquad (6.3)$$

The initial density of the system is therefore rigidly displaced. No distortion of the density in time takes place. In other words, every excitation of the system is an excitation of the center of mass part of the system, there is no energy transfer to the internal (relative) degrees of freedom of the system.

This statement is independent of the particle interaction.

The time-dependent wavefunction consists of the displaced initial (stationary) state $\Psi_0(\vec{r}_1 - \vec{x}(t), \vec{r}_2 - \vec{x}(t), ..., \vec{r}_N - \vec{x}(t))$ and suffers an additional time-dependent phase-shift given through

$$-iE_0t - iNS(t) + iN\frac{d\vec{x}}{dt} \cdot \vec{R}_{CM} \qquad (6.4)$$

where $\vec{R}_{CM} = \frac{1}{N}\sum_{j=1}^{N}\vec{r}_j$ is the center of mass operator and

$$S(t) = \int_0^t \left(\frac{1}{2}\dot{\vec{x}}^2(t') - \frac{1}{2}\vec{x}(t') \cdot \mathbf{K} \cdot \vec{x}(t')\right) dt' . \qquad (6.5)$$

$S(t)$ is equivalent to the classical action for the motion of the center of mass. The HPT Theorem is proved by changing the reference frame and rewriting the Schrödinger equation $(H_0 + N\vec{R}_{CM} \cdot \vec{E}(t))\Psi = i\frac{\partial}{\partial t}\Psi$ in an accelerated frame which moves according to $\vec{x}(t)$ ($\vec{x}(0) = 0$) with respect to the original reference frame. This corresponds to the Kramers-Henneberger Transformation [107].

The HPT constitutes a stringent test on many-body approximations, since it is one of the few exact properties known for a inhomogeneous electron gas. It therefore should also apply to TDDFT. General approximations for the exchange correlation functional, however, do not fulfill the HPT [106]. Restricting the initial-state to the many-body ground state Vignale [105] derived a simple symmetry property of the exchange correlation potential which is a necessary and sufficient condition for satisfying the HPT: The exchange-correlation potential observed from the accelerated Kramers-Henneberger frame has to transform by

$$V_{xc}[n'](\vec{r}, t) = V_{xc}[n](\vec{r} + \vec{x}(t), t) , \qquad (6.6)$$

where n' and n are the densities in the accelerated and rest frame respectively. Since in ALDA the functional dependence of the exchange-correlation potential is local in space and time, eq. (6.6) is fulfilled by ALDA.

The generalization to spin-density functional theory is straight-forward. In order that the HPT is satisfied the exchange-correlation potentials of the two different spin-degrees of freedom have to transform in an accelerated frame in correspondence with eq. (6.6) by

$$V_{\sigma,xc}[n'_\uparrow, n'_\downarrow](\vec{r}, t) = V_{\sigma,xc}[n_\uparrow, n_\downarrow](\vec{r} + \vec{x}(t), t) . \qquad (6.7)$$

Therefore also ALSDA satisfies the HPT. It is less obvious, if a self-interaction corrected ALSDA in the OEP treatment would satisfy the HPT. In ALSDA-SIC treated within the OEP approach also orbital densities are involved. In

44

the case of 2 electrons with opposite spins the orbital densities are equivalent to the spin-densities of the system, therefore eq. (6.7) will be satisfied in this special case. For spin-compensated triplet or singlet states the HPT is therefore fulfilled within ALSDA-SIC.

Chapter 7

One-particle observables - time-dependent dipole moment

In this chapter we study the accuracy of our TDDFT approach in comparing one-particle observables of the TDDFT and exact calculation. The one-particle observables relevant for the system under consideration are the time-dependent dipole moment $\langle Z \rangle = \langle \Psi(t) | z_1 + z_2 | \Psi(t) \rangle$ and the expectation value of the momentum in z-direction $\langle P_z \rangle = \langle \Psi(t) | \hat{p}_{z,1} + \hat{p}_{z,2} | \Psi(t) \rangle$. The dipole moment is defined without ambiguities within DFT, since it is entirely determined by the density through

$$\langle Z \rangle = \int d\vec{r} \, z \cdot n(\vec{r}); . \tag{7.1}$$

In the case of the harmonic potential also the expectation of the momentum in z-direction can be written as functional of the time-dependent density:

$$\langle P_z \rangle = \int d\vec{r} \, \frac{\partial}{\partial z} \cdot n(\vec{r}); . \tag{7.2}$$

In the special case of the harmonic oscillator the expectation of the Z and P_z are connected via $\langle P_z(t) \rangle = \frac{d}{dt} \langle Z(t) \rangle$. It will be shown that this exact relation also holds for the TDDFT system.

7.1 The dipole moment starting from the singlet ground state

In this chapter we analyze the quantitative errors of TDDFT reflected in the dipole expectation value introduced in eq. (7.1) starting from the singlet ground state of the harmonic 2-electron quantum dot. We analyze two
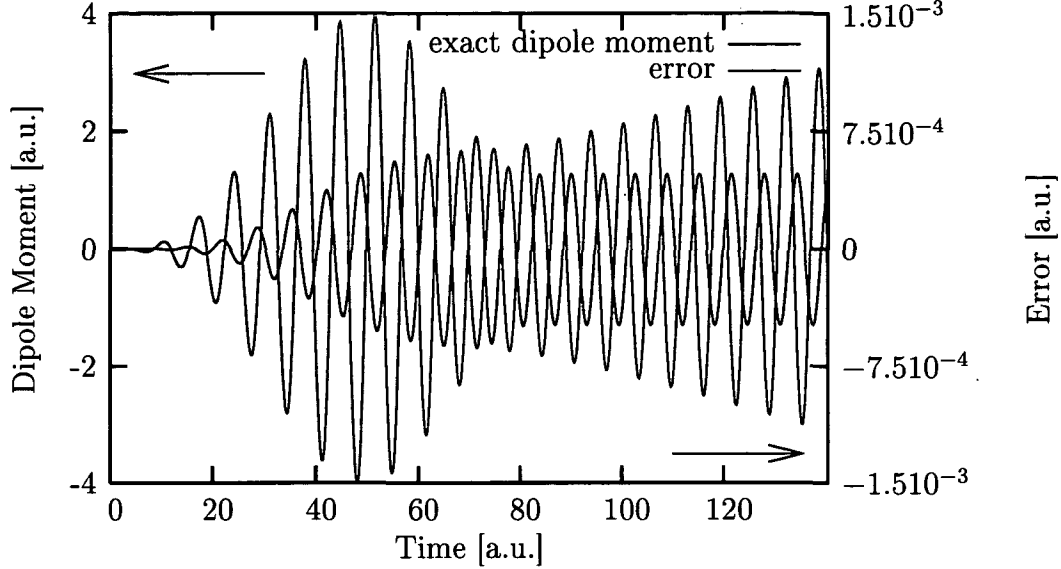
Figure 7.1: Comparison of the dipole moment of exact and TDDFT approach for the weakly correlated system at $\omega = 1$. Shown are the exact dipole moment (red line) and the absolute error (green line) $\langle Z(t) \rangle^{exact} - \langle Z(t) \rangle^{TDDFT}$. Note the different scale of the axes. The relative error of the TDDFT versus exact result is of the order of 0.1 percent. Parameters of the laser pulse: maximal field amplitude $A_0 = 0.3$, driving frequency $\omega_p = 0.884$, pulse duration $\tau = 90$

systems of different correlation strength, characterized by the oscillator frequency ω and different driving fields $E(t)$. Generally we can state that the TDDFT result stands in almost perfect agreement with the exact result starting from the singlet ground state, therefore illustrating the validity of the HPT within ALSDA.

Figure 7.1 and 7.3 show the time dependent dipole moment and the difference of TDDFT and exact calculation for the weakly correlated system of oscillator frequency $\omega = 1$ and the more correlated system at $\omega = 0.01$. In case of figure 7.1 the laser pulse has driving frequency $\omega_p = 0.884$, field amplitude $A_0 = 0.3$ and pulse length $\tau = 90$. The frequency of the laser pulse is chosen to be near the resonance. For this system the DFT ground state density is in excellent agreement with the exact ground state density, as analyzed in chapter 4.1 (see figure 4.1). Figure 7.1 shows the exact dipole moment (red line) and the error (green line) $\langle Z \rangle^{TDDFT} - \langle Z \rangle^{exact}$ of the TDDFT calculation.

Note the different scales of the ordinates. Plotting TDDFT and exact dipole-moment in one figure, the difference between both propagations could not be resolved. The relative error in the dipole-moment of the TDDFT propagation is of the order of 0.1 percent. We used a time-step of $\Delta t = 1.165 \ 10^{-2}$ in our calculations. This demonstrates the validity of the HPT. Additionally to the dipole moment, we directly checked the time-dependent density. The propagated density shows no deformations and, as stated by HPT, is only rigidly shifted in z-direction by the amount of the corresponding dipole moment. The HPT is therefore perfectly fulfilled by ALSDA if starting from the singlet ground state. We also checked on the second non-trivial one-particle observable, the time-dependent expectation value of the momentum operator in z-direction defined in eq. (7.2). The exact relation $\langle P_z(t) \rangle = \frac{d}{dt} \langle Z(t) \rangle$ between momentum expectation value and dipole expectation also holds in our TDDFT approach (not explicitly shown in figure 7.1). The error of the momentum expectation in TDDFT is comparable to the error of the dipole moment.

The discrepancies of TDDFT and exact dipole-moment are very small, nevertheless we will comment on the origin of the error. The error is not due to the approximation of the exchange-correlation potential, rather to the propagation method used to solve the non-linear Kohn-Sham equations. Initially the error is small and directly follows the dipole-moment. After the laser-pulse is switched off the error amplifies, like in a positive feedback loop. As already mentioned in the general survey of our numerical realization of TDDFT in chapter 3 we used a Suzuki-Trotter like split-operator method [144, 145] to propagate our initial Kohn-Sham orbital (see eq. (3.15)). In order to propagate the Kohn-Sham orbital from t to $t + \Delta t$ one would need the exchange-correlation potential evaluated for the density at time (and therefore Kohn-Sham orbitals) $t + \Delta t/2$. A simple solution to the problem would be to evaluate the electric field E at the mid-point $t + \Delta t/2$, whereas the exchange-correlation potential is determined at time t (method 1). This method increases the error from order $O(\Delta t^3)$ to $O(\Delta t^2)$. Recently it was proposed [144] to evaluate the exchange-correlation potential not with density $n(t)$ at time t, but performing the first step of the split-operator method and building the exchange correlation potential from this transient density (method 2). This should decrease the error and reestablish an order 2 method [144]. In our treatment this does not require an additional numerical effort and is simple to implement. Figure 7.2 shows the difference in performance of both methods, where the same step-width Δt was used in both calculations. The final error can be reduced by a factor of 10 by using method 2.

For the strongly correlated system of $\omega = 0.01$ we chose the following laser parameters: maximal field amplitude $A_0 = 0.045$, driving frequency $\omega_p = 0.097$,
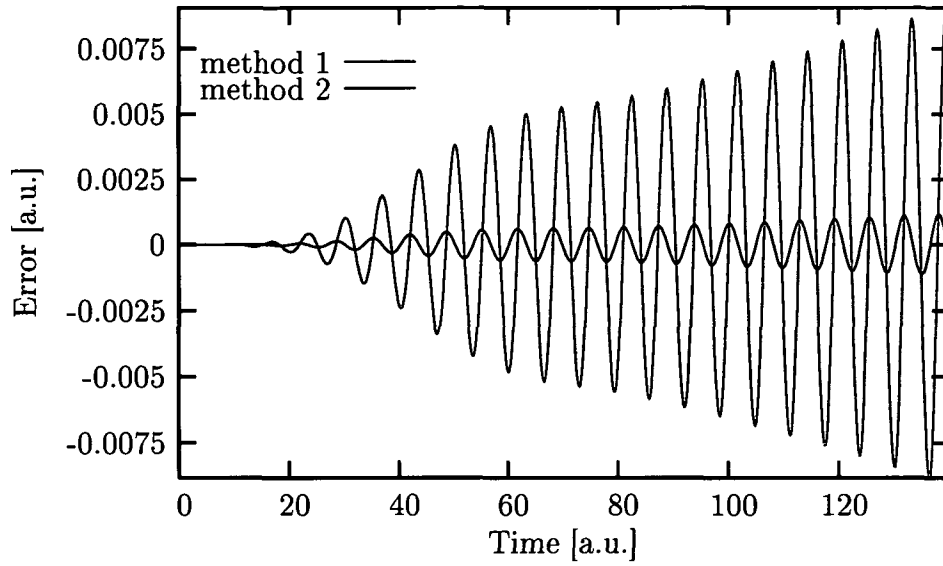
Figure 7.2: Comparison of the absolute error of the dipole moment for two different split-operator methods. Method 1 (red line) evaluates the exchange-correlation functional with the density at time t. Method 2 (green line) builds the exchange-correlation potential with the density obtained by performing the first propagation step of the split-operator (for details see eq. (3.15) of chapter 3). The error is significantly reduced in performing method 2, which actually does not increase the computational effort. The same time-step width is chosen ($\Delta t = 2.33 \ 10^{-2}$).
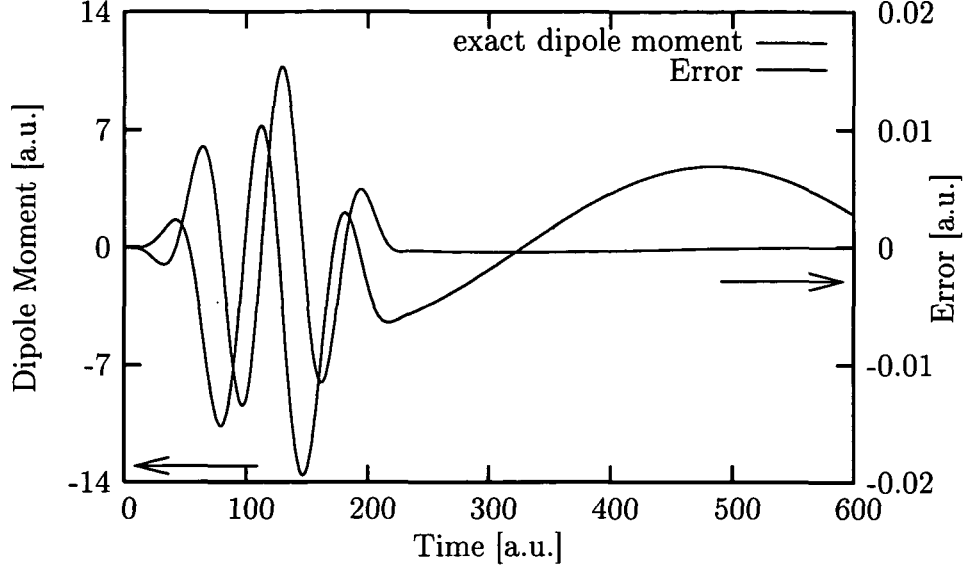
Figure 7.3: Comparison of the dipole moment within exact and TDDFT approach for the weakly correlated system at $\omega = 1$. Shown are the exact dipole moment (red line) and the absolute error (green line) $\langle Z(t) \rangle^{exact} - \langle Z(t) \rangle^{TDDFT}$. Parameters of the laser pulse: maximal field amplitude $A_0 = 0.045$, driving frequency $\omega_p = 0.097$, pulse duration $\tau = 244$

pulse duration $\tau = 244$. In the case of $\omega = 0.01$ the difference of the dipole moment of the exact calculation and the TDDFT calculation is also in the range of 0.1 percent. The ratio of exact to TDDFT solution never gets negative, showing an accurate description of the zeros of the dipole moment.

The accuracy of the dipole moment is independent of the degree of correlation of the system and is restricted by the propagation technique involved. This is only true for the system driven from a stationary state (Harmonic Potential Theorem). In a forthcoming chapter we will also study systems propagating form initial states different to stationary states. The quality of TDDFT calculations will dramatically decrease for such initial states.

Chapter 8

Occupation probabilities within TDDFT

8.1 Overview

In this chapter we attack the problem of calculating time-dependent many-particle observables within TDDFT. There are two independent possible sources of errors in TDDFT calculations. The first crucial ingredient is the time-dependent exchange correlation potential which determines the quality of the time-dependent electron density. A second independent source of error concerns the unknown functionals to calculate many-body observables such as occupation probabilities, ionization yields etc. In principle those quantities can be determined as a functional of the electron density. For the ionization yield approximations to this functional exist: absorbed density flux in an absorbing boundary of the system or partitioning of space in two regions representing the bound and ionized part of the density [6]. It is, however, not straight-forward to extend these approximations to state-to-state transition amplitudes.

The state-to-state transition amplitudes (S-matrix elements) are defined as the matrix elements of the long-time limit of the evolution operator U between a fixed initial state $|\Phi_i\rangle$ and a final state $\Phi_f\rangle$

$$S_{i,f} = \lim_{t \to \infty} \langle \Phi_f | U(t, -t) | \Phi_i \rangle \tag{8.1}$$

The evolution operator satisfies the integral operator equation

$$U(t, t_0) = 1 - i \int_{t_0}^{t} d\tau \, H(\tau) U(\tau, t_0) \tag{8.2}$$

with the initial condition $U(t_0, t_0) = 1$, $H(t)$ denotes the time-dependent system Hamiltonian. In our studies we restrict ourselves to Hamiltonians of

the form $H(t) = H_0 + V_{ext}(t)$ with the stationary Hamiltonian H_0 and some time-dependent external one-particle potential $V_{ext}(t)$ which is switched on at time $t = 0$ and switched off at $t = T$. The S-matrix in this case reduces to

$$S_{i,f} = \langle \Phi_f | U(T,0) | \Phi_i \rangle = \langle \Phi_f | \Phi_i(T) \rangle \, , \qquad (8.3)$$

and the channel states $|\Phi_i\rangle$ and $|\Phi_f\rangle$ are eigenstates of the stationary Hamiltonian H_0 and we introduced the propagated state $\Phi_i(T)\rangle := U(T,0)|\Phi_i\rangle$. In the case of the harmonic oscillator the indices i and f therefore stand for the set of quantum numbers $i := [N_{cm}^i, L_{cm}^i, n_{rel}^i, l_{rel}^i]$ and $f := [N_{cm}^f, L_{cm}^f, n_{rel}^f, l_{rel}^f]$ characterizing the final and initial states. For the angular quantum number of the c.o.m. system we will introduce the notation of capital letters ($L_{cm} = S, P, D, ...$), for the relative angular quantum number we use lower case letters ($l_{rel} = s, p, d, ...$). Evaluating the S-matrix at times $t > T$ only changes the general phase. The physical observable, invariant with respect to changes in the phase, is the state-to-state transition probability and is given by the square of the S-matrix

$$P(i,f)(t) = |S_{i,f}|^2(t) = |\langle \Phi_f | U(t,0) | \Phi_i \rangle|^2 \quad t > T. \qquad (8.4)$$

$P(i, f)$ is constant for $t > T$. To study the dynamics of the system we will also study time-dependent occupation probabilities at times $t < T$.

One aim of this thesis is to find functionals to approximate state-to-state transition amplitudes and probabilities within TDDFT, a problem which to our knowledge has so far not been attacked. This problem is decoupled from the challenge of finding new approximations to exchange-correlation functionals. In this work we propose different functionals to calculate S-matrix elements within TDDFT. The proposed functionals will depended implicitly on the time-dependent density and involve the time-dependent Kohn-Sham orbitals.

In spirit of time-dependent Hartree-Fock a first approximation for transition amplitudes would be to take the Slater determinants of Kohn-Sham orbitals as approximation to the full many-body wavefunction. Although the Kohn-Sham orbitals have a priori no physical meaning, they can be viewed as zeroth order approximation to the many-body wavefunction in terms of a coupling constant perturbation theory [124, 125]. Our approximation to the transition matrix element therefore implies to approximate the correlated initial $|\Phi_i\rangle$ by a Kohn-Sham Slater determinant $|\Phi^{DFT}\rangle = |n_1^i l_1^i m_1^i n_2^i l_2^i m_2^i\rangle$. For the ground state we have $|\Phi_i\rangle \simeq |0s0s\rangle$. The second approximation is to replace the exact time evolved state $|\Phi_i(t)\rangle$ in eq. (8.3) by the evolved Kohn-Sham determinant $\Psi^{TDDFT}(t)$. The transition amplitude then is calculated by

$$S_{i,f}(t) \simeq \langle \Phi_f | \Psi^{TDDFT}(t) \rangle \qquad (8.5)$$

A delicate question arises at this point: Which are the appropriate channel states Φ_f to project on the time-dependent Slater determinant? Do we project onto Slater determinants best suited to mimic the exact stationary-states of the system, or do we project onto the real eigenstates of the system Hamiltonian H_0? In the following chapters we are comparing both possibilities of final states. Since the total angular momentum and total angular momentum projection are good quantum numbers in our system the final states will in both cases be chosen as configuration states of well defined total angular momentum. We therefore distinguish to possible approximations to calculate transition amplitudes one consists in projecting onto Kohn-Sham configuration states of well defined angular momentum $|n_1 l_1 n_2 l_2 L_{tot} \ M_{tot}\rangle$, the other in projecting onto exact states $|N_{cm}L_{cm}n_{rel}l_{rel}L_{tot}\rangle$

$$S_{i,f}(t) \simeq \langle n_1 l_1 n_2 l_2 L_{tot} \ M_{tot}|\Psi^{TDDFT}(t)\rangle \qquad (8.6)$$

$$S_{i,f}(t) \simeq \langle N_{cm}L_{cm}n_{rel}l_{rel}L_{tot} \ M_{tot}|\Psi^{TDDFT}(t)\rangle \qquad (8.7)$$

Inherently connected to the choice of the optimal channel state will be the problem of the so-called spurious cross-channel correlation (oscillations in the transition amplitudes at asymptotic times) first diagnosed and analyzed in time-dependent Hartree-Fock studies. In table 8.1 we clarify the notation of different final and initial states used in the following sections.

Table 8.1: Notation of the different initial and final states used in our projection approach: The exact states and DFT configuration states are defined as states of well defined angular momentum L_{tot} and angular momentum projection M_{tot}. We restrict our studies on states of $M_{tot} = 0$, this quantum number will therefore be omitted. The total angular momentum number L_{tot} will be omitted if it can be deduced without any ambiguities from the coupling of the two involved angular momenta.

states	quantum numbers	notation
exact	$N_{cm}L_{cm}n_{rel}l_{rel}L_{tot}M_{tot}$	$L_{cm} = S, P, D, ...$ $l_{rel} = s, p, d, ...$ $L_{tot} = S, P, D, ...$
DFT	$n_1 l_1 m_1 n_2 l_2 m_2$	$l_1 = s, p, d, ...$ $l_2 = s, p, d, ...$
DFT configuration state functions	$n_1 l_1 n_2 l_2 L_{tot}M_{tot}$	$l_1 = s, p, d, ...$ $l_2 = s, p, d, ...$ $L_{tot} = S, P, D...$

8.2 Projection onto Kohn-Sham configuration states

For the following considerations we will evolve the Kohn-Sham system from its singlet ground state. We build a time-dependent Slater-determinant denoted with $\Psi^{TDDFT}(t)$ of the time-propagated Kohn-Sham orbital $\Phi_0(\vec{r}_1, t)$ which initially was in the Kohn-Sham ground state $\Phi_0(\vec{r}_1)$. $\Psi^{TDDFT}(t)$ is now treated as the time-dependent many-body wavefunction. The delicate question arising in TDDFT is how to choose the appropriate channel state onto which we project the time-dependent Kohn-Sham Slater-determinant $\Psi^{TDDFT}(t)$. The first method to calculate transition probabilities is to project the time-dependent Kohn-Sham determinant onto stationary Kohn-Sham Slater-determinants, approximating the wave-functions of exact stationary states. The exact eigenstates of the harmonic two-electron quantum have well defined total angular momentum. We therefore construct configuration state functions $|n_1 l_1 n_2 l_2 L M\rangle$ of well-defined total angular momentum L and angular momentum projection M built up from Kohn-Sham single-electron orbitals $|n_i l_i m_i\rangle$. Since we start out with $M = 0$ which is preserved by the time-dependent perturbation, we only have to consider configuration states with total $M = 0$. The symmetrized coordinate-space part of the singlet configuration state function reads [156]:

$$|n_1 l_1 n_2 l_2, L0\rangle := \begin{cases} \frac{1}{\sqrt{2}} \sum_m [\langle l_1 m\, l_2 -m|L0\rangle\, |n_1 l_1 m\rangle_1 \otimes |n_2 l_2 -m\rangle_2 & n_1 \neq n_2 \\ \quad + \langle l_2 -m\, l_1 m|L0\rangle\, |n_2 l_2 -m\rangle_1 \otimes |n_1 l_1 m\rangle_2] & \text{or } l_1 \neq l_2 \\ \\ \sum_m \langle l_1 m\, l_1 -m|L0\rangle\, |n_1 l_1 m\rangle_1 \otimes |n_1 l_1 -m\rangle_2 & n_1 = n_2 \\ & \text{and } l_1 = l_2 \end{cases}$$
(8.8)

$\langle l_1 m l_2 - m|L0\rangle$ denotes the Clebsch-Gordon coefficient.

In correspondence with eq. (8.6) the time-dependent occupation probability of the configuration state $|n_1 l_1 n_2 l_2, L0\rangle$ of the TDDFT Slater-determinant is then defined as

$$P(n_1 l_1 n_2 l_2 L0; t) := |\langle n_1 l_1 n_2 l_2, L0|\Psi^{TDDFT}(t)\rangle|^2 \,.$$
(8.9)

Since in our numerical approach the time-dependent Kohn-Sham orbitals $|\Phi(t)\rangle$ are expanded in the orthonormal basis of the stationary Kohn-Sham orbitals $|n_i l_i m_i\rangle$ of the ground state occupation, the overlap integral in eq. (8.9) is simple to calculate. The asymptotic limit (after the perturbation of the laser pulse) of eq. (8.9) can then be interpreted as transition- probability. In projecting onto the Kohn-Sham ground state configuration state
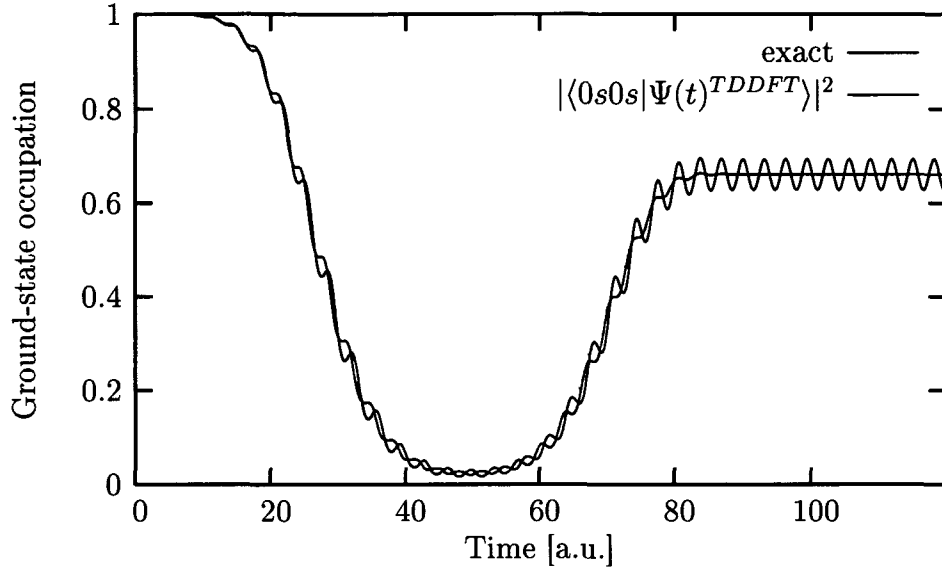
Figure 8.1: Comparison of ground state occupation probability of exact calculation (red) and TDDFT calculation (green) in the LSDA-SIC approximation for a confining frequency $\omega = 1$. Parameters of the laser pulse: maximal field amplitude $A_0 = 0.3$, driving frequency $\omega_p = 0.884$, pulse duration $\tau = 90$
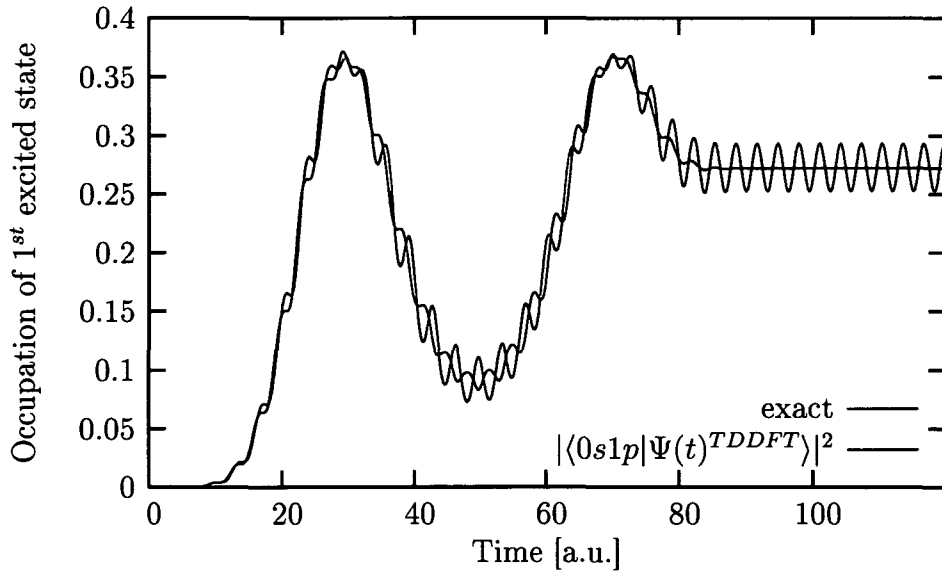

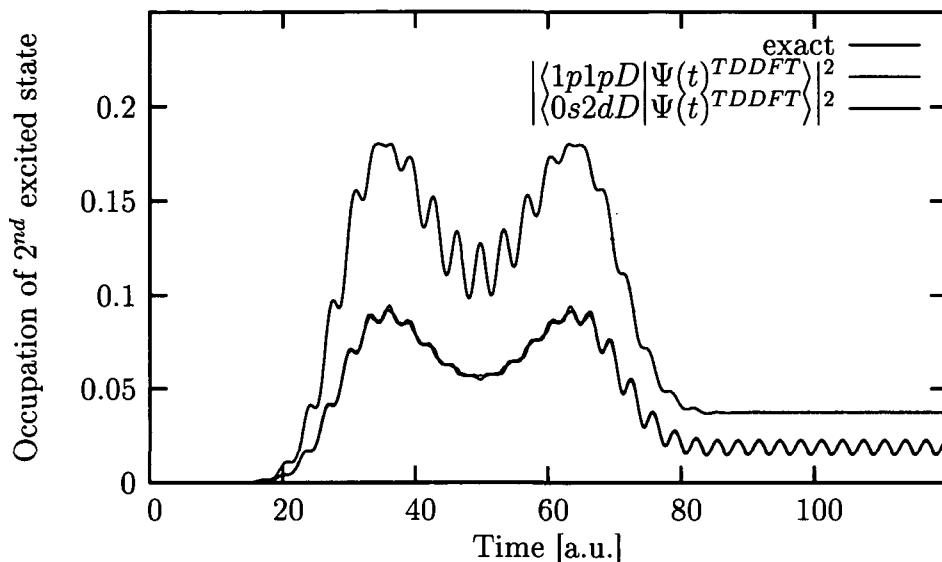Figure 8.2: Comparison of occupation probability of first excited state with total angular momentum $L = 1$ of exact calculation (red) and TDDFT calculation (green)

55

Figure 8.3: Comparison of occupation probability of second excited state $N_{cm}{=}2,L_{cm}{=}2,n_{rel}{=}0,l_{rel}{=}0$ with total angular momentum $L = 2$ of exact calculation (red) and TDDFT calculation (green)

function $|0s0s\rangle$ we therefore get a first guess of the ground state occupation probability within the TDDFT approach which we compare to the ground state occupation probability of the exact propagation. Figure 8.1 shows the comparison of exact versus TDDFT ground state occupation for the weakly correlated system of confining strength $\omega = 1$. The parameter of the laser pulse are chosen the same as in chapter 7.1. We see that the overall shape of the ground state occupation is very well described by our TDDFT approach of eq. (8.9). The laser pulse is switched off at $t = 90$. After that the exact system shows a ground state occupation probability of about 66 percent. Most of the missing population resides in the first excited state (see figure 8.2).

The TDDFT occupation probability is oscillating around the exact transition probability for times $t > 90$ in the absence of an external perturbation. These oscillations (named 'spurious cross-channel correlations') are known from the time-dependent Hartree-Fock calculations [58]. They are relics from the highly non-linear nature of Kohn-Sham (or TDHF) equations, which lack the principle of superposition.

After the excitation through the laser field, the system is in a coherent superposition of eigenstates of the unperturbed exact Hamiltonian. If one develops this coherent superposition in a basis (in the configuration state-functions),
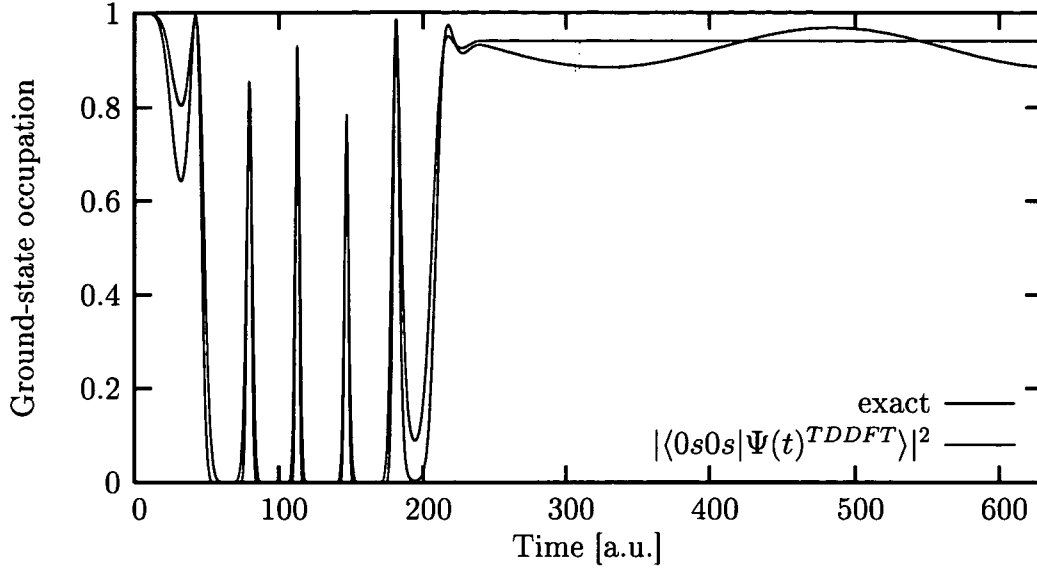
Figure 8.4: Comparison of ground state occupation probability of exact calculation (red) and TDDFT calculation (green) in the LSDA-SIC approximation for a confining frequency $\omega = 0.01$. Parameters of the laser pulse: maximal field amplitude $A_0 = 0.045$, driving frequency $\omega_p = 0.097$, pulse duration $\tau = 244$
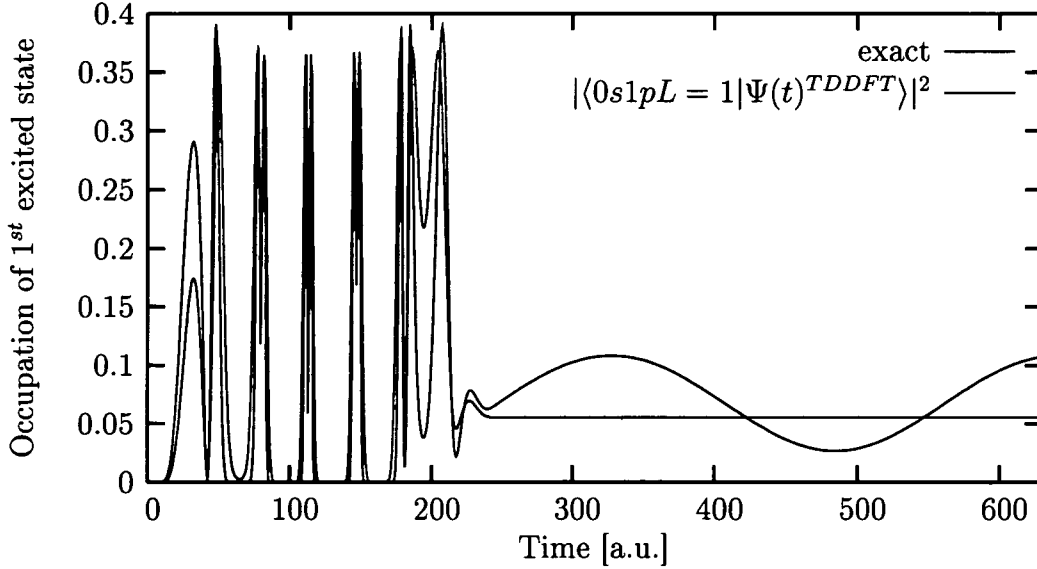

Figure 8.5: Comparison of occupation probability of first excited state with total angular momentum $L = 1$ of exact calculation (red) and TDDFT calculation (green)

which is not the eigenbasis, the occupation probabilities of this new basis states will necessarily oscillate. It should therefore not be astonishing that the TDDFT occupation probability calculated via projection onto the Kohn-Sham basis shows oscillations at asymptotic times. It is tempting to think that these oscillations should vanish if one projects onto the correct channel state (exact eigenstates of the system). This is, however, not true for a propagation through time-dependent Kohn-Sham equations. The time-evolved Kohn-Sham orbitals do not reliably represent the wavefunction but only the density. In general, this 'spurious cross-channel correlations' will therefore persist also when projecting onto the eigenstates of the system.

In the case of the weakly correlated system of $\omega = 1$ the exact and the DFT ground state wavefunction (Slater-determinant of ground state Kohn-Sham orbitals) have an overlap of 98.6 percent (see appendix D). The oscillations in the ground state occupation probability have an amplitude of around 7 percent. They therefore can not be damped out by projecting onto the exact eigenfunction. The projection onto the exact eigenstate will result in a shift of the TDDFT ground state occupation. The same will be true for the occupation of the first excited state, for which exact and the configuration state function $|0s1pL = 1\ 0\rangle$ of Kohn-Sham orbitals have an overlap of 98.1 percent.

Also in the case of strong correlation reliable results for occupation probabilities can be achieved. Considering the two-electron system with confining frequency of $\omega = 0.01$ the LSDA-SIC fails to reproduce the correct ground-state density profile (see figure 4.2). The exact and DFT ground state have an overlap of 83 percent (see table D.5 in appendix D). Nevertheless the occupation probabilities obtained by the TDDFT projection approach yield results in accordance with the exact solution. Figures 8.4 and 8.5 show a comparison of exact versus TDDFT results for the ground and the first excited state. As in the weakly correlated case the TDDFT occupation probabilities show cross-channel correlations after the switch-off of the laser pulse. Average over those oscillations results, however, in accurate transition probabilities. The parameters of the laser pulse in the case of the weakly confined quantum dot are: maximal field amplitude $A_0 = 0.045$, driving frequency $\omega_p = 0.097$, pulse duration $\tau = 244$.

In the following we will return to the weakly correlated system of $\omega = 1$. Regarding the second-excited state $N_{cm}=2$, $L_{cm}=2$, $n_{rel}=0$, $l_{rel}=0$ of total angular momentum $L = 2$ the situation is different (see figure 8.3). The exact state needs at least 2 configuration-state functions of Kohn-Sham orbitals to be reliably represented (see tables of appendix D), $|0s2dL = 2\ 0\rangle$ and $|1p1pL = 2\ 0\rangle$. Projection of the TDDFT wave-function onto each single configuration state-function therefore will not give a good approximation to

the occupation of the excited state. As can be seen in figure 8.3 the occupation probability for both configuration-state functions are equal in size and of the order of $1/2$ of the exact occupation probability of the lowest state of total angular momentum $L = 2$. In the case that a single configuration-state function of Kohn-Sham orbitals is a bad representative of an exact eigenstate $|N_{cm}L_{cm}n_{rel}l_{rel}\rangle$ of the system one therefore has to choose a different channel state to project on. The projection has to be performed onto the exact eigenstate of the system (or a linear combination of configuration-state functions significantly contributing to the exact eigenstate). How this is done is explained in the following section.

8.3 Projection onto exact eigenstates

In the last chapter we observed that for calculating occupation probabilities of states which are not well represented by a single configuration, projection of the time-dependent TDDFT wavefunction onto a configuration state function of Kohn-Sham orbitals is not the appropriate method. In correspondence with eq. (8.7) we therefore define the occupation probability by projecting the TDDFT wave-function onto exact eigenstates $|N_{cm}L_{cm}n_{rel}l_{rel}LM\rangle$ of well defined total angular momentum:

$$P(N_{cm}L_{cm}n_{rel}l_{rel}NM; t) := |\langle N_{cm}L_{cm}n_{rel}l_{rel}NM|\Psi^{TDDFT}(t)\rangle|^2 \qquad (8.10)$$

Starting from the singlet ground state with $n_{rel} = l_{rel} = 0$ the only states involved during time will be excitations of the center of mass. The total angular momentum equals the angular momentum of the center of mass, the angular coupled states $|N_{cm}L_{cm}n_{rel}l_{rel}LM\rangle$ are therefore trivial and characterized by $|N_{cm}L_{cm}0s\rangle$. The numerical implementation of eq. (8.10) is not straight forward. It is tricky to calculate the 6-dimensional integrals involved in the overlap $\langle N_{cm}L_{cm}0s|\Psi^{TDDFT}(t)\rangle$. As already mentioned in the first chapters we have developed a stationary as well as time-dependent configuration interaction (CI) code in the basis of Kohn-Sham configuration state functions. We therefore have the expansion of the 'exact' (converged result of the CI approach) eigenstates of the system in terms of Kohn-Sham configuration state functions. The overlap integral eq. (8.10) is then therefore straight forward to calculate.

In figure 8.6 we show a comparison of occupation probability of singlet ground state for the two different TDDFT projection-approaches proposed. Since the TDDFT-system starts from the DFT ground state, the overlap of exact and TDDFT wave-function at initial time $t = 0$ is not equal to unity
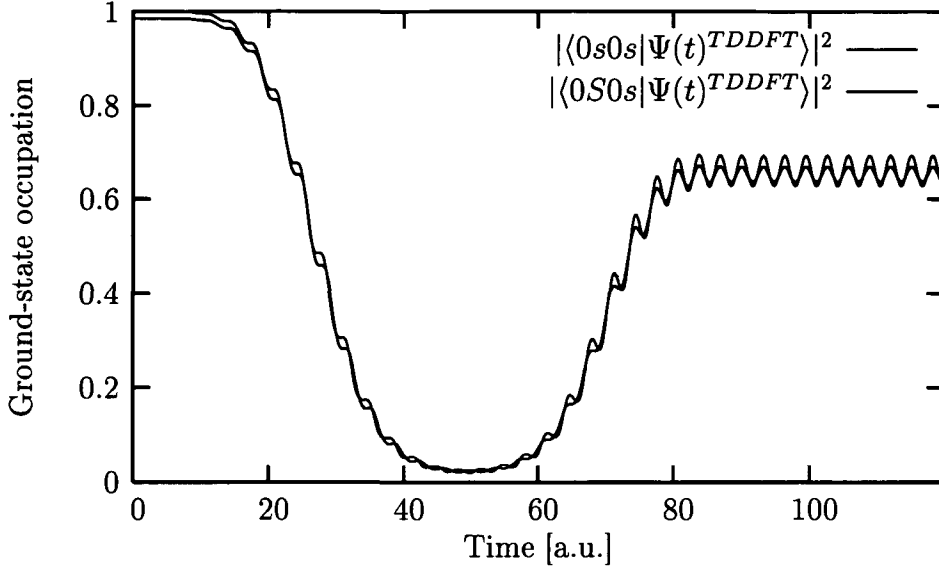
Figure 8.6: Comparison of occupation probability of singlet ground state of the two different TDDFT approaches proposed. The time-dependent TDDFT Slater-determinant is once projected onto the Kohn-Sham ground state (green line) and onto the exact, correlated ground state (blue line).

but 99.3 percent. Because of this large overlap the two approaches yield similar results. The cross-channel correlations are slightly damped by projecting onto the exact ground state but still are present. Hence, they can not be cured by projecting onto the exact eigenstates. Averaging over cross-channel correlations to define time-independent transition probabilities after switch-off of the perturbation yields a better result for the projection onto the DFT ground state. The projection onto the exact ground state therefore gives no improvement of the transition probability.

Based on a converged time-dependent CI calculation we observe that

$$|\langle 0S0s|\Psi^{TDDFT}(t)\rangle|^2 = |\langle 0s0s|\Psi^{exact}(t)\rangle|^2 \quad \forall t \, . \qquad (8.11)$$

The exact ground state occupation of the TDDFT wavefunction equals the projection of the total correlated wavefunction onto the Kohn-Sham ground state. The equality was observed in any regime of correlation. This observation demonstrates anew that the calculations are satisfying the HPT. At time $t = 0$ the TDDFT calculation starts out with the DFT ground state $|\Psi^{TDDFT}(0)\rangle = |0s0s\rangle$, the exact calculation propagates from the exact ground state $|\Psi^{exact}(0)\rangle = |0S0s\rangle$, and the equality $\langle 0S0s|\Psi^{TDDFT}(t)\rangle = \langle 0s0s|\Psi^{exact}(t)\rangle$ at time $t = 0$ is evident. The HPT states that the wavefunctions are subject of a rigid translation, the exact wavefunction as well as

the Kohn-Sham orbitals. Starting out from an overlap integral and at later times shifting either one or the other wave-function rigidly should yield in both cases the same overlap. This manifestation of the HPT only holds for the ground state. If one chooses, however, as initial state a different eigenstate of the system, as an example $|\Psi^{exact}(0)\rangle = |1P0s\rangle$ for the exact and $|\Psi^{TDDFT}(0)\rangle = |0s1p\rangle$ for the DFT system the equality $\langle 1P0s|\Psi^{TDDFT}(t)\rangle = \langle 1p0s|\Psi^{exact}(t)\rangle$ should hold.

Figure 8.7 shows a comparison of occupation probability for the first excited state of exact calculation and TDDFT wavefunction projected onto the exact first excited state. The overlap of DFT configuration state $|0s1p\rangle$ with the exact first excited state $|1P0s\rangle$ (center of mass mode is excited) is 99.0 percent. A comparison of figure 8.7 to the figure 8.2 (where the TDDFT wave-function is projected onto the DFT configuration state $|0s1p\rangle$) shows that projection onto the exact state gives slightly better results during the time of the perturbing laser pulse. Oscillations of the occupation probability at times around 50 are in better agreement with the exact occupation probability. For the transition amplitude, however, we find the result in accordance to the ground state transition. Defining the transition amplitude by averaging over the cross-channel correlations gives a better and very accurate result for the projection onto the DFT configuration state. We therefore state that if TDDFT configuration states have a large overlap with the exact eigenstates of the system the most accurate transition amplitudes are obtained by projecting the TDDFT Slater-determinant onto DFT configuration state functions and averaging over the cross-channel correlations.

The story changes dramatically when observing occupation probabilities of eigenstates which need two or more DFT configuration state functions to be built up. We restrict ourselves to the weakly correlated system of $\omega = 1$ and draw our attention onto the occupation of the exact second excited state of angular momentum $L_{cm} = 2$ (denoted as $|2D0s\rangle$). In this case the TDDFT wave-function has to be projected onto a linear superposition of relevant configuration state-functions, or onto the exact state. Figure 8.8 shows that projection onto the exact state $|2D0s\rangle$ gives excellent transition probabilities.

In the case of a weakly correlated system the method of projecting the Slater-determinant of time-dependent Kohn-Sham orbitals onto either exact eigenstates or Kohn-Sham configuration state-functions seems promising. The method of averaging over the cross-channel correlations is not rigorously justified, nevertheless it yields very accurate transition probabilities in the case of the driven ground state of the harmonic two-electron quantum dot. Despite this first success it should be pointed out that within the proposed projection mechanism it is not possible to define a well behaving transition amplitude
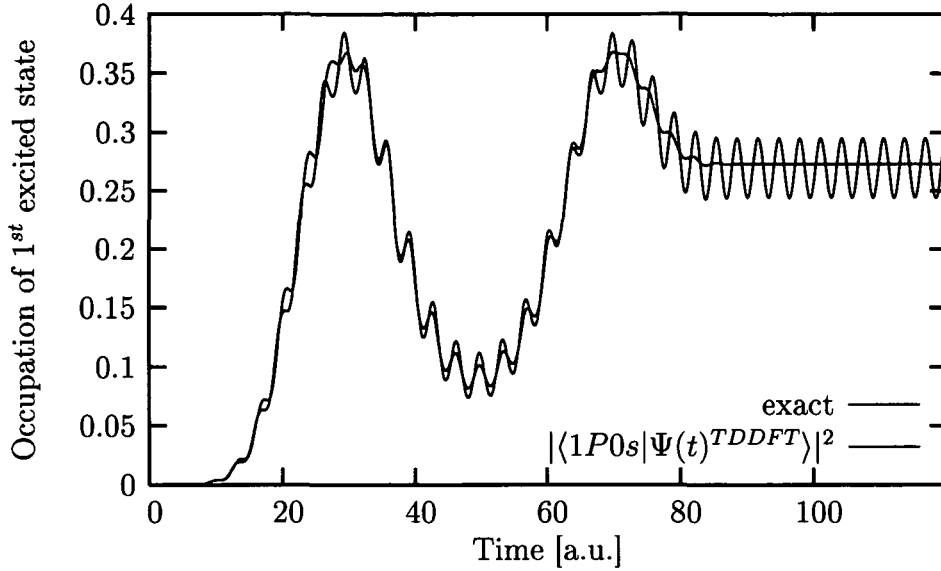
61

Figure 8.7: Comparison of occupation probability of first excited state with total angular momentum $L = 1$ of exact calculation (red) and TDDFT calculation (green) for a confining frequency $\omega = 1$. The TDDFT wave-function is projected onto the exact first excited state. Parameters of the laser pulse: maximal field amplitude $A_0 = 0.3$, driving frequency $\omega_p = 0.884$, pulse duration $\tau = 90$
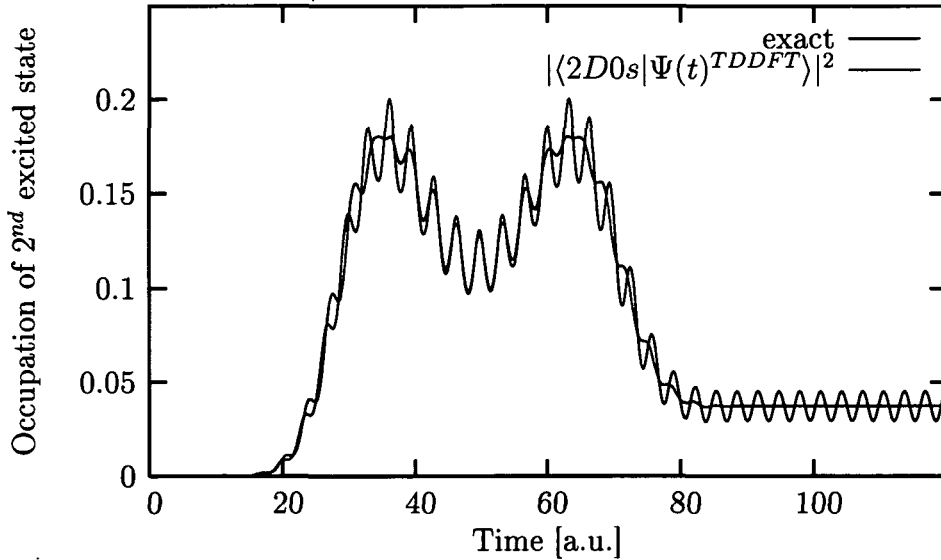

Figure 8.8: Comparison of occupation probability of second excited state $(N_{cm} = 2, L_{cm} = 2, n_{rel} = 0, l_{rel} = 0)$ of exact calculation (red) and TDDFT calculation (green) for a confining frequency $\omega = 1$. The TDDFT wavefunction is projected onto the exact first excited state. Pulse parameters as in figure 8.7

62

in the asymptotic limit of large times after the perturbation responsible for the transition is switched off. It was not possible to find appropriate channel states to project onto the TDDFT Slater-determinant which would give stationary occupation numbers after the perturbation vanished. We will show in the following that the situation will become worse if we consider more complex systems, i.e. the triplet ground state and systems which are not subject to the harmonic potential theorem.

Chapter 9

Propagation of the triplet ground state

In this chapter we assess the quality of TDDFT propagating the triplet ground state in an external laser field. As discussed in chapter 6 also the triplet ground state is subject to the harmonic potential theorem. In the case of a symmetric spin-part of the wavefunction with antiparallel spins $(|\uparrow\downarrow\rangle+|\downarrow\uparrow\rangle)$ the HPT should hold for ALSDA-SIC. The evolution of the triplet ground state, being the first excitation of angular momentum ($n_{rel} = 1$, $l_{rel} = 1$) of the internal (relative) degree of freedom and the ground state of the center of mass ($N_{cm} = 0$, $L_{cm} = 0$) is strongly related to the evolution of the singlet ground state. The time-propagation is only reflected in the center of mass (c.o.m.) part of the wavefunction, which is equal for singlet and triplet ground state. The time-dependent dipole moment is only related to the c.o.m. degree of freedom, hence identical for either singlet or triplet ground state as initial state. The second "invariant" of singlet or triplet ground-state propagation in an external field is the occupation of the ground state.

9.1 Dipole moment

In chapter 5 we have studied the performance of DFT with LSDA-SIC for the triplet ground state. We have found that the DFT triplet ground-state density obtained by spherical average of the effective Kohn-Sham potential is in better accordance with the exact density compared to the density obtained by not applying the spherical average. The latter has, however, the property to be stationary if propagated in time with the full angular dependence of the

Kohn-Sham potential. Our studies show that the initial state obtained by the full angular dependence of the effective Kohn-Sham potential gives better results in terms of the HPT. Starting with the triplet ground state obtained by spherical average the density undergoes deformations since the initial state is not Kohn-Sham eigenstate of the effective potential of full angular dependence. The distortions of the density at the beginning of the laser pulse are rather small but increase with time. For the following considerations we therefore propagate the initial state obtained by the full angular dependence of the Kohn-Sham potential.

Before analyzing the quality of the triplet ground-state propagation within ALSDA-SIC we consider an ALDA (adiabatic local density approximation) TDDFT calculation without inclusion of a self-interaction correction. The HPT is fulfilled in this case. Both Kohn-Sham orbitals are propagated in the same exchange-correlation potential

$$V_{xc}^{ALDA}[n] = \frac{\delta E_{xc}^{LDA}[n]}{\delta n} . \qquad (9.1)$$

Figure 9.1 shows the exact dipole moment and the error of the ALDA calculation. Comparing the error of the ALDA dipole moment of the triplet ground state to that of the singlet ground state (see figure 7.1) we observe a slight increase. Nevertheless the error stays moderate and ALDA gives an excellent dipole moment. The densities are rigidly transported according to the HPT.

We now turn to the ALSDA-SIC and include a self-interaction correction to the exchange-correlation potential. As discussed in chapter 6 ALSDA-SIC in principle satisfies the necessary and sufficient conditions to fulfill HPT if the spin-compensated two-electron system is considered. In the case of the triplet ground-state the ALSDA-SIC yields different exchange-correlation potentials for the different Kohn-Sham orbitals

$$V_{xc,\sigma}^{SIC}[n_\downarrow, n_\uparrow] = \frac{\delta E_{xc}^{LSDA}[n_\downarrow, n_\uparrow]}{\delta n_\sigma} - \int \frac{n_\sigma(\vec{r'}, t)}{|r - r'|} d\vec{r'} - \frac{\delta E_{xc}^{LSDA}[n_\sigma, 0]}{\delta n_\sigma} \quad n_\uparrow \neq n_\downarrow .$$
$$(9.2)$$

Figure 9.3 shows the error of the TDDFT dipole moment. A comparison of figure 9.3 with the error obtained by ALDA (see figure 9.1) shows that the error in the dipole moment increases drastically in the case of the ALSDA-SIC. After the laser pulse is switched off at times $t > 90$ the error increases and becomes comparative in size to the dipole moment. The time-step in the split-operator propagation was chosen as $\Delta t = 4.76 \, 10^{-3}$. Further decrease of the time step did not improve the result. To assess the error of the time-dependent density figure 9.4 shows snapshots of the reduced density at different times. The points in time at which the reduced density is
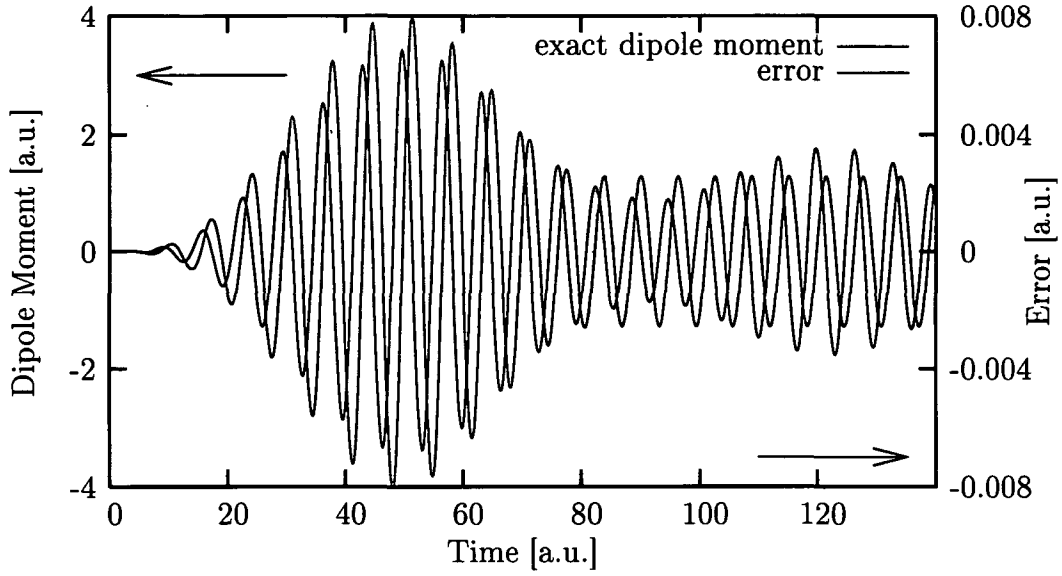
Figure 9.1: Time-dependent dipole moment of exact calculation (red line) and error of TDDFT ALDA calculation (green line) starting from the triplet ground state. The time-step in this calculation is $\Delta t = 4.76 \ 10^{-3}$. Parameters of the laser pulse: maximal field amplitude $A_0 = 0.3$, driving frequency $\omega_p = 0.884$, pulse duration $\tau = 90$
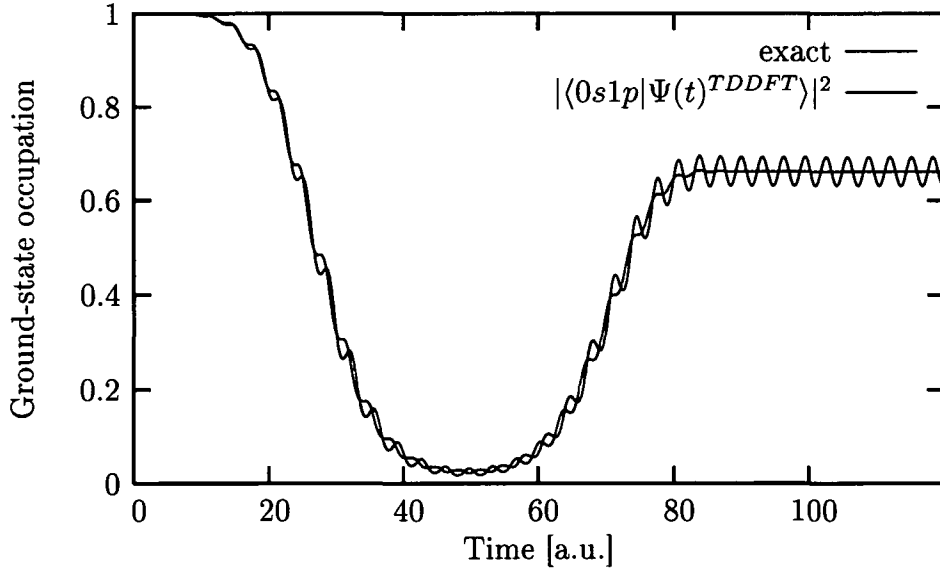

Figure 9.2: Comparison of triplet ground-state occupation probability of the exact (red line) and TDDFT ALDA (green line) calculation. The initial state was obtained without spherical averaging of the exchange-correlation potential (see chapter 5).
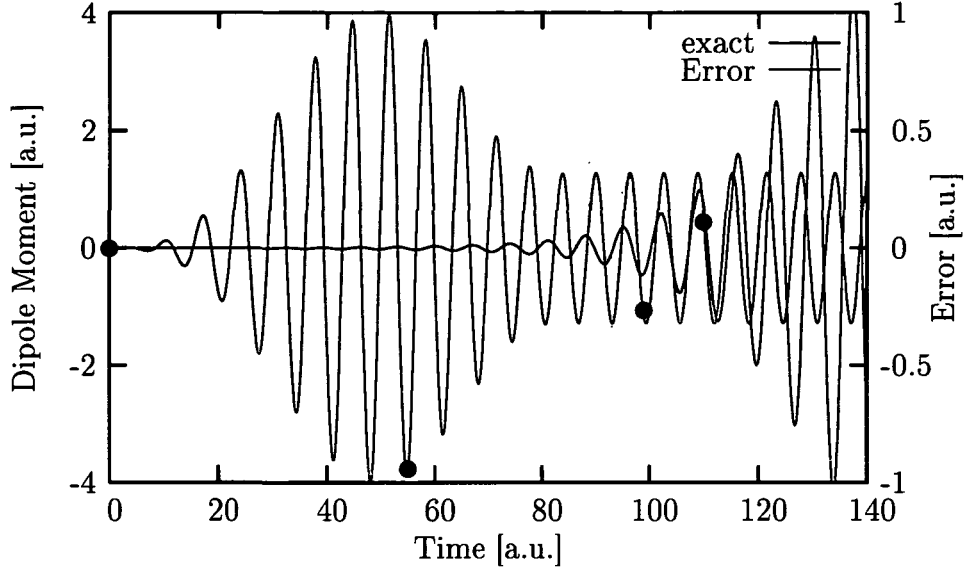
Figure 9.3: Time-dependent dipole moment of exact calculation (red line) and error of the ALSDA-SIC TDDFT calculation (green line) starting from the triplet ground state. The time-step in this calculation is $\Delta t = 4.76 \ 10^{-3}$, further decrease did not yield any improvements. The dots mark the points in time at which density snap-shots are made, which are shown in the subsequent figure. Parameters of the laser pulse: maximal field amplitude $A_0 = 0.3$, driving frequency $\omega_p = 0.884$, pulse duration $\tau = 90$
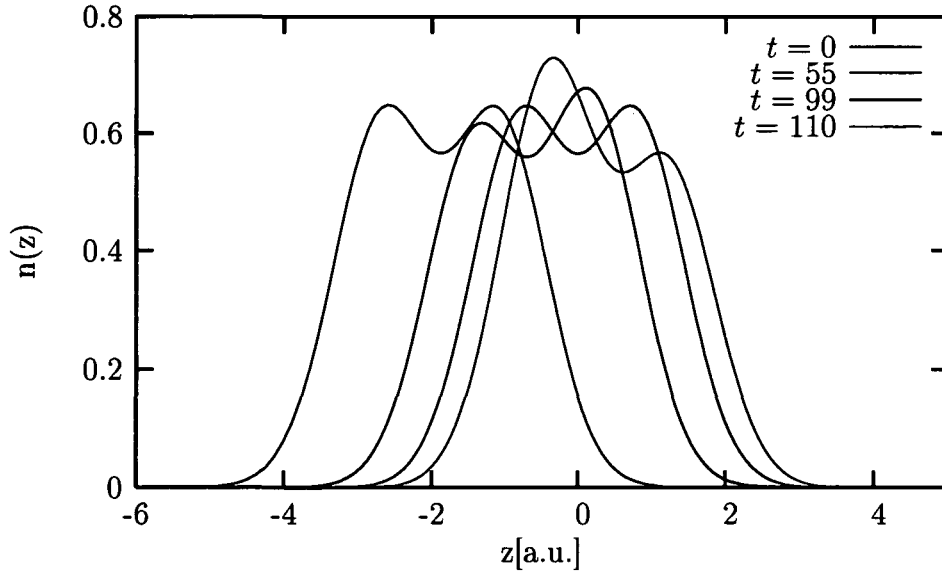

Figure 9.4: Reduced densities $n(z) = \int dx \int dy n(\vec{r})$ at different times t. The points in time t are marked in figure 9.3 with the corresponding color.

plotted are marked in figure 9.3. Whereas the HPT is still fulfilled until the maximum peak amplitude of the laser pulse is reached (at time $t = 55$ green line), violations of the HPT can be observed after switching off the pulse. The density is no longer rigidly transported, but gets deformed. The propagation is stable for times as long as the laser pulse is active. The free propagation of the coherent superposition after the switch-off of the laser pulse is not handled satisfactory in the ALSDA-SIC. In the next section we study time-dependent occupation probabilities to analyze the failure in more detail.

9.2 Occupation probabilities

In the case of the ALDA without self-interaction correction the TDDFT calculation gives, as in the singlet ground-state propagation, occupation probabilities in accordance to the exact result. Figure 9.2 shows a comparison of exact and ALSDA calculation of the triplet ground-state occupation.

In the last section we observed that by adding the self-interaction correction the HPT was no longer fulfilled and the error in the dipole moment was increasing. The failure of ALSDA-SIC for the triplet ground-state propagation will also be manifested in the occupation probabilities. Figure 9.5 shows the occupation of the triplet ground state of the Kohn-Sham Slater determinant as a function of time in comparison to the exact result. As long as the laser is active, the TDDFT occupation probabilities for the triplet ground-state propagation perform equally well as in the singlet case. The cross-channel correlations at times $t > 90$ suffer an additional drift, which is not observed in the case of the singlet ground-state occupation. At times $t > 120$ the TDDFT calculation breaks down. The problem seems not to be due to the propagation technique of the split-operator method. Evaluating the exchange-correlation potential at mid-points, as discussed in section 7.1, reduced the time-step for converged results from $\Delta t = 1.83 \ 10^{-4}$ to $\Delta t = 4.67 \ 10^{-3}$. The results in both converged cases are equal.

To study the dynamics of the ALSDA-SIC system in more detail, we examined the development of each time-dependent Kohn-Sham orbital. Figures 9.6 and 9.7 show a projection of the time-dependent Kohn-Sham orbitals $|\Phi_\uparrow(t)\rangle$ and $|\Phi_\downarrow(t)\rangle$ onto the Kohn-Sham triplet ground-state orbitals $|\Phi_\uparrow(0)\rangle \simeq |0s\rangle$ and $|\Phi_\downarrow(0)\rangle \simeq |1p\rangle$. At times $t > 90$ we observe that part of the occupation of $|0s\rangle$ is shoveled from $|\Phi_\downarrow(t)\rangle$ into $|\Phi_\uparrow(t)\rangle$ and vice-versa. At times $t > 130$ the Kohn-Sham orbitals change their role, so that $|\Phi_\downarrow(t)\rangle$ becomes the orbital with dominant $|0s\rangle$ component. This interchange, not observed in the case of the ALDA propagation, causes the break-down of the propagation. The
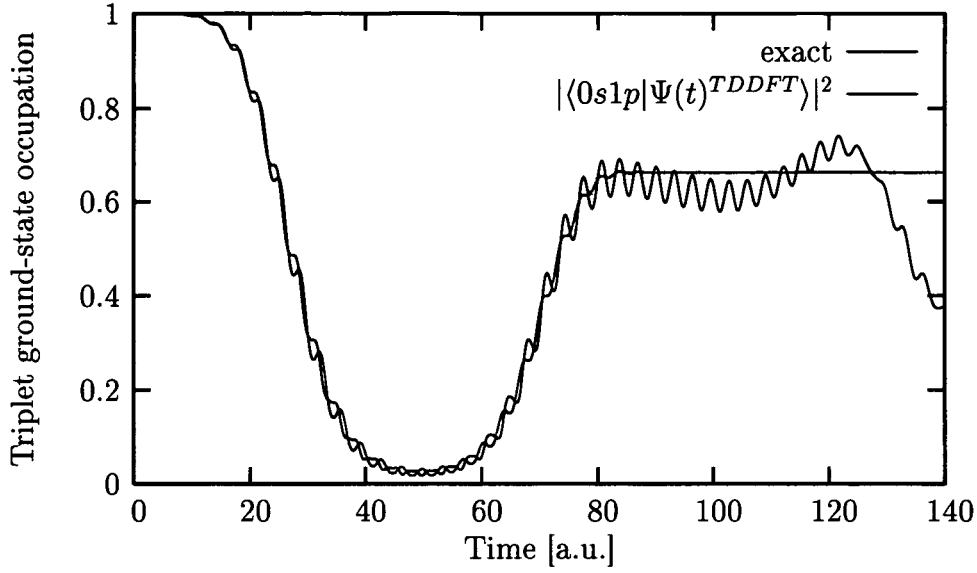
Figure 9.5: Comparison of triplet ground-state occupation probability of the exact (red line) and TDDFT ALSDA-SIC (green line) calculation. The initial state was obtained without spherical averaging of the exchange-correlation potential (see chapter 5).

driving force of this break-down is due to the Coulombic part of the self-interaction correction. The effective Kohn-Sham potentials are dominated by the external potential and the Hartee potential

$$V_{\uparrow}(\vec{r}, t) \simeq V_{ext}(\vec{r}, t) + \int \frac{n_{\downarrow}(\vec{r'}, t)}{|r - r'|} d\vec{r'} \tag{9.3}$$

$$V_{\downarrow}(\vec{r}, t) \simeq V_{ext}(\vec{r}, t) + \int \frac{n_{\uparrow}(\vec{r'}, t)}{|r - r'|} d\vec{r'} . \tag{9.4}$$

Initially when the external laser field is small the densities $n_\sigma(t)$ are only slightly shifted from the ground-state densities, the propagation is stable. As the amplitude of the laser pulse increases $V_{ext}(t)$ is the dominant part of the effective potential and the Hartree potential can be neglected. After switch-off of the laser pulse the spin-densities $n_\sigma(t)$ are far from equilibrium, as can be seen from the expectation of the dipole moment. The dynamics of the system is dominated by the Hartree potentials. Small numerical errors in the propagated densities $n_\sigma(t)$ are reflected asymmetrically in the effective Kohn-Sham potentials V_σ of eq. (9.3). This asymmetry results in an amplification of the error like in a positive feedback loop and the propagation of the Kohn-Sham orbitals breaks down.
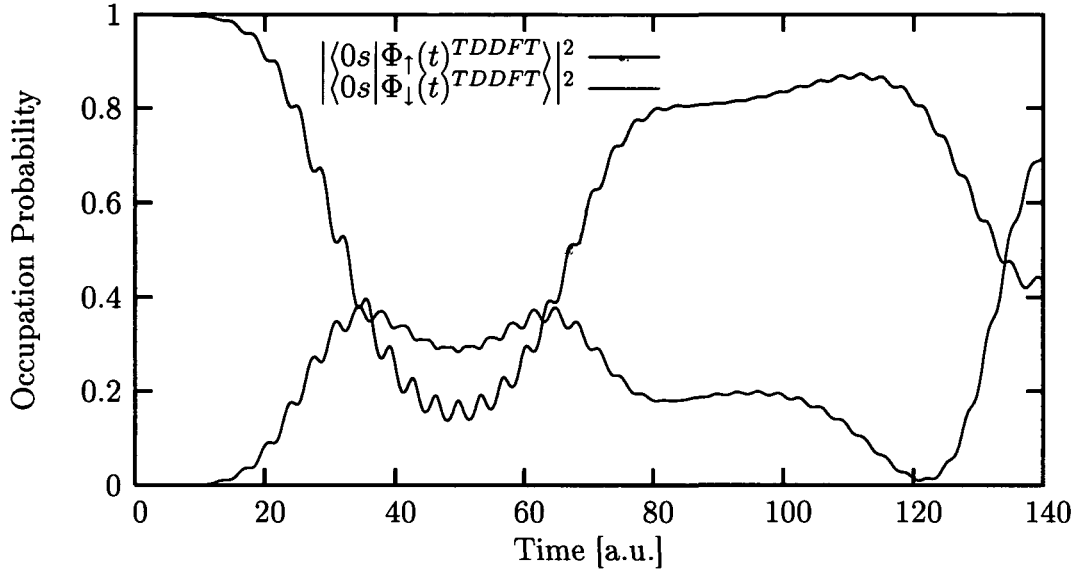
Figure 9.6: Time-dependent occupation of the $|\Phi_\uparrow(0)\rangle \simeq |0s\rangle$ Kohn-Sham orbital of the time-dependent Kohn-Sham orbitals $|\Phi_\uparrow(t)\rangle$ (red line) and $|\Phi_\uparrow(t)\rangle$ (green line) of the ALSDA-SIC calculation

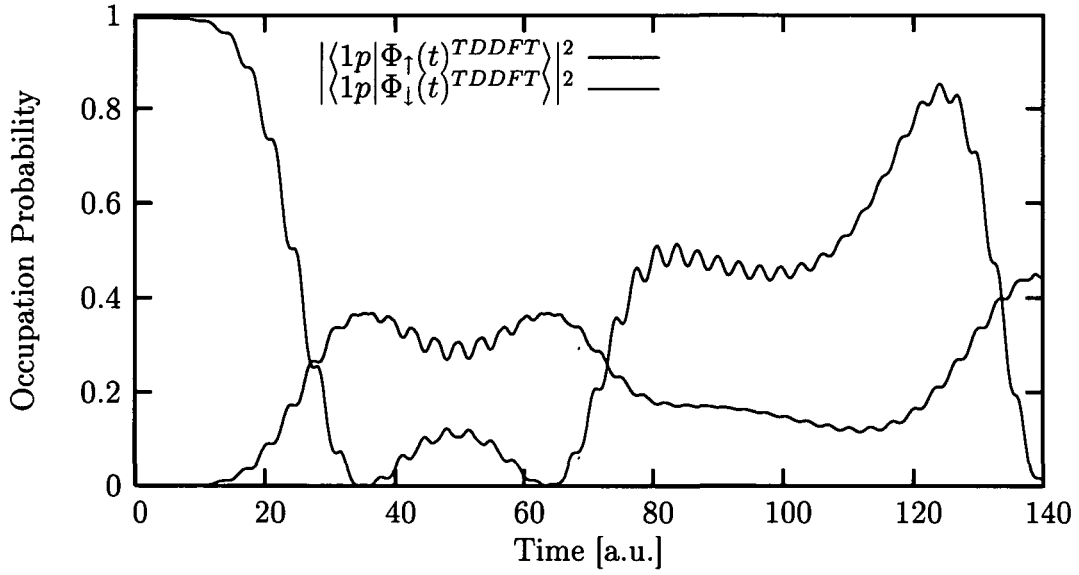

Figure 9.7: Time-dependent occupation of the $|\Phi_\downarrow(0)\rangle \simeq |1p\rangle$ Kohn-Sham orbital of the time-dependent Kohn-Sham orbitals $|\Phi_\uparrow(t)\rangle$ (red line) and $|\Phi_\uparrow(t)\rangle$ (green line) of the ALSDA-SIC calculation

Chapter 10

Time-dependent configuration interaction

In this chapter we introduce the method of time-dependent configuration interaction (CI) based on Kohn-Sham orbitals. This method is introduced with the goal to compare TDDFT calculations to 'exact' solutions of the many-particle Schrödinger equation in the case that the Hamiltonian is no longer separable (for example helium in an external laser field). For those systems the CI calculation provides a reference calculation to be compared, for example, with TDDFT calculations.The method will also prove useful for the harmonic two-electron quantum dot. Choosing an initial state which is not an eigenstate of the harmonic oscillator but a coherent superposition of eigenstates, the Hamiltonian stays separable and the problem can in principle be solved in just taking care of the center of mass motion. In the following chapter we will study occupation probabilities of arbitrary initial states and want to compare them to occupation numbers from TDDFT calculations. For this purpose it is necessary to expand the exact eigenstates in product-functions of Kohn-Sham orbitals. For strongly correlated states (small ω) it is, however, computationally demanding, since one has to calculate several overlap integrals (6-dimensional integrals). It will therefore be useful to use a configuration approach. Once the basis expansion has converged, it can be directly compared to the TDDFT calculations.

The CI method is a basis-expansion method, where the correlated many-body wavefunctions are expanded in a product basis of one-particle orbitals. In view of the application we will construct our product-basis from Kohn-Sham one-particle orbitals $|n_i l_i m_i\rangle$ provided by solution of the time-independent Kohn-Sham equation with ground state occupation eq. (3.10). Concentrating the analysis only on singlet states with anti-symmetric spin part of the wavefunction the coordinate-space part of the product functions of Kohn-Sham

71

orbitals has to be symmetrized. In addition we construct basis-functions of well defined total angular momentum L (configuration state functions), which is a good quantum number in the system we are going to study. The symmetrized coordinate-space part of the singlet configuration state function is therefore characterized by the pair of one-particle (Kohn-Sham) quantum numbers (n_1, l_1, n_2, l_2) and the total angular momentum and angular momentum projection (L, M) and reads [156]:

$$|n_1 l_1 n_2 l_2, L0\rangle := \begin{cases} \frac{1}{\sqrt{2}} \sum_m [\langle l_1 m \ l_2 -m | L0 \rangle \ |n_1 l_1 m\rangle_1 \otimes |n_2 l_2 -m\rangle_2 & n_1 \neq n_2 \\ \quad + \langle l_2 -m \ l_1 \ m | L0 \rangle \ |n_2 l_2 -m\rangle_1 \otimes |n_1 l_1 m\rangle_2] & \text{or } l_1 \neq l_2 \\ \\ \sum_m \langle l_1 l_1 m \ -m | L0 \rangle \ |n_1 l_1 m\rangle_1 \otimes |n_1 l_2 -m\rangle_2 & n_1 = n_2 \\ & \text{and } l_1 = l_2 \end{cases} \quad (10.1)$$

$\langle l_1 m \ l_2 -m | L0 \rangle$ denotes the Clebsch-Gordon coefficient. We restrict our considerations to total angular momentum projection $M = 0$, since our initial states and time-dependent perturbation are chosen such way that no higher components of M come into play. In taking all possible combinations of configurations and angular momentum quantum numbers the basis $\{|n_1 l_1 n_2 l_2, L0\rangle\}$ becomes complete. In practice the basis will be truncated. The total two-electron wavefunction $\Psi(t)$ is expanded into the basis of configuration state functions

$$|\Psi(t)\rangle = \sum_{n_1, l_1, n_2, l_2, L} a(n_1, l_1, n_2, l_2, L; t)|n_1 l_1 n_2 l_2, L0\rangle , \quad (10.2)$$

where the sum extends over all possible two-particle configurations and angular momenta of the truncated basis. In our calculations we implemented different truncated basis sets which can be systematically enlarged. One can, for example, restrict each single-particle momentum quantum number l_i and main quantum number n_i to be smaller than a defined values l_{max} and n_{max}. Also the total angular momenta involved can be restricted to L_{max}.

To simplify the notation we introduce the symbol $I := (n_1, l_1, n_2, l_2, L)$ denoting the set of quantum numbers of a configuration-state function. The short notation for eq. (10.2) then simply reads $|\Psi(t)\rangle = \sum_I a_I(t)|I\rangle$. The time-dependent two-electron Schrödinger equation in an external one-particle potential $V(\vec{r}, t)$ is then transformed into a system of coupled equations which reads

$$i\frac{d}{dt}a_I(t) = \epsilon_I a_I(t) + \sum_{I'} a_{I'}(t) \left(\langle I'|V^{ext}(t)|I\rangle + \langle I'|V_{ee}|I\rangle - \langle I'|V_{xc}|I\rangle \right) \quad (10.3)$$

where $\epsilon_I = \epsilon_{n_1,l_1} + \epsilon_{n_2,l_2}$ is just the sum of the Kohn-Sham energies of the configurations entering in configuration state I. The matrix elements involved in eq. (10.3) are matrix elements with respect to the configuration state functions of eq. (10.1) (denoted with $\Phi_I(\vec{r}_1, \vec{r}_2)$ in coordinate space) of the external time dependent perturbation (time-dependent laser-field in dipole approximation)

$$\langle I'|V^{ext}(t)|I\rangle = \int\int d\vec{r}_1 d\vec{r}_2 \Phi_{I'}^*(\vec{r}_1, \vec{r}_2)(V^{ext}(\vec{r}_1)+V^{ext}(\vec{r}_2))\Phi_I(\vec{r}_1, \vec{r}_2) , \quad (10.4)$$

the matrix element of the exchange-correlation potential

$$\langle I'|V_{KS}(t)|I\rangle = \int\int d\vec{r}_1 d\vec{r}_2 \Phi_{I'}^*(\vec{r}_1, \vec{r}_2)(V^{KS}(\vec{r}_1) + V^{KS}(\vec{r}_2))\Phi_I(\vec{r}_1, \vec{r}_2) ,$$
$$(10.5)$$

where $V^{KS}(\vec{r}) = V_H(\vec{r}) + V_{xc}^{SIC}(\vec{r})$ is the sum of Hartree potential and exchange correlation potential (including self-interaction correction terms to the Hartree potential) of the ground state occupation, and the Coulomb-matrix element

$$\langle I'|V_{ee}(t)|I\rangle = \int\int d\vec{r}_1 d\vec{r}_2 \Phi_{I'}^*(\vec{r}_1, \vec{r}_2)\frac{1}{|\vec{r}_1 - \vec{r}_2|}\Phi_I(\vec{r}_1, \vec{r}_2) . \quad (10.6)$$

Whereas the matrix elements eqs. (10.4) and (10.5) are one-particle matrix elements (see appendix C.2), the Coulomb matrix element of eq. (10.6) is a two-particle matrix element, involving a 6-dimensional integral. In the appendix C.1 we will introduce a numerically efficient way to calculate the Coulomb-matrix elements.

The set of coupled differential equations eq. (10.3) is solved by means of a Runge-Kutta method. The initial conditions of eq. (10.3) may be either chosen as a configuration-state function, setting one specific $a_I(t = 0) = 1$, to a superposition of Kohn-Sham configuration state functions (as we will study in the free propagation starting from a coherent superposition of eigenstates) or to the "exact" eigenstate of the system. For the latter we have to solve the time-independent Schrödinger equation

$$\epsilon_I a_I(0) + \sum_J a_J(0) \left(\langle J|V^{ext}(t)|I\rangle + \langle J|V_{ee}|I\rangle - \langle J|V_{xc}|I\rangle\right) = E a_I(0) \quad (10.7)$$

by solving the eigenvalue equation of the matrix $\langle J|V^{ext}(t) + V_{ee} - V_{xc}|I\rangle + \epsilon_I \delta_{I,J}$. This provides the 'exact' total energy eigenvalues E and the corresponding expansion of the exact eigenfunctions in terms of the configuration-state functions (and hence in Kohn-Sham orbitals). The exact ground state
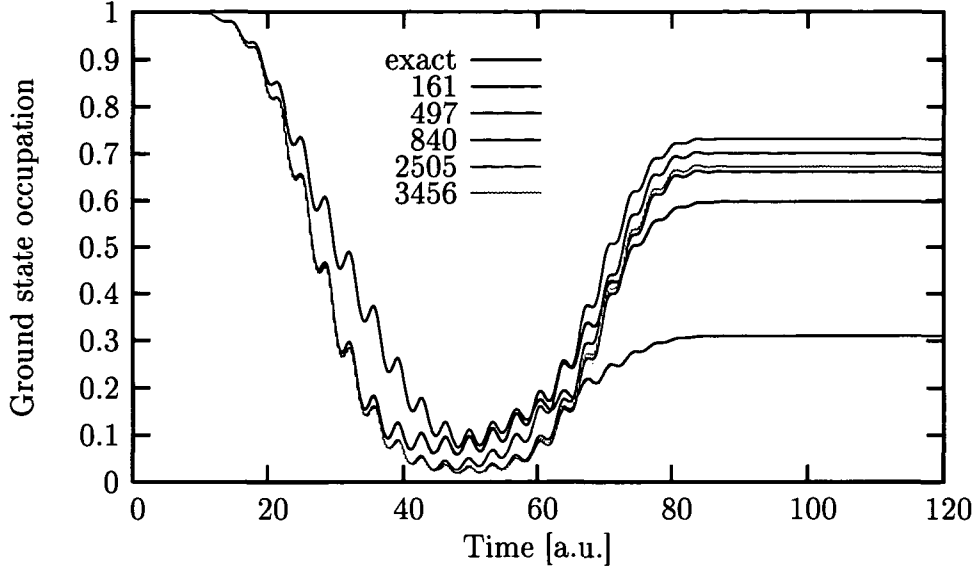
Figure 10.1: Comparison of ground state occupation of exact (red line) and CI calculation of different numbers of configuration states. Parameters of the laser pulse: maximal field amplitude $A_0 = 0.3$, driving frequency $\omega_p = 0.884$, pulse duration $\tau = 90$
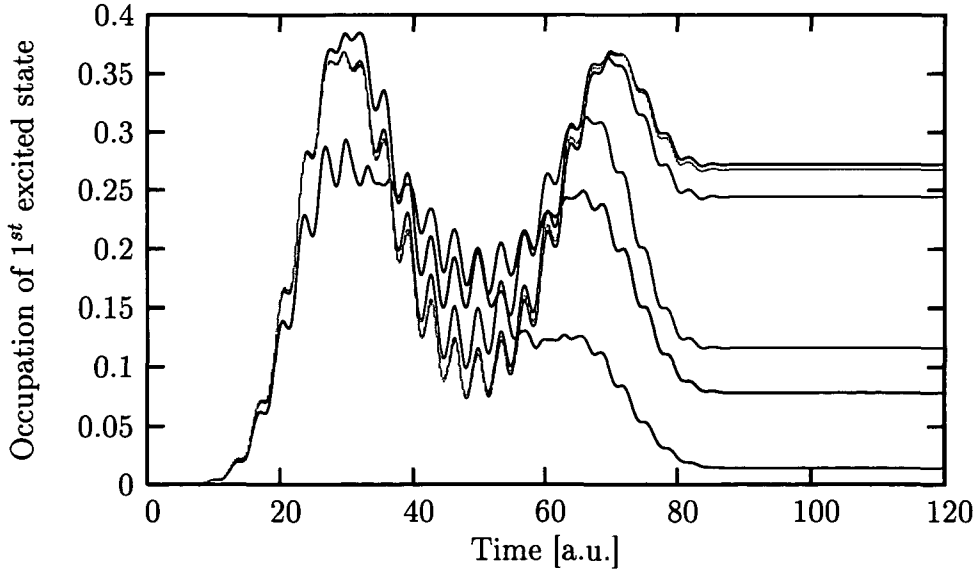

Figure 10.2: Comparisons of occupation of the first excited state of angular momentum $L = 1$ of exact and CI calculations. The color code is chosen as in the upper figure.

energy is approached monotonically from above when increasingly more configurations are added. The ground state energy of 161 configurations is $E_0 = 3.7339$, with 5053 configurations we obtain $E_0 = 3.7308$ as compared to the exact value of $E_0 = 3.7301$. Also the wavefunction itself converges monotonically. As a measure for convergence we have studied the overlap of the CI wavefunction with the DFT ground state compared to the overlap of the exact wavefunction with the DFT ground state. Starting with 116 configurations the overlap is 0.99258, with 5053 configurations we find an overlap of 0.99290 in comparison to the exact overlap of 0.99295.

Figures 10.1 and 10.2 demonstrate the convergence properties of the CI expansion in the case of the laser driven two-electron quantum dot. Plotted is a comparison of ground state occupation probabilities of the exact calculation and CI calculations of different numbers of basis-states included. Convergence was reached for approximatively 6000 two-particle basis functions with maximal total and one-particle angular momentum quantum number of $L = 10$. The maximal one-particle principal quantum number involved is $n = 8$. It is observed that the convergence of the ground state occupation is not monotonic in that the final value of the occupation is first underestimated, increasing the number of configuration it is overestimated to finally converge to the exact result (see figure 10.1). The occupation of the first excited state approaches the correct result in a monotonic way.

Chapter 11

Free propagation of coherent superposition of DFT orbitals

The Kohn-Sham equations (eq. (3.10)) are highly non-linear and therefore violate the superposition principle. In this chapter we are studying the performance of TDDFT in propagating a coherent superposition of eigenstates in the absence of an external perturbation. We start out with a coherent superposition of Kohn-Sham orbitals as initial state and propagate this state within TDDFT. On the other hand we propagate the initial state exactly. This can be done by expanding Kohn-Sham configuration state functions in the exact eigenbasis of the system. The overlap integrals of DFT configuration state functions with exact eigenfunctions are lengthy to calculate with increasing angular momentum quantum numbers involved. In appendix D we give some numerical values of overlap integrals of the weakly and highly correlated quantum dot, for $\omega = 1$ and $\omega = 0.01$ respectively. In order to have a benchmark to test TDDFT calculations for Helium we developed a time-dependent configuration interaction (CI) method (see chapter 10). The exact propagation of a coherent superposition can be easily handled with our CI code.

The initial condition of the time-dependent Kohn-Sham orbitals are chosen as coherent superposition of 2 different stationary Kohn-Sham orbitals $|n_1, l_1, 0\rangle$, $|n_2, l_2, 0\rangle$, $(n_1 \neq n_2 \vee l_1 \neq l_2)$

$$|\Phi_\uparrow(0)\rangle = \alpha|n_1, l_1, 0\rangle + \sqrt{1 - \alpha^2}e^{i\beta}|n_2, l_2, 0\rangle$$
$$|\Phi_\downarrow(0)\rangle = |\Phi_\uparrow(0)\rangle \tag{11.1}$$

where $\alpha, \beta \in \mathbb{R}$, $\alpha^2 \leq 1$. Solving the time-dependent Kohn-Sham equations within the basis of static DFT orbitals (see chapter 3) we therefore are able to calculate straightforwardly occupation probabilities of 2-particle DFT configuration states (see eq. (8.8)) according to eq. (8.9) . Initially only the
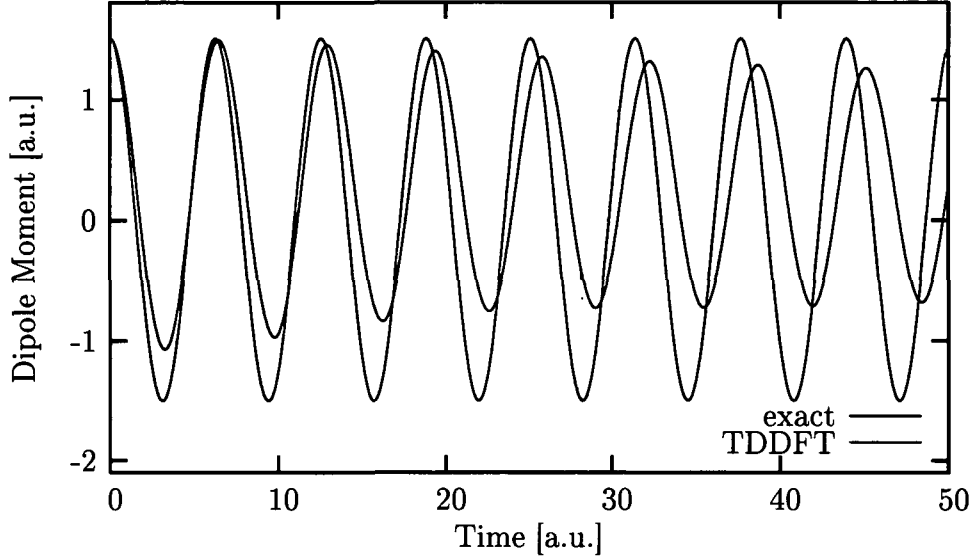
Figure 11.1: Comparison of time-dependent dipole moment of exact and TDDFT calculation for a coherent superposition. The initial state is for both TDDFT and exact calculation the product-function of the single-particle Kohn-Sham orbital $|\Phi(0)\rangle = \frac{1}{\sqrt{2}}|1s0\rangle + \frac{1}{\sqrt{2}}|1p0\rangle$. Confining strength $\omega = 1$.

occupation probabilities

$$P(n_1, l_1, 0, n_2, l_2, 0, t = 0) = 2\alpha^2(1 - \alpha^2) \qquad (11.2)$$

$$P(n_1, l_1, 0, n_1, l_1, 0, t = 0) = \alpha^4 \quad \text{and} \qquad (11.3)$$

$$\sum_L P(n_2, l_2, n_2, l_2, L, 0, t = 0) = (1 - \alpha^2)^2 \qquad (11.4)$$

are different from zero. It can not be expected that the system evolves within the subspace of the initially occupied configuration states.

In the following analysis we restrict ourselves to the weakly correlated system of confining strength $\omega = 1$. TDDFT calculations for initial states to which HPT applies were very promising in this correlation regime. The initial state under consideration is the singlet state constructed from a superposition of the ground state and first excited Kohn-Sham orbital

$$|\Phi_\uparrow(0)\rangle = |\Phi_\downarrow(0)\rangle = \frac{1}{\sqrt{2}}|1s0\rangle + \frac{1}{\sqrt{2}}|1p0\rangle . \qquad (11.5)$$

Figure 11.1 shows a comparison of the time-dependent dipole moment of TDDFT and exact (converged CI) calculation of the initial state of eq. (11.5).

Initially the dipole moment of both calculations are in accordance. After the first half cycle, however, the two calculations show considerable discrepancies. Initially the frequency of the oscillations in the dipole moment is well described by TDDFT, after the first cycle, one observes a shift to a lower frequency in the TDDFT dipole moment. The performance of TDDFT is therefore considerably degraded if one chooses an initial condition which is not subject to the HPT.

The situation becomes even worse when comparing the occupation numbers of TDDFT and exact calculation. Figure 11.2 shows a comparison of occupation numbers of DFT configuration state functions for the exact (CI) and the TDDFT calculation for the initial condition of eq. (11.5). Since TDDFT and exact calculation start out from the same initial state, the projection of the TDDFT and of the exact wavefunction onto the DFT configuration states $|0s0s\rangle$ and $|0s1p\rangle$ are equal at time $t = 0$ but diverge thereafter. Since the coherent superposition is a pure superposition of the center of mass mode ($0S,1P,2D$ and $2S$), the difference of the energies involved correspond to the frequencies of 2ω and ω. Those frequencies are reflected in the occupation probabilities of the DFT configuration states of the exact wavefunction (red and blue line), the dominant frequency is 2ω. The occupation probability of the DFT configuration states of the TDDFT wave-function, however, shows a major frequency component of ω, which is the oscillation frequency of the dipole moment (see figure 11.1).

The comparison of the dipole moment of exact and TDDFT propagation shows that the density is not correctly propagated in the present TDDFT approach. The shape of the time-dependent densities of exact and TDDFT calculation are different (not shown here). One could therefore argue that the failure of calculating occupation probabilities for states which are not subject to the HPT is due to the wrong exchange correlation potential used, which is not able to reproduce the right density. In the following chapter we will, however, demonstrate that even if the exact exchange correlation potential was known, it would not be possible by our simple projection method to construct reliable occupation probabilities.
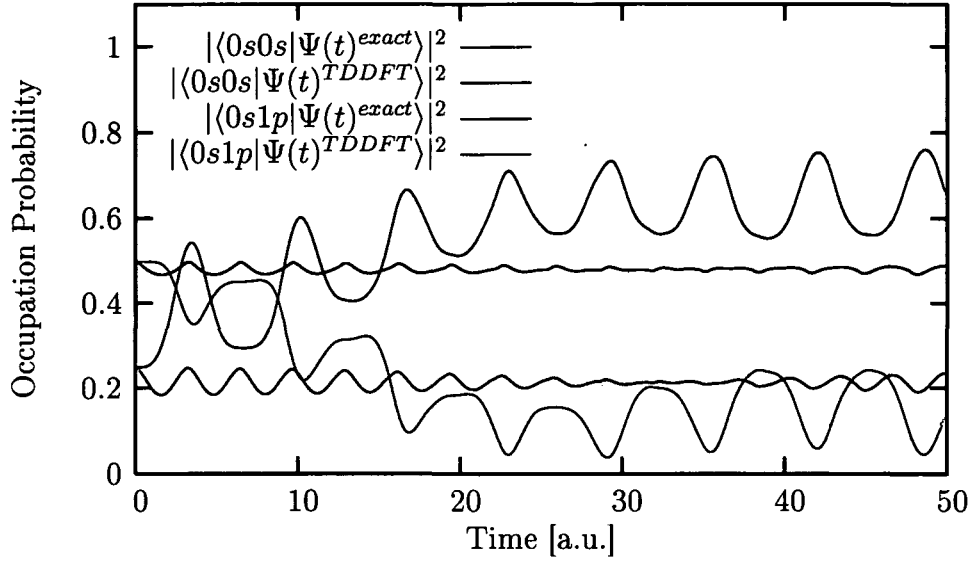
Figure 11.2: Shown is a comparison of occupation probabilities of Kohn-Sham configuration-state functions ($|0s0s\rangle$ and $|0s1p\rangle$) of a propagated coherent superposition of states of exact (red and blue line) and TDDFT (green and magenta) system. The initial state is for both TDDFT and exact calculation the product-function of the single-particle Kohn-Sham orbital $|\Phi(0)\rangle = \frac{1}{\sqrt{2}}|1s0\rangle + \frac{1}{\sqrt{2}}|1p0\rangle$. The confining strength of the parabolic well is $\omega = 1$.
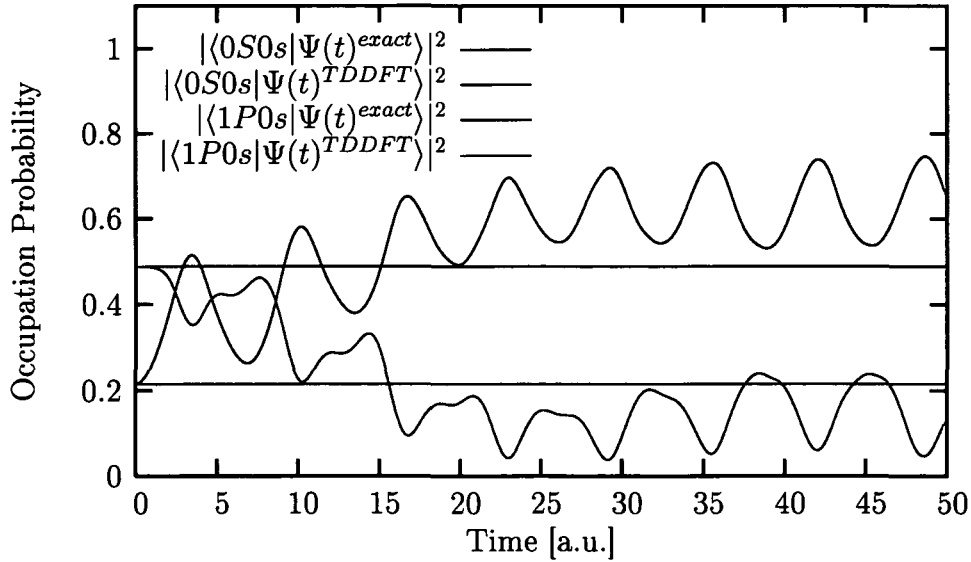

Figure 11.3: Shown is a comparison of occupation probabilities of exact eigenstates ($|0S0s\rangle$ and $|1P0s\rangle$) of a propagated coherent superposition of states of exact (red and blue line) and TDDFT (green and magenta).

Chapter 12

Exact Kohn-Sham scheme

In this chapter we will show the results of a realization of an 'exact' time-dependent Kohn-Sham scheme. For the special case of a singlet two-electron system the exact exchange correlation potential can be determined, therefore providing all the prerequisites needed to calculate the exact Kohn-Sham orbitals. In the last chapter we observed that in the case of starting from a coherent superposition as initial state ALSDA-SIC fails to reproduce the density. Also the projection mechanism to calculate state-to-state transition amplitudes failed. The reason of failure can lie in the wrong exchange-correlation potential, or may indicate a more fundamental difficulty. To answer this principal question we performed propagations of coherent superpositions of states in the exact time-dependent exchange correlation potential [158].

12.1 Construction of the exact exchange-correlation potential

In the case of a two-electron singlet system it is possible to construct the exact time-dependent exchange correlation potential [48]. For simplicity of notation it is derived for the one-dimensional problem, generalization to 3 dimension is straight forward. The two electrons are considered to occupy both the same orbital. The Kohn-Sham equations reduce to a single one-particle equation for the doubly occupied orbital $\phi_0(x, t)$

$$\left(-\frac{1}{2}\frac{d^2}{dx^2} + V_{ext}(x, t) + V_H(x, t) + V_{xc}(x, t) \right) \phi_0(x, t) = i\frac{\partial}{\partial t}\phi_0(x, t) . \quad (12.1)$$

The density of the system is just given by $n(x, t) = 2|\phi_0(x, t)|^2$. The Kohn-Sham orbital can be decomposed into a unitary complex function $e^{if(x,t)}$ and

a real function $|\phi_0(x,t)|$ and thus rewritten in terms of the density.

$$\phi_0(x,t) = \sqrt{\frac{n(x,t)}{2}}e^{if(x,t)} .$$ (12.2)

The constraint that $V_{xc}(x,t)$ should be a real function results in an ordinary differential equation in x which determines the phase $f(x,t)$ of the orbital in terms of the exact density up to the initial conditions for $f(x,t=0)$ and its derivative

$$\frac{\partial}{\partial x}\left(\frac{\partial f(x,t)}{\partial x}n(x,t)\right) = -\frac{\partial n(x,t)}{\partial t}$$ (12.3)

and an explicit equation for the exchange correlation potential in terms of the exact density and the phase

$$V_{xc}(x,t) = \frac{1}{4}\frac{\partial^2 ln\,[n(x,t)]}{\partial r^2} + \frac{1}{8}\left|\frac{\partial ln\,[n(x,t)]}{\partial x}\right|^2 - V_{ext}(x,t)$$

$$-V_H(x,t) - \frac{1}{2}\left|\frac{\partial f(x,t)}{\partial x}\right|^2 - \frac{\partial f(x,t)}{\partial t} .$$ (12.4)

In the static limit equation (12.4) reduces to

$$V_{xc}^{static}(x) = \frac{1}{4}\frac{\partial^2 ln\,[n(x)]}{\partial x^2} + \frac{1}{8}\left|\frac{\partial ln\,[n(x)]}{\partial x}\right|^2 - V_{ext}(x) - V_H(x)$$ (12.5)

which corresponds to the exchange correlation potential that recovers any density $n(x)$ of a static problem as its ground-state density. As a consequence the first four terms in equation (12.4) correspond to the exchange correlation potential of a system which has the density at time t as a ground-state density and the last two terms are the corrections due to the time-dependence of the phase. This causes computational problems. If the density has a node at a finite point x, it usually means that the static potential is diverging at that point x. For the exchange correlation potential to be finite the phase $f(x,t)$ has to cancel this infinity which numerically is not feasible. Also an initial state whose density has a node would account for a divergent exchange correlation potential. Hence we are forced to restrict our studies to cases where no nodes arise in the density over time.

12.2 One-dimensional model system

We study two different one-dimensional model two-electron systems [152, 153]. The first system is characterized by the one-dimensional harmonic

oscillator potential $V_{ext}(x) = \frac{1}{2}\omega^2 x^2$ ($\omega = 0.25$), the second system under consideration is a 1-dimensional helium atom with the model potential $V_{ext}(x) = -\frac{2}{\sqrt{x^2+b^2}}$. The time-dependent Schrödinger equation of these systems is given by

$$i\frac{\partial}{\partial t}\Psi(x_1,x_2,t) = \left[\sum_{i=1,2}\left(-\frac{1}{2}\frac{\partial^2}{\partial x_i^2} + V_{ext}(x_i)\right) + \frac{1}{\sqrt{(x_1-x_2)^2+b^2}}\right]\Psi(x_1,x_2,t)\,,$$

(12.6)

where b is a parameter commonly introduced to allow the electrons to bypass each other without passing through a singularity. We set the parameter $b = 0.7408$ in order to get a ground-state energy for the model helium atom that is close to the ground-state energy of the three-dimensional helium atom. The partial differential equation 12.6 is discretized on a two-dimensional equidistant spatial grid and solved by means of a Runge-Kutta algorithm. For details see reference [158]. The exact solution provides us the exact density $n(x,t)$, from which we are able to construct the exact exchange correlation potential.

12.3 Propagation of a coherent superposition

First we consider the propagation from a coherent superposition of exact eigenstates of the one-dimensional harmonic quantum dot. The exact system starts from a superposition from the exact ground-state $|0\rangle$ and exact first-excited state $|1\rangle$

$$|\Psi(t=0)\rangle = \frac{1}{\sqrt{2}}\left(|0\rangle + |1\rangle\right)\,.$$

(12.7)

The time-propagation of the exact state $|\Psi(t)\rangle$ is therefore given by

$$|\Psi(t)\rangle = \frac{1}{\sqrt{2}}\left(e^{-iE_0 t}|0\rangle + e^{-iE_1 t}|1\rangle\right)\,,$$

(12.8)

where E_0 and E_1 denotes the exact energy eigenvalue of the ground and first excited state. The exact initial $|\Psi(0)\rangle$ state gives rise to a initial density $n(0)$ and hence an exact exchange-correlation potential $V_{xc}(0)$ according to eq. (12.5). The initial Kohn-Sham orbital $|\phi_0\rangle$ is then given by the ground state of the Kohn-Sham equation with $V_{xc}(0)$. Exact and Kohn-Sham system therefore start from different states $|\Psi(t=0)\rangle$ and $|\Phi(t=0)\rangle = |\phi_0\phi_0\rangle$ respectively, which have, however, the same density $n(0)$. The overlap of the different initial states is $\langle\Phi(t=0)|\Psi(0)\rangle = 0.736$. The Kohn-Sham orbitals $|\phi_0\rangle$ are propagated with the exact exchange correlation potential resulting
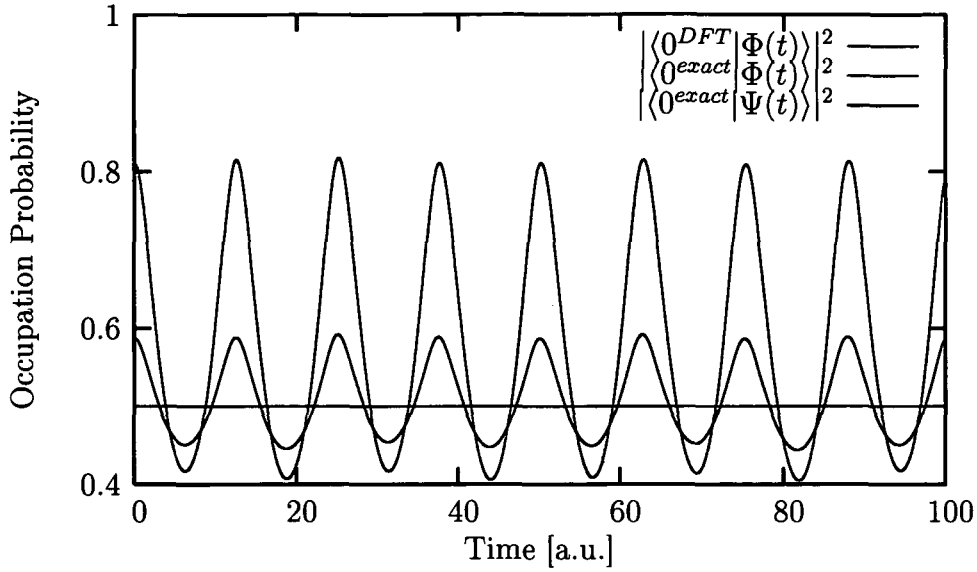
Figure 12.1: One-dimensional quantum dot with $\omega = 0.25$. Shown is a comparison of the exact ground-state occupation probability (blue) and occupation probabilities for TDDFT via projection of the Kohn-Sham Slater-determinant onto the ground state Kohn-Sham configuration (red) and onto the exact ground state (green). The exact exchange correlation potential was used. Initial state is a coherent superposition of exact states: $|\Psi(t = 0)\rangle = \frac{1}{\sqrt{2}}(|0\rangle + |1\rangle)$.

Figure 12.2: Same as in figure 12.1 but for the first excited state.

Figure 12.3: One-dimensional Helium model. Shown is a comparison of the exact ground-state occupation probability (blue) and occupation probabilities for TDDFT via projection of the Kohn-Sham Slater-determinant onto the ground-state Kohn-Sham configuration (red) and onto the exact ground state (green). The exact exchange correlation potential was used. Initial state is a coherent superposition of exact states: $|\Psi(t=0)\rangle = \frac{1}{\sqrt{2}}(|0\rangle + |1\rangle)$.
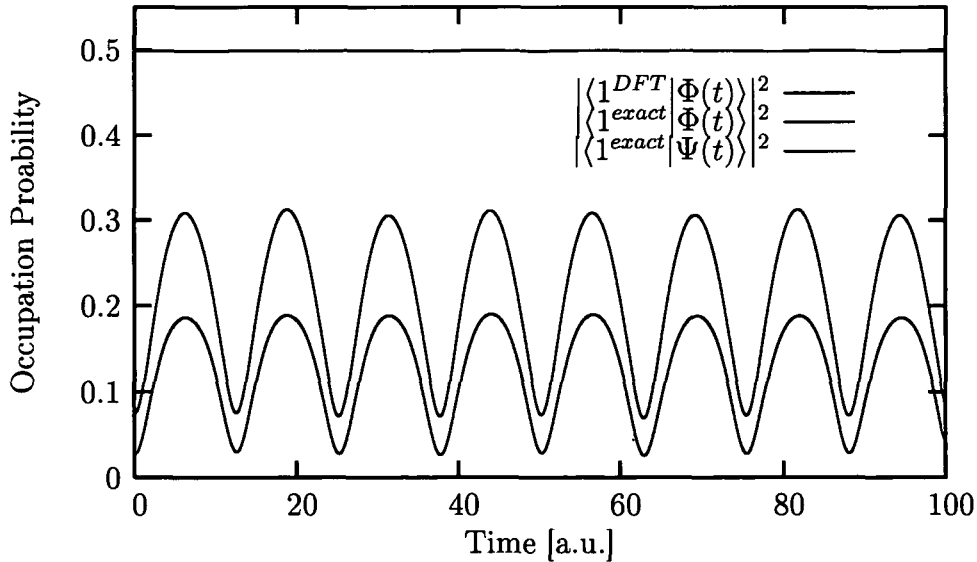

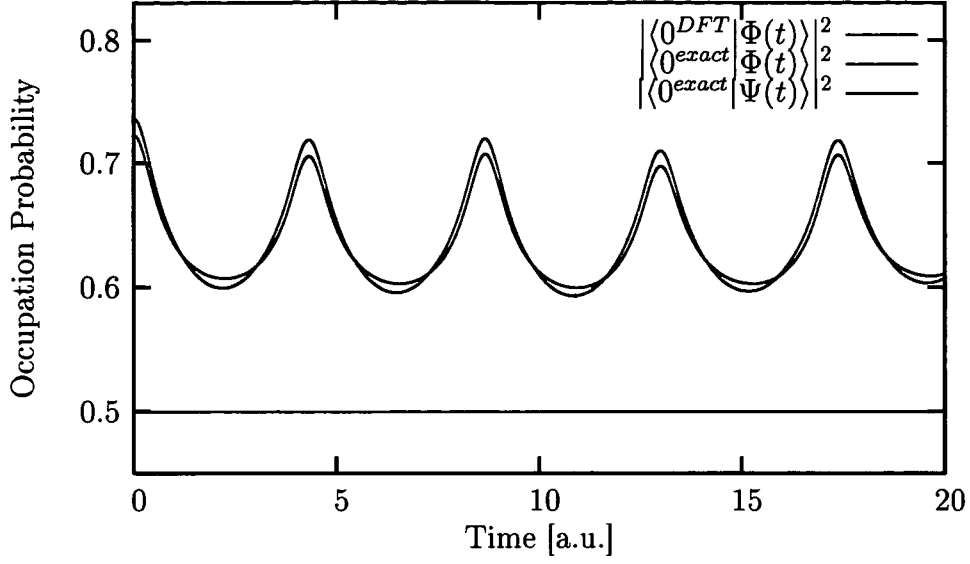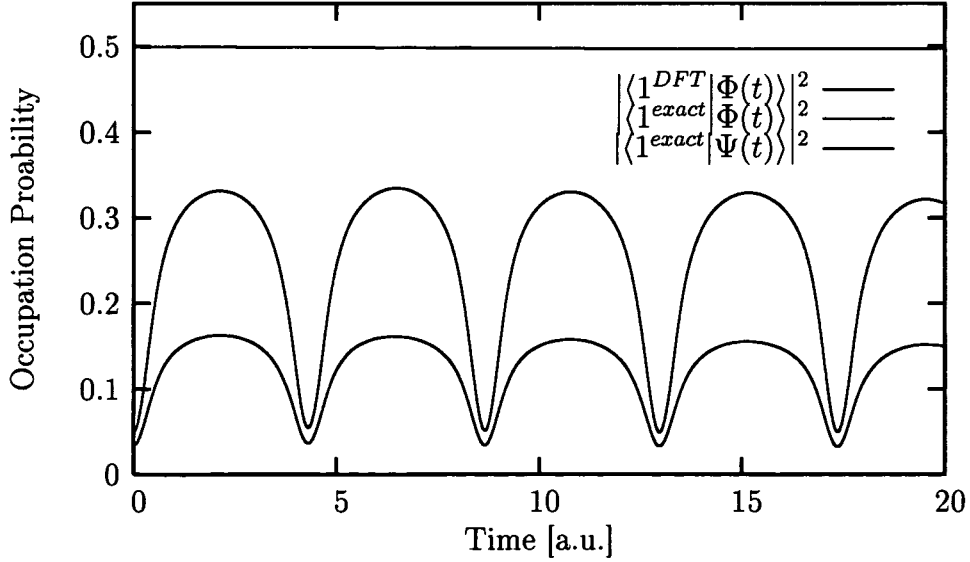Figure 12.4: Same as in figure 12.3 but for the first excited state.

from the exact density $n(t)$ (see eq. (12.4)), therefore the densities $n(t)$ of exact and Kohn-Sham scheme are identical. We then tried to calculate occupation probabilities within TDDFT by the projection method we introduced in chapter 8. Figures 12.1 and 12.2 show a comparison of exact and TDDFT occupation probabilities for the quantum dot of the ground state and first excited state respectively. The projection of the TDDFT wave-function (Slater-determinant of Kohn-Sham orbitals) onto the exact ground state (denoted with $\langle 0^{exact}|\Phi(t)\rangle$, green line) of the system oscillates around the exact ground-state occupation value of 0.5. Projection onto the product function of Kohn-Sham ground-state orbitals (denoted with $\langle 0^{DFT}|\Phi(t)\rangle$) does not give a reliable occupation probability. In the case of occupation of the first excited state both TDDFT occupation probabilities fail (see figure12.2). Figures 12.3 and 12.4 show the results for the one-dimensional Helium model. In this case, not even the ground-state occupation oscillates around the exact result.

Even with the knowledge of the exact exchange-correlation potential the projection mechanism of time-dependent Kohn-Sham Slater-determinants onto either exact or Kohn-Sham configuration states does not provide reliable occupation probabilities. The problems in determining occupation probabilities for a propagation of a coherent superposition in the three-dimensional case of the harmonic oscillator therefore is not only due to the incorrect exchange-correlation potential.

As already mentioned in the general overview of TDDFT in chapter 3 there exist different time-dependent Kohn-Sham schemes starting from different initial states (with the same density as the exact system), all in principle reproducing the exact time-dependent density of the system [10]. The time-dependent Kohn-Sham orbitals and hence approximate many-body wave-functions are different for different fixed Kohn-Sham initial-states. The quality of our projection mechanism therefore would rely on the choice of the initial state.

In the following we are considering therefore exact and Kohn-Sham system propagating from the same initial state. The initial state is chosen as the exact Kohn-Sham ground state. $|\Psi(t=0)\rangle = |0^{DFT}\rangle$ of the one-dimensional quantum dot. The Kohn-Sham system is propagated with the exact time-dependent exchange-correlation potential. Figure 12.5 shows a comparison of ground-state occupation probabilities of the exact wave-function (blue line) and TDDFT occupation probabilities by the projection-method. The Kohn-Sham Slater-determinant was projected onto the exact (green line) as well as the DFT ground state (red line). For comparison the projection of the exact wave-function onto the DFT ground state is plotted (magenta line). It is not possible to deduce any reasonable ground-state occupation probability based

on the projection-method of TDDFT results. As can be seen directly from the figure also time-average over the oscillations of the different occupation probabilities of TDDFT would give wrong results. The discrepancy of the projection of exact and TDDFT wavefunction onto the DFT ground state is not as large as in the case of the quantum dot of chapter 11. In particular both projections have the same frequency components, which was not fulfilled in the case of ALSDA-SIC (see figure 11.2).

Those studies of a simple one-dimensional model systems demonstrated that even with the knowledge of the exact exchange correlation potential it was not possible to reliably construct occupation probabilities based on the projection of Kohn-Sham Slater-determinants onto either exact or DFT channel states. We tested the projection-method onto different Kohn-Sham schemes starting either from the same initial state of exact and Kohn-Sham propagation or from different initial states but the same initial densities. In both cases the results are rather dispiriting.
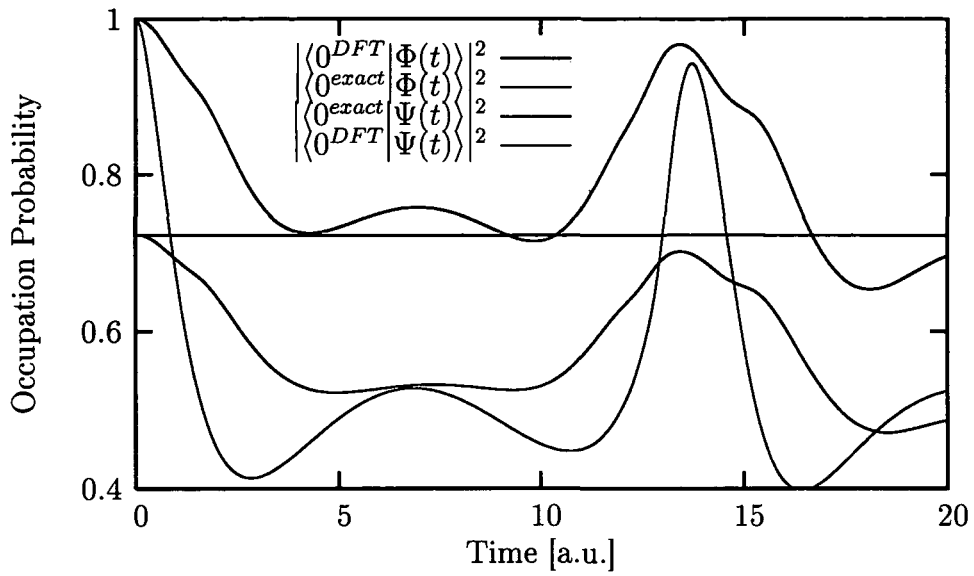
Figure 12.5: One-dimensional quantum dot with $\omega = 0.25$: Shown is a comparison of the exact ground-state occupation probability (blue) and occupation probabilities for TDDFT via projection of the Kohn-Sham Slater-determinant onto the ground-state Kohn-Sham configuration (red) and onto the exact ground state (green). Also the projection of the exact time-dependent wavefunction onto the Kohn-Sham ground state is given (magenta). The exact exchange correlation potential was used. Initial state: Kohn-Sham ground state for both systems

Chapter 13

Functional-integral approach to transition matrix elements

In chapter 8 some progress was made in calculating time-dependent occupation probabilities within TDDFT where a projection method was proposed. The Slater-determinant of the time-dependent Kohn-Sham orbitals was projected either onto Kohn-Sham configuration state functions or exact eigenfunctions of the system under consideration. At asymptotic times after switch-off of a perturbative laser field we observed oscillations of the occupation probabilities obtained by our projection method. We showed that these oscillations persist by projecting onto exact eigenstates of the unperturbed Hamiltonian. It was not possible to find appropriate channel states to project on to obtain a time-independent transition amplitude at asymptotic times. In other words, we failed to define a state-to-state transition matrix element (or S-matrix) within TDDFT by usual means.

The above described problem is well known from nuclear reaction time-dependent Hartree-Fock calculations [58]. Several similar methods based on a functional integral approach were proposed to circumvent the problem of cross-channel correlation [60, 61, 62, 63, 67] Starting point is the S-matrix defined as the matrix elements between initial $|\Phi_i\rangle$ and final $|\Phi_f\rangle$ state of the long-time limit of the interaction-picture evolution operator S:

$$S_{i,f} = \langle\Phi_f|S|\Phi_i\rangle = \lim_{\tau\to\infty}\langle\Phi_f|U_0(0,\tau)U(\tau,-\tau)U_0(-\tau,0)|\Phi_i\rangle , \qquad (13.1)$$

where $U_0(0,\tau)$ denotes the time-evolution operator in the Schrödinger picture corresponding to the field-free many-body Hamiltonian

$$H_0 = \sum_i\left(-\frac{1}{2}\vec{\nabla}_i^{\,2} + V_{ext}(\vec{r}_i)\right) + \frac{1}{2}\sum_{i,j}\frac{1}{|\vec{r}_i - \vec{r}_j|} \qquad (13.2)$$
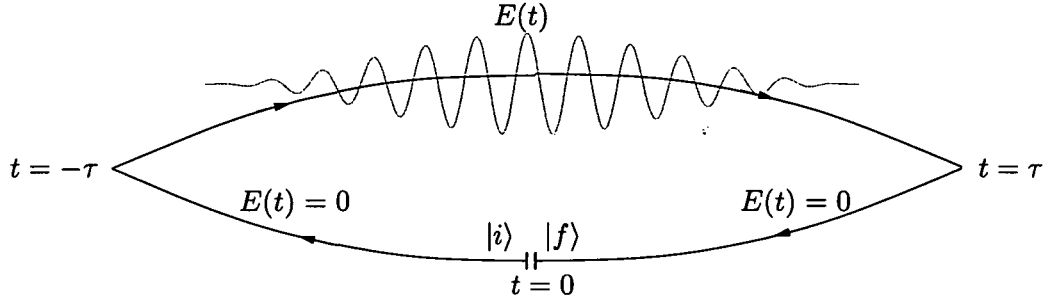
Figure 13.1: Time evolution for the S-matrix in the interaction picture for a perturbation starting at $t = -\tau$ and ending at $t = +\tau$: The system starts out from the initial state $|\Phi_i\rangle$ and is evolved backwards in time to $t = -\tau$ with the perturbation turned off. At time $t = -\tau$ perturbation sets in (in our case a time-dependent electric field $E(t)$), the state is forward propagated according to the Hamiltonian including $V(t)$ to $t = +\tau$. Backward propagation to $t = 0$ in the perturbation-free case $V(t) = 0$ closes the time-loop.

and $U(0, \tau)$ the propagator in the case of a time-dependent perturbation $V(t) = \sum_i v(\vec{r}_i, t)$ corresponding to the Hamiltonian $H = H_0 + V(t)$. The perturbation potential is supposed to be zero at asymptotic times $\lim_{t \to -\infty} V(t) = \lim_{t \to \infty} V(t) = 0$. The channel states $|\Phi_i\rangle$ and $|\Phi_f\rangle$ are eigenstates of H_0.

The mean-field method introduces two independent approximations. The channel functions $|\Phi_i\rangle$ and $|\Phi_f\rangle$, solutions of a stationary many-body problem, have to be approximated in practice by a single Slater-determinant, or a sum of a few determinants. The second major approximation concerns the many-body propagators U and U_0. In this method U is rewritten by Hubbard-Stratonovich representation [59] as a functional integral over an auxiliary mean field $\sigma(\vec{r}, t)$, thereby involving only a one-body Hamiltonian. The many-body evolution operator is decomposed into a superposition of an infinite number of one-body propagators. The functional integral is then approximated by the method of stationary phase. The mean field $\sigma(\vec{r}, t)$ which renders the phase stationary is given by

$$\sigma(\vec{r}, t) = Re \left\{ \frac{\langle \Phi_f(t)|\hat{\rho}|\Phi_i(t)\rangle}{\langle \Phi_f(t)|\Phi_i(t)\rangle} \right\} , \qquad (13.3)$$

where $\hat{\rho}$ denotes the one-particle density operator. Rather than a mean potential, $\sigma(\vec{r}, t)$ is a mean density of the system. $|\Phi_i(t)\rangle$ ($|\Phi_f(t)\rangle$) denotes the initial (final) state propagated forward (backward) in time according to the Hamiltonian $H_\sigma(t) = \sum_i h_\sigma^{(i)}$, where $h^{(i)}_\sigma$ denotes a Hartree-like one-body Hamiltonian. $\sigma(\vec{r}, t)$ is treated as source in the Hartree-like term of

$h_\sigma^{(i)}$, rather than the electron-density $n(\vec{r}, t)$. The one-body Hamiltonians $h_\sigma^{(i)}$ which determine the time-evolution

$$i\frac{\partial}{\partial t}|\Phi_i(t)\rangle = \sum_i h_\sigma^{(i)}|\Phi_i(t)\rangle \qquad (13.4)$$

are given by

$$h_\sigma^{(i)}(t) = -\frac{1}{2}\vec{\nabla}_i^2 + V_{ext}(\vec{r}_i) + v(\vec{r}_i, t) + \int d\vec{r}\,\frac{\sigma(\vec{r}, t)}{|\vec{r} - \vec{r}_i|}. \qquad (13.5)$$

Eqs. (13.3), (13.4) together with (13.5) constitute a self-consistency problem for $\sigma(\vec{r}, t)$, $|\Phi_i(t)\rangle$ and $|\Phi_f(t)\rangle$. Due to the definition of the S-matrix in the interaction picture the time t in eqs. (13.5) and (13.3) has to be varied in a loop from $t = 0$ to $t = -\tau$ ($V(t) = 0$), where the external perturbation $V(t)$ starts, to $t = +\tau$ (end of the perturbation) and back to $t = 0$ ($V(t) = 0$). Figure 13.1 shows a sketch of the time cycle.

Unlike TDDFT, where the exchange-correlation potential possesses an initial state dependence, in the mean-field approach $\sigma(\vec{r}, t)$ also depends on the final state $|\Phi_f\rangle$. $\sigma(\vec{r}, t)$ is deduced self-consistently to 'connect' initial to final state.

So far, in the derivation of eqs. (13.5) and (13.3) neither exchange effects (particle statistics) nor two-body correlations have been taken into account. The inclusion of exchange effects is possible but cumbersome [60], since it incorporates second order corrections to the stationary phase approximation. This could be circumvented by introducing a non-local mean field σ. Exchange effects would already be accounted for in the zero order stationary phase approximation. Choosing single Slater-determinants as channel states the resulting equations are similar to time-dependent Hartree-Fock equations, with a Fock-like contribution, which is non-local in space. In the following we propose a slightly different approach, closely connected to TDDFT where locality in space can be maintained.

Adapted to our original problem, we approximate the channel states $|\Phi_i\rangle$ and $|\Phi_f\rangle$ through single Slater-determinants of stationary Kohn-Sham orbitals. Eqs. (13.3) and (13.4) then reduce to one-particle Hartree-like equations. The similarity to the time-dependent Kohn-Sham equations is tempting to introduce exchange and correlation effects by addition of the Kohn-Sham exchange-correlation potential. The exchange correlation potential is then treated as a functional of the mean field σ rather than the electron density, in analogy to the original mean field approach. In this case the self-consistency problem can be solved in a sequence of time-dependent Kohn-Sham like equations. In addition we introduce in analogy to the spin-densities of TDDFT mean fields for spin up $\sigma_\uparrow(\vec{r}, t) = Re\left\{\frac{\langle\Phi_f(t)|\hat{\rho}_\uparrow|\Phi_i(t)\rangle}{\langle\Phi_f(t)|\Phi_i(t)\rangle}\right\}$
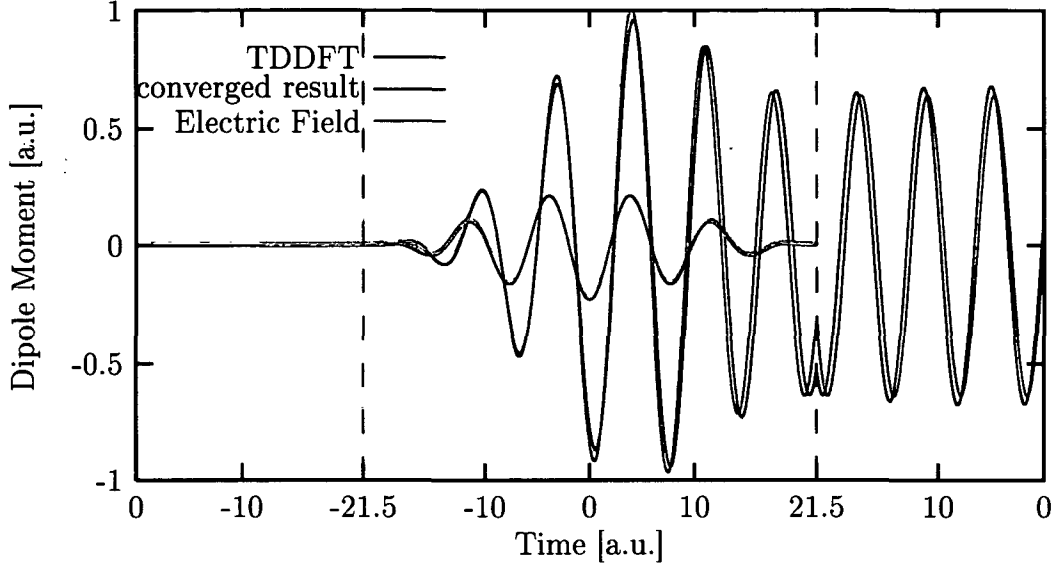
Figure 13.2: Shown is the time-dependent dipole moment of the TDDFT result (red) and the converged mean-field result (blue). Also shown is the electric field (green). Parameters of the laser pulse: maximal field amplitude $A_0 = 0.23$, driving frequency $\omega_p = 0.804$, pulse duration $\tau = 43$. The time axes corresponds to the time loop of figure 13.1. $t = -21.5$ denotes the point where the laser pulse is turned on. At the end of the laser pulse ($t = 21.5$) the time-propagation is reversed, therefore producing the cusp in the dipole moment.

and spin down $\sigma_\downarrow = Re\left\{\frac{\langle\Phi_f(t)|\hat{\rho}_\uparrow|\Phi_i(t)\rangle}{\langle\Phi_f(t)|\Phi_i(t)\rangle}\right\}$ where $\hat{\rho}_\uparrow$ ($\hat{\rho}_\downarrow$) denotes the spin-projection of the density operator. The total mean field then decomposes into $\sigma = \sigma_\uparrow + \sigma_\downarrow$. This allows us to use the spin-density dependent self-interaction corrected ALDA exchange correlation potential. In contrast to the original mean-field approach, the present Kohn-Sham like approach can not be deduced rigorously by means of the Hubbard-Stratonovich representation and contains an heuristic aspect.

We apply the proposed approach to the model system of two electrons in the harmonic oscillator. We denote the final (initial) channel state of the singlet system by $|\Phi_f\rangle = |\phi_f^\uparrow, \phi_f^\downarrow\rangle$ ($|\Phi_i\rangle = |\phi_i^\uparrow, \phi_i^\downarrow\rangle$), where $\phi_f^\uparrow$ denotes a one-particle orbital of configuration (n, l, m) of the final spin-up electron. The mean fields then are given by

$$\sigma(\vec{r}, t) = \sigma_\uparrow + \sigma_\downarrow = Re\left\{\frac{\phi_f^{\uparrow*}(\vec{r}, t)\phi_i^\uparrow(\vec{r}, t)}{\langle\phi_f^\uparrow(t)|\phi_i^\uparrow(t)\rangle} + \frac{\phi_f^{\downarrow*}(\vec{r}, t)\phi_i^\downarrow(\vec{r}, t)}{\langle\phi_f^\downarrow(t)|\phi_i^\downarrow(t)\rangle}\right\} , \quad (13.6)$$

91

and the Hamiltonian of eq. (13.5) is replaced by

$$h_\sigma = \frac{\vec{p}^2}{2m} + \frac{m\omega^2}{2}\vec{r}^2 + \int d\vec{r}' \frac{\sigma(\vec{r}',t)}{|\vec{r}-\vec{r}'|} - E(t)z + V_{xc}[\sigma_\uparrow,\sigma_\downarrow](\vec{r},t) \ . \qquad (13.7)$$

Eq. (13.7) together with eq. (13.6) are solved self-consistently by means of an iterative scheme. As a first guess for $\sigma(\vec{r},t)$ we start out with the density $n(\vec{r},t)$ of the TDDFT problem, the first trial $|\Phi_i(t)\rangle^{(1)}$ is the TDDFT propagated state. The second iteration is a TDDFT backwards propagation of the final state $|\Phi_f(t)\rangle^{(2)}$ with $\sigma(\vec{r},t)$ calculated through eq. (13.6) with the instantaneous $|\Phi_f(t)\rangle^{(2)}$ and $|\Phi_i(t)\rangle^{(1)}$ of the first iteration. The third iteration is a forward propagation of $|\Phi_i\rangle$ with σ calculated from the instantaneous $|\Phi_i(t)\rangle^{(3)}$ and $|\Phi_f(t)\rangle^{(2)}$ and so on. The S-matrix element is then calculated through $S_{i,f} = \langle \Phi_f|\Phi_i(t)\rangle$, where T denotes the time $t = 0$ after going through the whole time-loop of figure 13.1.

Figures 13.2 and 13.3 show results of a converged calculation. The time-dependent laser field is symmetric against time-reversal and of pulse length $\tau = 43$, driving frequency $\omega_p = 0.804$ and peak field amplitude $A_0 = 0.23$. The frequency of the confining parabolic potential was chosen as $\omega = 1$. Figure 13.2 shows the time-dependent dipole moment of the TDDFT calculation (red line), which serves as initial guess of the iteration cycle. The time axes in figures 13.2 and 13.3 is chosen conform to figure 13.1. The system starts out from the DFT ground state at time $t = 0$ and is backwards propagated in time to time $t = -21.5$ where the laser pulse sets in. The wavefunction is propagated forward in time for the duration of the pulse until $t = 21.5$. At this instant the wavefunction is propagated backwards to the initial time $t = 0$. Because of the time-reversal at $t = 21.5$ the dipole moment shows a cusp at this instant in time. In figure 13.2 also the converged result of the dipole moment is shown (blue line), which is slightly different from the TDDFT result and is hence no longer in accordance with the exact dipole moment. The time-dependent density in this mean-field approach therefore depends on the question which is posed and no longer describes the evolution of the exact density. Choosing a different final state would alter the result of the density. Figure 13.3 shows the development of the occupation numbers within the functional-integral approach. The initial TDDFT occupation is shown (red line) as well as the result of the first iteration (green line) and the converged (result). From the converged occupation probability the transition amplitude after the end of the pulse can be deduced, which is defined as the occupation probability at the end of the time-loop at time $t = 0$ which in this case would be $|\langle 0s0s|\Phi_i(t = 0)\rangle|^2 = 0.6$. The exact ground-state transition probability is 0.663, the original TDDFT transition amplitude oscillates around this exact value, the average over the oscillations
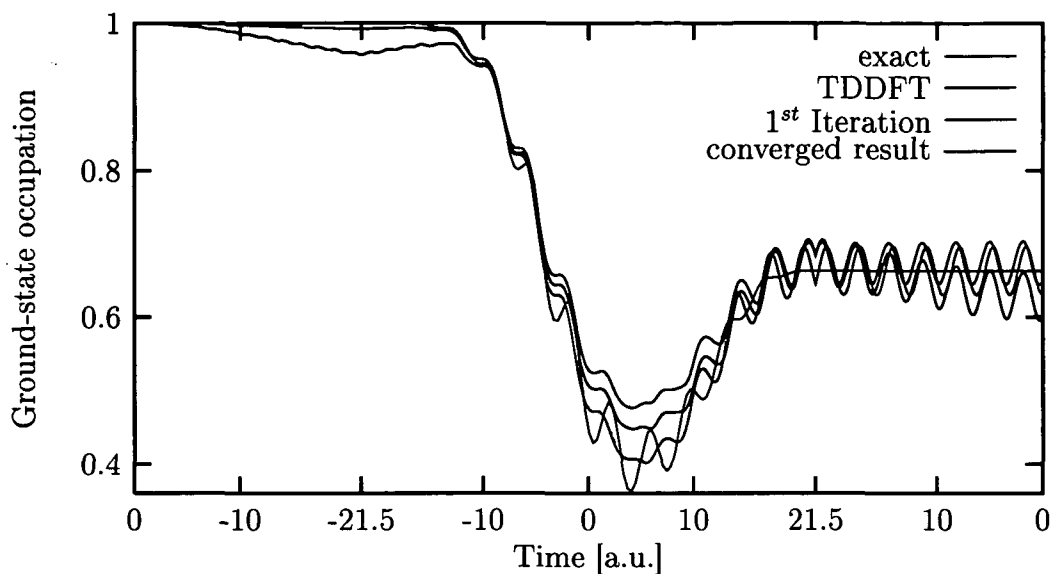
Figure 13.3: Time-dependent ground-state occupation probability of the exact (black line), th TDDFT calculation (red line),the first iteration (green line) and the converged result (blue line). Time axes as in figure13.2 corresponding to the time-loop of figure 13.1.
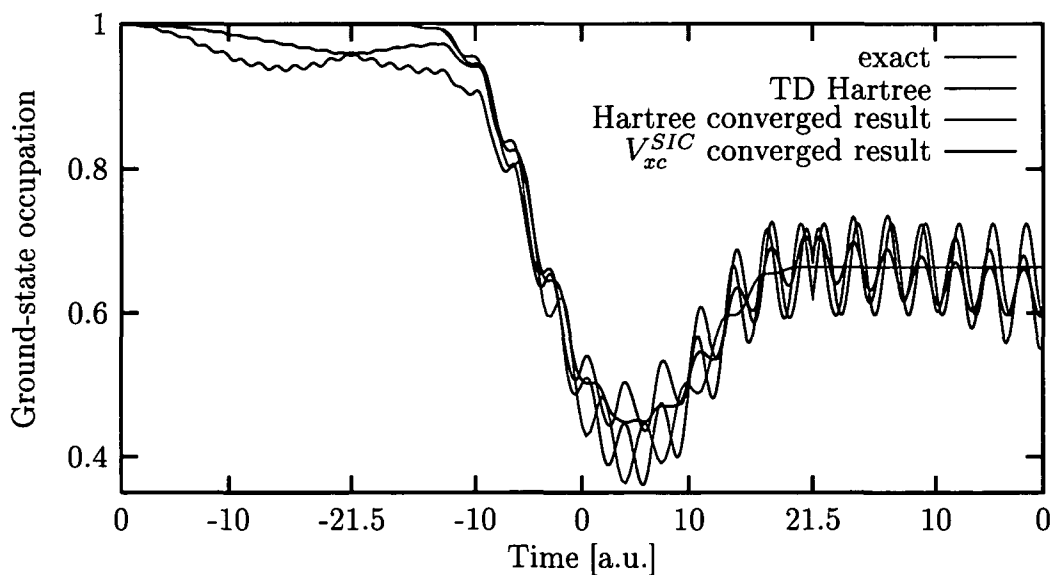
Figure 13.4: Shown is a comparison of ground-state occupation probabilities of the exact solution (black), of the original Hartree-like functional integral approach (time-dependent Hartree result in red, the converged functional integral result based on eq. (13.5) in green) and TDDFT based approached (converged functional integral result based on eq. (13.7) in blue)

would yield the same quantity. The functional integral approach, although rigorously defining a transition amplitude, does not improve on the TDDFT results averaged over the cross-channel correlations.

Moreover we face convergence problems of the functional integral approach. Convergence could not be reached for the general case, only in the case of symmetric laser pulses $E(t) = E(-t)$ and equal initial and final state. The case of different final and initial states gives two different results for $S_{i,f}$ of forward and backward propagations ($\langle \Phi_f | \Phi_i(t) \rangle$ or $\langle \Phi_f(0) | \Phi_i \rangle$ respectively). To compare or modified approach relying on eq. (13.7) to the original Hartree-based approach calculations have been performed according to eq. (13.5). We observe that the new approach including exchange-correlation effects generally gives better transition probabilities (see figure 13.4 for a comparison of the ground-state occupation probabilities). Averaging over cross-channel correlations of pure TDDFT or Hartree results gave identical results which are in the case of the system satisfying the HPT in excellent agreement with exact transition probabilities.

Besides the approach of defining well-behaved transition amplitudes via the Hubbard-Stratonovich operator identity and stationary phase method there exists another class of proposed methods to define transition amplitudes which relies on variational principles [74, 73, 71]. A recent published review article [71] gives an overview of those methods. Basic idea is to pose a Frenkel's variational problem for an expectation value of a given observable with general action-like functionals. These methods should provide equations of motion best suited to the observable to be measured. In some sense the dynamics of the approximated system will depend on the observable which is measured, which is also the case of the mean-field method described in this chapter. A connection of those variational methods to the stationary phase mean-field method was established [71]. Depending on how one restricts the variational space of wave-functions different methods can be derived. It could be shown that the time-dependent Hartree-Fock approximation appears as the best mean-field equation for predicting averages of single-particle observables (within this variational approach). For many-body observables like transition probabilities other mean-field equations can be derived, similar to those obtained by the functional integral approach applied in this work [71, 72]. Those coupled-channel equations have not been solved, the variational functional, however, served to improve time-dependent Hartree-Fock transition amplitudes [72, 74]. Those functionals for improving transition matrix elements of a given mean-field approximation are very similar to the perturbative approach we study in the next chapter.

94

Chapter 14

Perturbation theory

Although wavefunctions built from Kohn-Sham orbitals do not possess a rigorous physical meaning we demonstrated in chapter 8 that in some cases they can serve to reliably represent many-particle wavefunctions. Occupation probabilities obtained by projecting the Kohn-Sham wavefunctions onto Kohn-Sham configuration state functions, however, show cross-channel correlations and it is not possible to define a S-matrix with a proper asymptotic time limit. Nevertheless the Kohn-Sham wavefunctions can serve as a basis for perturbation theory [121]. Connections of DFT with various perturbation approaches exist and in some cases were applied. In the following we will give an overview of existing combinations of perturbation theory and density functional theory.

14.1 Combination of DFT and perturbation expansions

Different combinations of ground state density functional theory and perturbation theory can be found in the literature. The major part of perturbation theories in DFT seeks after the construction of implicit density functionals, i.e. exchange-correlation energy functionals which depend explicitly on occupied and unoccupied Kohn-Sham orbitals. Formally this perturbation approach is solved by a coupling-constant perturbation theory of Görling and Levy [124, 125], the practical use of which is limited. A related theory [137] consists in a combination of many-body perturbation theory (MBPT) [122, 123] and DFT for ground-state energies, which was recently proposed [134, 135, 138]. The second-order orbital energy functional of MBPT serves as an approximated energy functional for the optimized-effective potential method (OEP)[89, 90, 91]. Given a total energy functional depending explic-

itly on single-particle orbitals, the OEP method provides the variationally best orbitals that minimize the total energy expression, under the constraint that the one-particle orbitals are solutions of Kohn-Sham equations with a local exchange-correlation potential. It was demonstrated that in principle the exchange-correlation potential obtained from second order MBPT via the OEP method is divergent at large distances [131, 132, 133]. In numerical implementations with finite-basis set representation those divergencies, however, do not appear [136]. Another study simulated the perturbation series of the exchange-correlation theory to all orders [130]. For some systems this series turned out to be divergent. Improvements of the energies compared to the OEP exchange only case could, however, be demonstrated for the helium isoelectronic series [134]. Moreover the exchange and correlation potentials obtained from this approach show the correct qualitative behavior and are in excellent agreement with potentials obtained from very accurate many-body wavefunctions [140]. A connection of this MBPT OEP approach to the second order Görling-Levy coupling-constant perturbation theory was established [137]. These methods, however, are restricted to improve only the total energy and the exchange-correlation potential and provide no perturbation expansion for the wavefunctions.

A different method is to improve energies obtained from a conventional DFT calculation by performing Rayleigh Schrödinger perturbation theory. Studies on different simple molecules (water molecule, LiH, HF) indicate that many-body perturbation expansions based on DFT-orbitals (of different exchange-correlation potentials) are all divergent [141]. In the best case an oscillatory behavior of the energy with respect to the exact energy as a function of the order of the perturbation theory is observed. The general case shows divergence of the perturbation series, i.e. the error increased with the order of the perturbation-parameter.

For the time-dependent regime perturbation theory only served so far for formal considerations [127, 128, 9, 126]. In the following the performance of first-order time-dependent perturbation theory will be studied in the case of the laser-driven harmonic two-electron quantum dot. We seek to improve on the TDDFT transition-matrix element.

14.2 Time-dependent perturbation theory

Thinking of the time-dependent Kohn-Sham Hamiltonian as unperturbed Hamiltonian of the total many-body system one is led to apply perturbation theory in order to keep track of the residual Coulomb interaction, which is not described through the mean field Hamiltonian. In spirit of many-

body perturbation theory one therefore takes as 'unperturbed Hamiltonian' the sum of the one-particle Kohn-Sham Hamiltonians of the time-dependent system

$$H_0[n_\uparrow, n_\downarrow](t) = \sum_{i=1,2} H^{KS}[n_\uparrow, n_\downarrow](\vec{r}_i) \tag{14.1}$$

$$= \sum_{i=1,2} \left[-\frac{1}{2}\vec{\nabla}_i^2 + V_{ext}(\vec{r}_i, t) + V_H[n](\vec{r}_i, t) + V_{xc}^{SIC}[n_\uparrow, n_\downarrow](\vec{r}_i, t) \right] ,$$

and is therefore a functional of the time-dependent density. The perturbation $V = H - H_0$ to the total Hamiltonian of eq. (2.4) then results as

$$V(\vec{r}_1, \vec{r}_2, t) = V_{ee}(\vec{r}_1, \vec{r}_2) - \sum_{i=1,2} \left[V_H[n](\vec{r}_i, t) + V_{xc}^{SIC}[n_\uparrow, n_\downarrow](\vec{r}_i, t) \right] , \tag{14.2}$$

where the interaction potential $V_{ee}(\vec{r}_1, \vec{r}_2) = \frac{1}{|\vec{r}_1 - \vec{r}_2|}$ is the Coulomb-potential. Aim of the perturbation approach is to expand the exact time-evolution operator $U(t, t_0)$ satisfying

$$U(t, t_0) = 1 - i \int_{t_0}^{t} H(\tau)U(\tau, t_0)d\tau \tag{14.3}$$

with the initial condition $U(t_0, t_0) = 1$ in terms of the Kohn-Sham evolution operator $U_0(t, t_0)$

$$U_0(t, t_0) = 1 - i \int_{t_0}^{t} H_0(\tau)U(\tau, t_0)d\tau \tag{14.4}$$

with $U_0(t_0, t_0) = 1$. It should be noted that already the unperturbed Hamiltonian $H_0(t)$ is time-dependent. The perturbation expansion of the evolution operator is then given by [75]

$$U(t, t_0) = U_0(t, t_0) + \sum_{n=1}^{\infty} U_n(t, t_0) \quad \text{with} \tag{14.5}$$

$$U_n(t, t_0) = (-i)^n \int_{t>\tau_n>\tau_{n-1}>..>\tau_1>t_0} d\tau_n d\tau_{n-1}...d\tau_1 \; U_0(t, \tau_n)V(\tau_n)U_0(\tau_n, \tau_{n-1})...$$

$$...U_0(\tau_2, \tau_1)V(\tau_1)U_0(\tau_1, t_0)$$

The aim is to calculate the first-order correction to the Kohn-Sham transition matrix element we defined in chapter 8 by the projection mechanism $\langle \Phi_f | U_0(t, t_0) | \Phi_i \rangle = \langle \Phi_f | \Phi_i(t) \rangle$, where $|\Phi_i\rangle = |\Phi_i(t_0)\rangle$ denotes the initial state of the Kohn-Sham system and

$$|\Phi_i(t)\rangle := |U_0(t, t_0)[n_i]\Phi_i\rangle \tag{14.6}$$

97

is the self-consistently propagated Kohn-Sham wavefunction. The evolution operator is a functional of the time-dependent density $n_i(t)$ of the propagated initial state. The final state $|\Phi_f\rangle$ in chapter 8 was either chosen as a Kohn-Sham configuration state function, or an eigenstate of the exact Hamiltonian at $t < t_0$. Due to the complexity of the numerical implementation of the perturbation approach the final state $|\Phi_f\rangle$ has to be restricted to a Kohn-Sham configuration state. The first-order corrected Kohn-Sham transition probability then reads

$$
\begin{aligned}
\langle \Phi_f | U(t,t_0) | \Phi_i \rangle &\simeq \langle \Phi_f | \Phi_i(t) \rangle - i \int_{t_0}^{t} d\tau \langle \Phi_f | U_0(t,\tau) V(\tau) U_0(\tau,t_0) | \Phi_i \rangle \\
&\simeq \langle \Phi_f | \Phi_i(t) \rangle - i \int_{t_0}^{t} d\tau \langle \Phi_f(\tau) | V(\tau) | \Phi_i(\tau) \rangle ,
\end{aligned}
\tag{14.7}
$$

where $|\Phi_f(\tau)\rangle := U_0(\tau,t_0)[n_i(\tau)]|\Phi_f(\tau)\rangle$ denotes the backwards propagated final state. The state $|\Phi_f(\tau)\rangle$ is not propagated self-consistently but by the Hamiltonian $H_0[n_i(\tau)]$ of the forward propagated initial state $|\Phi_i(\tau)\rangle$. In addition to the solution of the time-dependent Kohn-Sham equations one therefore has to store the wavefunction $|\Phi_i(\tau)\rangle$ in the time-interval $\tau \in [t_0, t]$. In a second step the final state $|\Phi_f(\tau)\rangle$ is propagated backwards in the self-consistent field of $|\Phi_i(\tau)\rangle$ and the matrix-elements $\langle \Phi_f(\tau) | V(\tau) | \Phi_i(\tau) \rangle$ have to be evaluated at each time-step.

For a first estimate of the magnitude of the first-order correction the case of 'forward-scattering' is examined. We start from the ground state of the two-electron parabolic dot. The final state at time t is chosen as the forward propagated initial state at time t: $|\Phi_f\rangle = \Phi_i(t)\rangle$. Eq. (14.7) then reduces to

$$
\langle \Phi_f | U(t,t_0) | \Phi_i \rangle \simeq 1 - i \int_{t_0}^{t} d\tau \langle \Phi_i(\tau) | V(\tau) | \Phi_i(\tau) \rangle ,
\tag{14.8}
$$

because $|\Phi_f(\tau)\rangle = |\Phi_i(\tau)\rangle$ for all $\tau \in [t_0, t]$. The first order correction involves therefore the Hartree-energy since $\langle \Phi_i(\tau) | V_{ee} | \Phi_i(\tau) \rangle = \frac{1}{2} E_H[n(\tau)]$. Neglecting the correlation part in V_{xc}^{SIC} the matrix element $\langle \Phi_i(\tau) | \sum_{j=1,2} V_{xc}^{SIC}(\vec{r}_j) | \Phi_i(\tau) \rangle \simeq E_H[n(\tau)]$. Therefore eq. (14.8) becomes

$$
\langle \Phi_f | U(t,t_0) | \Phi_i \rangle \simeq 1 + \frac{1}{2} i \int_{t_0}^{t} d\tau \, E_H[n(\tau)] ,
\tag{14.9}
$$

the first order correction is therefore proportional to the time integral of the Hartree-energy. In the case of the harmonic quantum dot the Coulomb energy does not change in time, the integral in eq. (14.9) therefore grows linearly with t. The first order-correction to the transition probability therefore diverges
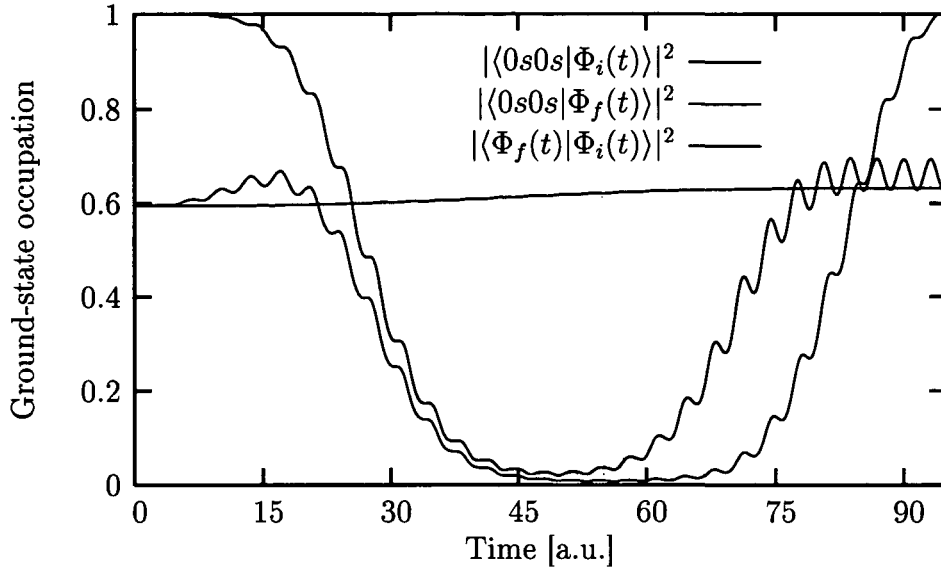
Figure 14.1: Shown are Kohn-Sham ground-state occupation probabilities of forward propagated initial state $|\Phi_i(0)\rangle = |0s0s\rangle$ and backwards propagated final state $U_0(\tau, t_f)|\Phi_f(t_f) = U_0(\tau, t_f)|0s0s\rangle$. Further shown is the overlap of both wave-functions $|\langle\Phi_f(\tau)|\Phi_i(\tau)\rangle|^2$
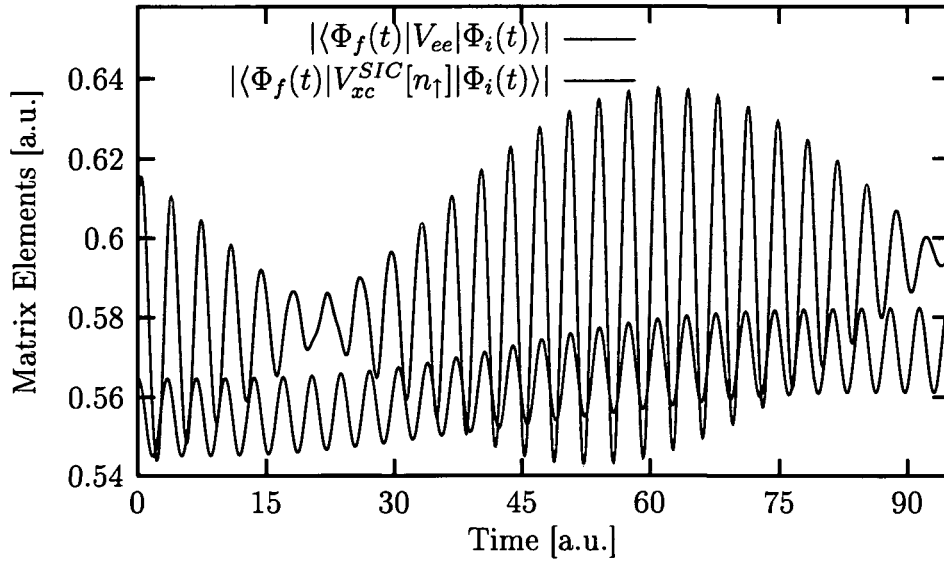
Figure 14.2: Shown are the time-dependent matrix-elements of the Coulomb-interaction (red line) and the exchange-correlation potential $V_{xc}^{SIC}[n_\uparrow]$ of one spin-component (red line). The matrix elements are of the same order of magnitude during the whole time-interval. The first order correction in the perturbation series therefore diverges.

quadratically with t. In the case of forward scattering one is tempted to interprete eq. (14.9) as a Taylor expansion of

$$\langle \Phi_f | U(t, t_0) | \Phi_i \rangle \simeq 1 \cdot \exp \left\{ +\frac{1}{2} i \int_{t_0}^{t} d\tau E_H[n(\tau)] \right\} , \qquad (14.10)$$

truncated after the first order contribution of the exponent. Indeed eq. (14.10) can be derived by means of a variational principle [69] we will introduce in a forthcoming chapter. Eq. (14.10) therefore only explores a trivial phase effect and does not contribute to an improvement of the transition matrix element.

The choice of the final state in the 'forward scattering' is pathological in the sense that the first order term in most cases will result in a transition amplitude greater than one. In the following therefore a different choice of the final state will be made. It will be demonstrated, however, that nevertheless the first order correction is divergent. The final state is chosen as the DFT ground state so that $|\Phi_f(t_f)\rangle = |\Phi_i(t_0)\rangle = |0s0s\rangle$. We consider the weakly correlated system of $\omega = 1$ The system is propagated in the laser pulse with parameters identical to those of chapter 8: maximal field amplitude $A_0 = 0.3$, driving frequency $\omega_p = 0.884$, pulse duration $\tau = 90$. Figure 14.1 shows the ground-state occupation of the forward propagated initial state as well as the backwards propagated final state. The overlap $|\langle \Phi_f(\tau) | \Phi_i(\tau) \rangle|^2$ stays at around 60 percent for the entire time-interval. In figure 14.2 we show the absolute value of the matrix-elements of the Coulomb-interaction V_{ee} and the exchange correlation potential V_{xc}^{SIC}, which are comparable in magnitude during the whole time-period. Since in the integral determining the first-order correction the sum $\sum_{i=1,2} V_{xc}^{SIC}(\vec{r}_i)$ enters the perturbation series for the transition-matrix element diverges linearly with time t. Calculations of the one-dimensional Helium model introduced in section 12.2 also show a diverging first-order correction (not shown).

As in the case of forward scattering diagrams of different order of perturbation theory could be resummed resulting in a phase similar to eq. (14.10), which in the general case will be complex. It is, however, a delicate question which diagrams to choose in the resummation. In the case of stationary many-body perturbation theory the expansion is in principle divergent and in general the inclusion of higher order diagrams does not necessarily improve the result [139].

In chapter 15 we will introduce a variational approach which circumvents the problem of resummation and the choice of the physically correct diagrams and yields an expression which in the case of forward scattering reduces to eq. (14.10).

First order Rayleigh-Schrödinger perturbation theory is therefore in general

not a suitable tool to improve on TDDFT transition probabilities. The problems of perturbation expansions in the inter-particle potential observed for ground state density functional theory seem to be even worse when time-dependent systems are considered.

Chapter 15

Variational approach

In chapter 14 we developed a first-order time-dependent perturbation theory in which the time-dependent Kohn-Sham Hamiltonian was used as the "unperturbed" Hamiltonian. We observed that the first-order correction to the state-to-state transition matrix element was linearly divergent in time. Resummation of diagrams of different order may result in a complex phase, but it is per se a difficult and delicate task to decide which diagrams to resum. In this chapter we will introduce a variational approach, initially proposed as purely formal tool in the theory of atomic collisions [69] which later served to improve on time-dependent Hartree-Fock calculations for transition probabilities [70, 72, 73, 74]. First-order time-dependent perturbation theory can be derived by means of this variational approach. An approximate expression for the transition matrix element which would correspond to a resummation of different higher order terms of the perturbation series can be derived by additional constraints on the variational functional [69, 70].

15.1 Interrelation of the perturbation theory and the variational approach

In this section we introduce a variational approach for the transition matrix element. It will be demonstrated that this variational method and the first-order perturbation theory are inherently connected. We use a slightly different derivation as originally proposed in [69].

The basics underlying the variational approach consists in an action-like functional, the stationary value of which yields the transition matrix element

$$S_{i,f}(t_f) = \langle \Phi_f | U(t_f, t_0) | \Phi_i \rangle = \langle \Phi_f | \Phi_i(t_f) \rangle , \qquad (15.1)$$

where $U(t, t_0)$ (see eq. (14.3)) denotes the evolution operator according to the full Hamiltonian of eq. (2.4). The generalized action functional which yields the transition matrix element is given by

$$J(\Psi_f, \Psi_i) = -i \int_{t_0}^{t_f} dt \left\langle \Psi_f(t) \left| H - i\frac{d}{dt} \right| \Psi_i(t) \right\rangle + \langle \Psi_f(t_f) | \Psi_i(t_f) \rangle \quad (15.2)$$

in which the wavefunctions $|\Psi_i\rangle$ and $|\Psi_f\rangle$ satisfy the initial and final conditions

$$|\Psi_i(t_0)\rangle = |\Phi_i\rangle \quad \text{and} \quad |\Psi_f(t_f)\rangle = |\Phi_f\rangle . \quad (15.3)$$

Variation of the functional with respect to the time-dependent wave-functions $|\Psi_i\rangle$ and $|\Psi_f\rangle$ and keeping only linear terms in the variation results in

$$\delta J(\Psi_f, \Psi_i) = \quad \langle \Psi_f(t_f) | \delta \Psi_i(t_f) \rangle + \frac{1}{i} \int_{t_0}^{t_f} dt \left\langle \delta \Psi_f(t) \left| H - i\frac{d}{dt} \right| \Psi_i(t) \right\rangle$$

$$+ \frac{1}{i} \int_{t_0}^{t_f} dt \left\langle \Psi_f(t) \left| H - i\frac{d}{dt} \right| \delta \Psi_i(t) \right\rangle . \quad (15.4)$$

Partial integration of the last term in eq. (15.4) and taking into account the boundary conditions of the variation $\delta \Psi_i(t_0) = 0$ and $\delta \Psi_f(t_f) = 0$ yields

$$\delta J(\Psi_f, \Psi_i) = \frac{1}{i} \int_{t_0}^{t_f} \left\langle \delta \Psi_f(t) \left| H - i\frac{d}{dt} \right| \Psi_i(t) \right\rangle dt$$

$$+ \frac{1}{i} \int_{t_0}^{t_f} \left\langle \Psi_f(t) \left| H + i\frac{\overleftarrow{d}}{dt} \right| \delta \Psi_i(t) \right\rangle dt , \quad (15.5)$$

where the arrow at the top of the operator $\frac{d}{dt}$ denotes that the time-derivative acts on the left side onto $\Psi_f(t)$. The stationary value of the general action integral is hence reached in the case that $\Psi_i(t)$ and $\Psi_f(t)$ satisfy the Schrödinger equations

$$H|\Psi_i(t)\rangle = i\frac{d}{dt}|\Psi_i(t)\rangle \quad \text{with} \quad |\Psi_i(t_0)\rangle = |\Phi_i\rangle \quad (15.6)$$

$$H|\Psi_f(t)\rangle = i\frac{d}{dt}|\Psi_f(t)\rangle \quad \text{with} \quad |\Psi_f(t_f)\rangle = |\Phi_f\rangle \quad (15.7)$$

and the stationary value of the action equals the transition-matrix element

$$J^{stat}(\Psi_i, \Psi_f) = S_{i,f}(t_f) = \langle \Psi_f(t_f) | \Psi_i(t_f) \rangle . \quad (15.8)$$

For states Φ_i and Φ_f not satisfying the exact Schrödinger eqs. (15.6) and (15.7) but which differ little from the exact solution Ψ_i and Ψ_f respectively

the functional $J(\Phi_i, \Phi_f)$ of eq. (15.2) yields an improved transition matrix-element $S_{i,f}(t_f)$ which differs from the exact value of $S_{i,f}(t_f)$ by a second order quantity.

According to the decomposition of the Hamiltonian H in chapter 14 the total Hamiltonian H is split off into the Kohn-Sham Hamiltonian of eq. (14.1) and a time-dependent perturbation:

$$H = \sum_{i=1,2} H^{KS}[n_\uparrow, n_\downarrow](\vec{r}_i) + V(\vec{r}_1, \vec{r}_2, t) \qquad (15.9)$$

with $V(\vec{r}_1, \vec{r}_2, t)$ being the perturbation defined in eq. (14.2). The solution corresponding to the "unperturbed" Kohn-Sham Hamiltonian $\sum_{i=1,2} H^{KS}(\vec{r}_i)$ is the Slater determinant of the time-dependent Kohn-Sham orbitals $|\Phi_i(t)\rangle = A|\phi_{i,\uparrow}(t)\phi_{i,\downarrow}(t)\rangle$ and for the back-wards propagated state $|\Phi_f(t)\rangle = A|\phi_{f,\uparrow}(t)\phi_{f,\downarrow}(t)\rangle$ with the initial and final conditions $|\Phi_i(t_0)\rangle = |\Phi_i\rangle$ and $|\Phi_f(t_f)\rangle = |\Phi_f\rangle$ respectively. A denotes the operator which anti-symmetrizes the product wavefunctions. The initial and final states are chosen as a product of stationary Kohn-Sham orbitals. The improved transition matrix-element according to eq. (15.2) hence is

$$S_{i,f}(t_f) \simeq \langle \Phi_f(t_f)|\Phi_i(t_f)\rangle - i \int_{t_0}^{t_f} dt \, \langle \Phi_f(t) \,|V(\vec{r}_1, \vec{r}_2, t)|\, \Phi_i(t)\rangle \ , \qquad (15.10)$$

which equals the result eq. (14.7) of the first-order perturbation theory obtained in chapter 14.

15.2 Phase-invariant variational approach

In time-dependent density functional theory the exchange-correlation potential $V_{xc}[n_\uparrow, n_\downarrow](t)$ is only determined up to an arbitrary purely time-dependent potential $\tilde{V}(t)$. The improved transition amplitude of eq. (15.10) is, however, not invariant under changing the potential from $V(\vec{r}_1, \vec{r}_2, t)$ to $V(\vec{r}_1, \vec{r}_2, t) + \tilde{V}(t)$. To get an improved expression for an approximated value of the S-matrix invariant with respect to changes of the potential by a purely time-dependent potential the original functional eq. (15.2) is extended to [69]

$$\begin{aligned} J(\Psi_f, f_f, \Psi_i, f_i) &= \langle \Psi_f(t_f)|\Psi_i(t_f)f_i(t_f)\rangle \\ &\quad -i \int_{t_0}^{t_f} dt \left\langle \Psi_f(t)f_f(t) \left| H - i\frac{d}{dt} \right| \Psi_i(t)f_i(t) \right\rangle \end{aligned} \qquad (15.11)$$

where the wavefunctions Ψ_i and Ψ_f are multiplied by purely time-dependent functions $f_i(t)$ and $f_f(t)$ with the additional condition $f_i(t_0) = f_f(t_f) = 1$.

The functional of eq. (15.11) is in first turn varied with respect to wavefunctions. The procedure is the same as in the case of the simpler functional of eq. (15.2). The functional of eq. (15.11) gets stationary with respect to variations in $|\Psi_i\rangle$ and $|\Psi_f\rangle$ if $|\Psi_i\rangle$ fulfill the modified Schrödinger equations

$$H|\Psi_i(t)f_i(t)\rangle = i\frac{d}{dt}|\Psi_i(t)f_i(t)\rangle \quad \text{with} \quad |\Psi_i(t_0)f_i(t_0)\rangle = |\Phi_i\rangle \quad (15.12)$$

$$H|\Psi_f(t)f_f(t)\rangle = i\frac{d}{dt}|\Psi_f(t)f_f(t)\rangle \quad \text{with} \quad |\Psi_f(t_f)f_f(t_f)\rangle = |\Phi_f\rangle (15.13)$$

In a second step the functional is varied with respect to the functions f_f and f_i. The request that the functional is stationary determines the purely time-dependent functions

$$f_i(t) = \exp\left\{-i\int_{t_0}^{t} d\tau \frac{\langle \Psi_f(\tau)|H - i\frac{d}{d\tau}|\Psi_i(\tau)\rangle}{\langle \Psi_f(\tau)|\Psi_i(\tau)\rangle}\right\} \quad (15.14)$$

$$f_f^*(t) = \exp\left\{i\int_{t_f}^{t} d\tau \frac{\langle \Psi_f(\tau)|H + i\frac{d}{d\tau}|\Psi_i(\tau)\rangle}{\langle \Psi_f(\tau)|\Psi_i(\tau)\rangle}\right\} \quad (15.15)$$

Introducing eqs. (15.14) and (15.15) in the modified Schrödinger eqs. (15.12) and (15.13) they reduce to the original eqs. (15.6) and (15.7). The stationary functional of eq. (15.11) gives the transition amplitude. Introducing the stationary values of f_f and f_i of eqs. (15.14) and (15.15) into the functional of eq. (15.11) we obtain as in the case of section 15.1 an approximate expression for the transition matrix element [69] which yields

$$S_{i,f}(t_f) \simeq \langle \Phi_f(t_f)|\Phi_i(t_f)\rangle \cdot \exp\left\{-i\int_{t_0}^{t_f} dt \frac{\langle \Phi_f(t)|V(\vec{r}_1,\vec{r}_2,t)|\Phi_i(t)\rangle}{\langle \Phi_f(t)|\Phi_i(t)\rangle}\right\},$$
$$(15.16)$$

as in the previous section Φ_i and Φ_f denote the forward and backward propagation of the Kohn-Sham Slater determinants in the Kohn-Sham Hamiltonian. The quantity in the exponent is generally complex, so that eq. (15.16) does not describe a trivial phase effect. This raises the question of the unitarity of the S-matrix, which should satisfy $\sum_f |S_{i,f}(t_f)|^2 = 1$. It is not clear if eq. (15.16) preserves the unitarity condition, this point requires further investigation. Eq. (15.16) differs from the exact transition amplitude by a second order quantity. In contrast to eq. (15.10) the expression of eq. (15.16) is invariant with respect to changes of the exchange-correlation by a purely time-dependent potential $\tilde{V}(t)$.

An alternative derivation of the approximative transition amplitude of eq.

(15.16) uses a single variation with respect of to Ψ_i and Ψ_f of the functional [70]

$$J(\Psi_i, \Psi_f) = \int_{t_0}^{t_f} dt \frac{\langle \Psi_f(t) \left| i\frac{d}{dt} - H \right| \Psi_i(t) \rangle}{\langle \Psi_f(t) | \Psi_i(t) \rangle} - i \ln \langle \Psi_f(t_f) | \Psi_i(t_f) \rangle. \quad (15.17)$$

The connection of the perturbation theory to the variational approach, however, is less obvious in this formulation. Searching for the time-dependent wavefunctions which render the effective action eq. (15.17) stationary under the constraint that the wavefunctions are Slater determinants yields the time-dependent Hartree-Fock equations [70]. From this variational point of view Kohn-Sham Slater determinants are therefore not best suited. Nevertheless the functional of eq. (15.16) applied to the Kohn-Sham determinants may yield an improvement over the transition amplitudes obtained by the TDDFT projection approach.

In our analysis we restrict ourselves to time-symmetric laser pulses with $E(t) = E(\tau - t)$. The pulse parameters are chosen in accordance to chapter 13 as: maximal field amplitude $A_0 = 0.23$, driving frequency $\omega_p = 0.804$, pulse duration $\tau = 43$. In contrast to the perturbation approach of chapter 14, where the backwards propagation of the final state has to be performed in the self-consistent Hamiltonian of the forward propagated initial state, in the variational approach we are free to choose the Hamiltonian. One choice, in accordance with the the perturbation theory is the self-consistent Kohn-Sham Hamiltonian of the forward propagated initial state. As an alternative the final state is backwards propagated self-consistently. In the following final and initial state are chosen as the DFT ground state $|0s0s\rangle$.

As it is the case for the time-dependent Hartree-Fock Hamiltonian the Kohn-Sham Hamiltonian violates the time-reversal symmetry. In contrast to the full many-body Hamiltonian including a symmetric laser pulse with $E(t) = E(\tau - t)$ the Kohn-Sham Hamiltonian of the self-consistently propagated initial state $H^{KS}[n_0](t)$ is no longer symmetric against time-reversal, i.e. $H^{KS}[n_0](t) \neq H^{KS}[n_0](\tau - t)$. Backwards propagation in the self-consistent Hamiltonian of the forwards propagated state therefore will lead to different wavefunctions. Figure 15.1 demonstrates this fact and shows the time-dependent ground-state occupation of the forward propagated initial state versus the ground-state occupation of the backwards propagated final state. Not only is the backwards propagated state $\Phi_f(t_f - t)$ different from the forward propagated $\Phi_i(t)$, but also the backwards propagated states $\Phi_f(t)$ generated from different final times t_f are distinct. Surprisingly we observe $|\Phi_f(0)\rangle = |\Phi_i(t_f)\rangle$ $\forall t_f$ (initial conditions $|\Phi_f(t_f)\rangle = |0s0s\rangle$ and $|\Phi_i(0)\rangle = |0s0s\rangle$, i.e. the backwards propagated state $\Phi_f(0)$ equals the forward propagated state at final time $\Phi_i(t_f)$. The Kohn-Sham Hamiltonian, no

106
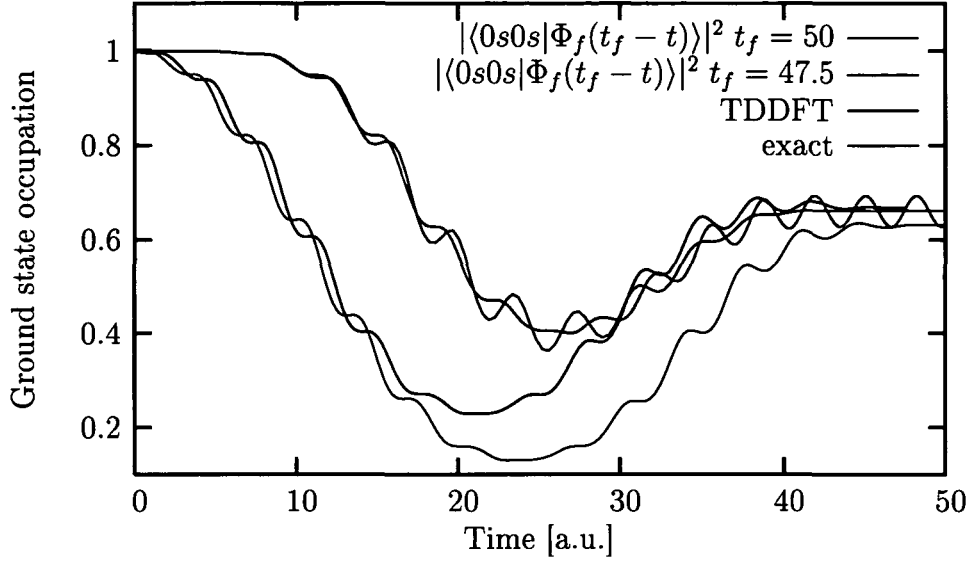
Figure 15.1: Shown are the ground-state occupation of the exact (green) and Kohn-Sham wavefunction (red) in comparison to the ground-state occupation of the backwards propagated $|0s0s\rangle$ Kohn-Sham orbital which is propagated in the self-consistent field of the forward propagated Kohn-Sham orbital from different end-times $t = 50$ (blue) and $t = 47.5$ (green).
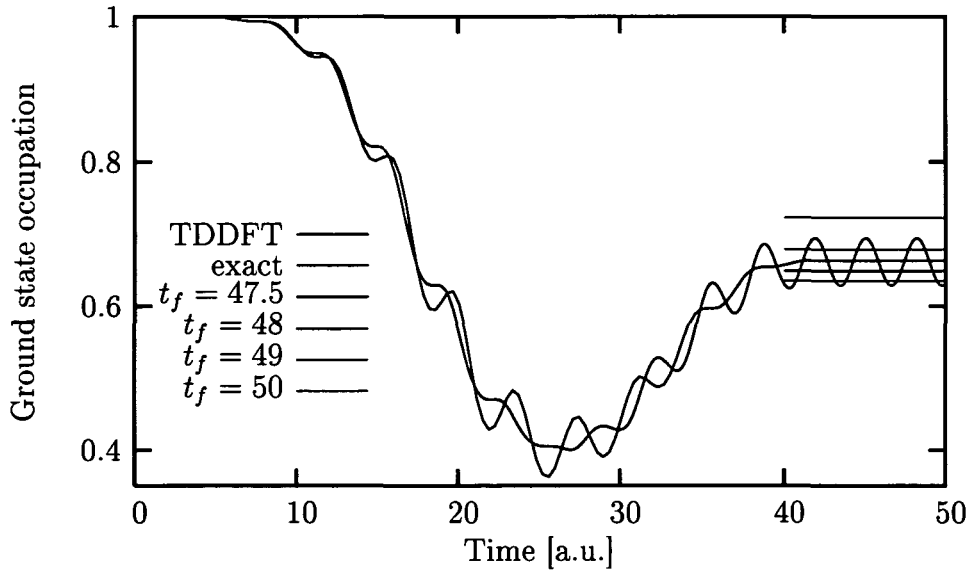

Figure 15.2: Ground-state occupation of the exact (green) and the Kohn-Sham wavefunction (red) and final occupation probabilities of the variational approach at different times t_f of eq. (15.16)

longer symmetric with respect to time-reversal symmetry, nevertheless preserves the quality that the final states of backward and forward propagation are identical.

Figure 15.2 shows the exact and TDDFT ground-state occupation probability and the result of the variational approach of eq. (15.16) at different final times t_f. The variational approach results in occupation probabilities which are distinct for different final times t_f. The reason of the oscillations lies in the real part of the exponent of eq. (15.16) which in the case of the harmonic quantum dot is oscillating with respect to t_f. Those oscillations imply either an increase or decrease of the TDDFT transition amplitude $\langle \Phi_f(t_f) | \Phi_i(t_f) \rangle$. Unfortunately the corrections do not chancel the oscillations in the TDDFT transition amplitude. The amplitude of the cross-channel correlations are even higher than those of the pure TDDFT calculation.

We also performed calculations by self-consistent backward propagation of the final state. No substantial difference to the former results could be observed. The cross-channel correlations persist and are enlarged in comparison to the TDDFT result. The transition amplitudes for fixed final time t_f only differ little upon the choice of the Hamiltonian of the backward propagation. The general conclusion we can draw from these studies is that variational approaches based on functionals of the form of eq. (15.10) to calculate transition amplitudes are not suited to improve on TDDFT results.

Chapter 16

Density functional for state-to-state transition amplitudes

In chapter 8 we have introduced a projection method to define state-to-state transition amplitudes within TDDFT. In this approach the Kohn-Sham wavefunctions are interpreted as many-body wavefunctions and are projected either onto Kohn-Sham configuration state functions or onto exact eigenfunctions of the system to obtain state-to-state transition amplitudes. The transition probabilities obtained this way show cross-channel correlations after the switch-off of the external field and have no well defined asymptotic limit. Attempts to correct the oscillating transition amplitudes by combination of TDDFT with other many-body approaches such as the functional integral approach, many-body perturbation theory and the variational approach failed. The functionals proposed in chapter 8 to calculate the S-matrix within TDDFT (see eqs. (8.6) and (8.7)) depend on the time-dependent Kohn-Sham orbitals and are not directly deduced from the time-dependent density. These functionals are implicit density functionals, i.e. they are implicitly depending on the density via the Kohn-Sham orbitals.

In this chapter we introduce a new functional to deduce the S-matrix which explicitly depends on the time-dependent density. It will be shown that the S-matrix obtained this way has a well defined asymptotic limit, i.e. time-dependent occupation probabilities after switch-off of the laser pulse do not show cross-channel correlations and are stationary.

We restrict the following considerations to two-electron systems. The generalization to more electrons is, however, straight forward. Starting point is the expression of the exact time-dependent wavefunction in terms of the

time-dependent S-matrix:

$$\Psi(\vec{r}_1, \vec{r}_2, t) = \sum_f S_{f,i}(t)\Phi_f(\vec{r}_1, \vec{r}_2) , \tag{16.1}$$

where the S-matrix for arbitrary times t is defined as

$$S_{i,f} = \langle \Phi_f | U(t,0) | \Phi_i \rangle \tag{16.2}$$

and $U(t,0)$ denotes the exact time-evolution operator, $|\Phi_i\rangle$ denotes the initial state and the sum in eq. (16.1) includes all possible final states $|\Phi_f\rangle$, which are eigenstates of the full many-body Hamiltonian. The time-dependent density is therefore given by

$$n(\vec{r}, t) = \sum_{f,f'} S_{f,i}(t)S^*_{f',i}(t)\rho^{(1)}_{f',f}(\vec{r}, \vec{r}) \tag{16.3}$$

where $\rho^{(1)}_{f,f'}(\vec{r}, \vec{r})$ denotes the diagonal element of the generalized one-particle reduced density matrix defined by

$$\rho^{(1)}_{f',f}(\vec{r}_1, \vec{r}_2) = \int d\vec{r}\, \Phi^*_{f'}(\vec{r}_1, \vec{r})\Phi_f(\vec{r}_2, \vec{r}) . \tag{16.4}$$

Defining the time-dependent transition density matrix by

$$T_{f',f}(t) = S^*_{f',i}(t)S_{f,i}(t) \tag{16.5}$$

the time-dependent density is given by

$$n(\vec{r}, t) = \sum_{f,f'} T_{f',f}(t)\rho^{(1)}_{f',f}(\vec{r}, \vec{r}) = \text{Tr}\left[T(t)\rho^{(1)}(\vec{r})\right] . \tag{16.6}$$

Knowing the reduced density matrix $\rho^{(1)}_{f,f'}(\vec{r}, \vec{r})$ and the time-dependent density $n(\vec{r}, t)$ (either from an exact calculation or a TDDFT calculation) it should therefore be possible to deduce the transition probabilities $T_{f,f}(t) = |S_{f,i}(t)|^2$ by inversion of eq. (16.6). Our primary interest therefore lies in the diagonal elements of the transition density matrix $T_{f',f}(t)$ at times after the switch-off of the external perturbation $t > \tau$. For those times the exact wavefunction is in a coherent superposition of different final states and the transition density matrix evolves as

$$T_{f',f}(t + \Delta t) = T_{f',f}(t) \exp\{-i(E_{f'} - E_f)\Delta t\} , \tag{16.7}$$

hence it only depends on the energy difference of the exact energy eigenvalues E_f. To extract the transition probabilities $T_{f,f}(t)$ a time-average of the density and eq. (16.6) is performed which yields

$$\bar{n}(\vec{r},t) = \frac{1}{t-\tau}\int_\tau^t n(\vec{r},t')dt' = \sum_{f,f'} \rho^{(1)}_{f',f}(\vec{r},\vec{r})\frac{1}{t-\tau}\int_\tau^t T_{f',f}(t')dt' . \quad (16.8)$$

The time-integral over the the transition matrix $T_{f',f}(t)$ reads

$$\frac{1}{t-\tau}\int_\tau^t T_{f',f}(t')dt' = \frac{1}{t-\tau}T_{f',f}(\tau)\int_0^{t-\tau} \exp\left\{-i(E_{f'}-E_f)\Delta t\right\} d(\Delta t) , \quad (16.9)$$

which for a time window $\Delta t = t - \tau$ satisfying $\Delta t|E_{f'} - E_f| \gg 2\pi$ reduces to

$$\lim_{t\to\infty}\frac{1}{t-\tau}\int_\tau^t T_{f',f}(t')dt' = T_{f',f}(\tau)\delta_{f,f'}. \quad (16.10)$$

In the long-time limit we therefore get

$$\bar{n}(\vec{r}) = \lim_{t\to\infty}\frac{1}{t-\tau}\int_\tau^{\tau+t} n(\vec{r},t') \, dt' = \sum_f \rho^{(1)}_{f,f}(\vec{r},\vec{r}) \, T_{f,f}(\tau) , \quad (16.11)$$

from which we can determine the transition probabilities $T_{f,f}(\tau)$ by inversion of the density matrix $\rho^{(1)}_{f,f}(\vec{r},\vec{r})$. Eq. (16.11) constitutes the read-out functional of the transition probabilities in dependence of the time-averaged density $\bar{n}(\vec{r})$.

In a practical calculation the sum in eq. (16.11) is truncated to a few final states $f = 0, ..., n_f$. The problem consists in evaluating the diagonal elements of the reduced density matrix $\rho^{(1)}_{f,f}(\vec{r},\vec{r})$ at n_f+1 distinct points r_i $i = 0, ..., n_f$, so that the matrix $R_{f,i} := \rho^{(1)}_{f,f}(\vec{r_i},\vec{r_i})$ does not become near singular and is invertible. The state-to-state transition probabilities then become

$$T_{f,f}(\tau) = \sum_{i=0}^{n_f} \bar{n}(\vec{r_i})R^{-1}_{f,i} \quad f = 0, 1, .., n_f . \quad (16.12)$$

We test this new density functional to calculate state-to-state transition amplitudes by means of the one-dimensional two-electron quantum dot with the Hamiltonian of eq. (2.2). We use the exact time-dependent density $n(x,t)$ in order to deduce the transition probabilities from the laser-driven ground state. In this way errors of the exchange-correlation potential can be ruled out and the quality of the proposed functional for state-to-state transition

probabilities can be directly assessed. The sum in eq. (16.11) is truncated after the second excited state, so that we take final states with c.o.m. quantum numbers $f = 0, 1, 2$ into account. In figure 16.1 we the exact time-dependent occupation probabilities of the ground and the first excited state compared to the transition probabilities obtained by inversion of

$$\bar{n}(x,t) = \frac{1}{t-\tau} \int_\tau^t n(x,t')dt' = \sum_f \rho_{f,f}^{(1)}(x,x) \, T_{f,f}(t) \qquad (16.13)$$

to read out approximate values $T_{f,f}(t)$ of the transition probabilities. At large times $T_{f,f}(t)$ approaches the exact transition probability. The validity of the proposed approach is therefore illustrated.

In the special case of the harmonic oscillator only final states with energy differences of multiples of the frequency ω come into play. Therefore it is sufficient to restrict the time-average of eq. (16.6) to the period $\Delta t = 2\pi/\omega$ involving the smallest possible energy difference of exact eigenstates. We therefore get a different time-average of the density, denoted with $\tilde{n}(x,t)$, than that obtained by eq. (16.13). The new functional of the time-averaged density $\tilde{n}(x,t)$ in this special case reads

$$\tilde{n}(x,t) = \frac{1}{\Delta t} \int_{t-\Delta t/2}^{t+\Delta t/2} n(x,t')dt' = \sum_f \rho_{f,f}^{(1)}(x,x) \, \tilde{T}_{f,f}(t) \qquad (16.14)$$

The transition probabilities $\tilde{T}_{f,f}(t)$ obtained by inversion of eq. (16.14) are up to computational inaccuracies stationary. The transition probabilities $T_{f,f}(t)$ obtained by inversion of eq. (16.13) approach $\tilde{T}_{f,f}(t)$ at large times. Figure 16.2 shows exact occupation probabilities in comparison to transition probabilities obtained by eq. (16.14) in the case of the ground-state propagation of the one-dimensional two-electron quantum dot in an external laser field. The exact transition probabilities and the counterpart obtained by the density functional coincide within the graphical resolution.

In the following analysis the density functional approach is tested in the case of the propagation of a coherent superposition of eigenstates in an external laser field. This arbitrary initial state, not subject to the HPT, explores a more complicated dynamics. In addition to the translation the shape of the density gets modified. As demonstrated in chapter 12 for the "exact" Kohn-Sham scheme the projection approach completely failed to deduce reliable occupation probabilities even in the absence of an external laser field. We consider the initial state composed of the ground state and the first excited state of the one-dimensional two-electron harmonic dot

$$|\Phi_i\rangle = \frac{1}{\sqrt{2}} \left(|0\rangle + |1\rangle \right) . \qquad (16.15)$$

Figure 16.1: Shown are the exact ground-state occupation (red) and the occupation of the first excited state (green) compared to the transition probabilities $T_{f,f}(t)$ obtained by inversion of eq. (16.13) (blue for the ground state and magenta for the first excited state). The oscillator frequency is $\omega = 0.25$. Parameters of the laser pulse: maximal field amplitude $A_0 = 0.07$, driving frequency $\omega_p = 0.1839$, pulse duration $\tau = 168$

Figure 16.2: Shown are the same quantities as in figure 16.1, however, for the inversion of eq. (16.14). The transition probabilities of the exact calculation and those obtained by the proposed density functional agree within the resolution of the plot.
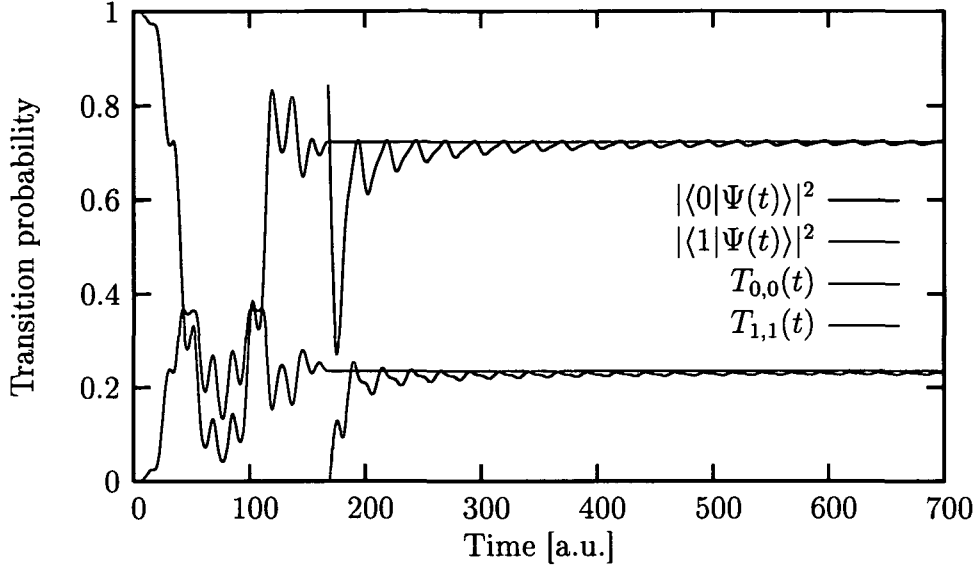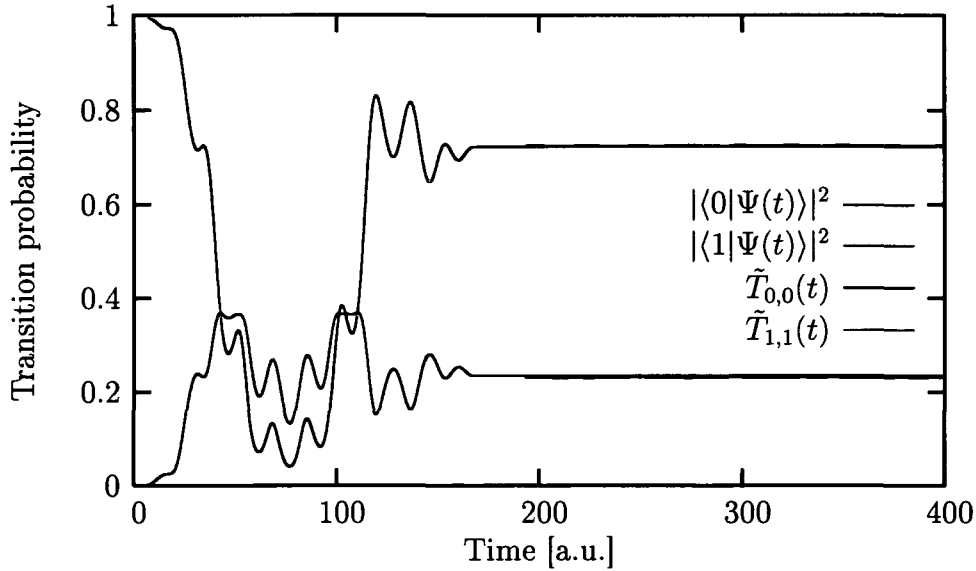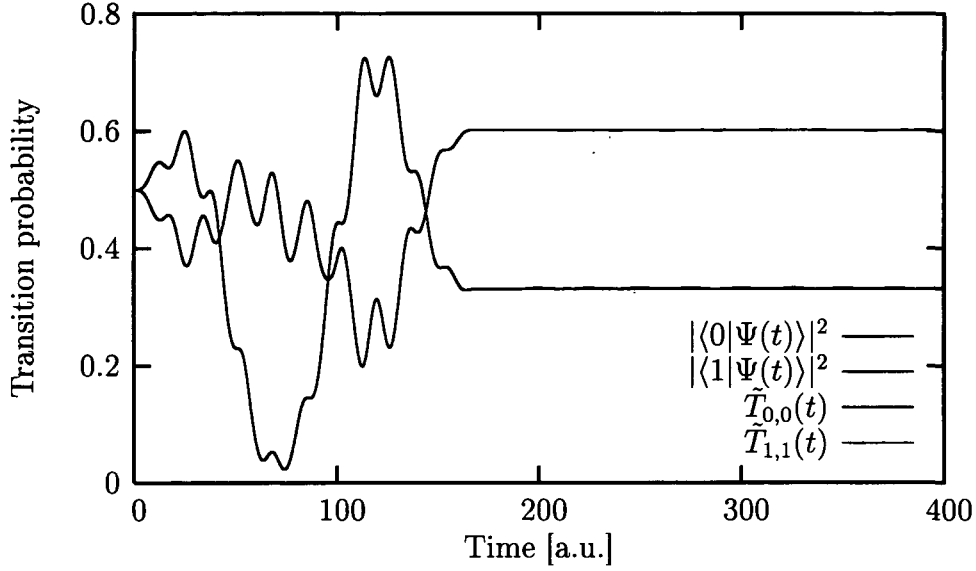
113

Figure 16.3: Shown are the exact ground-state occupation (red) and the occupation of the first excited state (green) compared to the transition probabilities $\tilde{T}_{f,f}(t)$ obtained by inversion of eq. (16.14) for the propagation of a coherent superposition (blue for the ground state, magenta for the first excited state). The transition probabilities of the exact calculation and those obtained by the proposed density functional coincide within the graphic's resolution. Parameters of the laser pulse: maximal field amplitude $A_0 = 0.03$, driving frequency $\omega_p = 0.1839$, pulse duration $\tau = 168$

As in the previous case of the ground-state propagation we take the exact time-dependent density $n(x, t)$ to evaluate eq. (16.14). Figure 16.3 shows the exact occupation probabilities of the ground state $|0\rangle$ and the first excited state $|1\rangle$ in comparison to the transition probabilities obtained by inversion of eq. (16.14). The agreement is perfect within the resolution of the plot. Small errors in the transition probabilities are due to numerical errors and the the truncation of the sum in eq. (16.14) to only three final states.

The results obtained in the case of the one-dimensional two-electron quantum dot are promising. More complex systems as the one-dimensional helium model are currently investigated. The drawback of the proposed density functional is that in principle the diagonal elements of the exact reduced one-particle density matrices $\rho_{f,f}^{(1)}$ have to be known. In other words, the knowledge of the exact stationary states of the system under consideration is essential. The implications of approximating the density matrices $\rho_{f,f}^{(1)}$ on the usefulness of the proposed functional have to be studied. For systems

114

in which many final states are occupied appropriate positions r_i have to be deduced in order to get invertible density matrices $R_{f.i} = \rho_{f,f}^{(1)}(r_i)$. In the case of helium in external laser fields the important question arises how the continuum of electronic states should be treated within the proposed approach. The promising results of the one-dimensional two-electron quantum dot are encouraging to attack those open problems in the near future.

Chapter 17

Conclusions

We presented a critical case study probing the quality of time-dependent density functional theory (TDDFT) applied to laser-matter interactions. Our model consists of two electrons, which are interacting via Coulomb force and confined in three dimensions by a harmonic oscillator potential. The electrons interact with a laser pulse treated in the dipole approximation. The dynamics of the system can be solved exactly and the exact results were used to benchmark the performance of TDDFT.

As exchange-correlation potential we chose the self-interaction corrected local adiabatic spin density approximation (ALSDA-SIC). The numerical integration of the time-dependent Kohn-Sham equations was performed on a grid using a pseudo-spectral method for optimal discretization. We applied an efficient split-operator method in the DFT energy representation of the unperturbed system.

The system evolves from different initial states. In a first study the singlet and triplet ground states were considered as initial states. As eigenstates of the harmonic dot these initial states are subject to the harmonic potential theorem (HPT) which states that the initial density is rigidly shifted without being distorted. The dynamics of the density satisfying the HPT is completely determined by the classical motion of the center of mass. We analyzed the time-dependent dipole moment and the time-dependent density profiles of the TDDFT calculation and compared them to the exact solution. The HPT is perfectly satisfied within ALSDA-SIC in the case of the propagation from the singlet ground state. Problems arise for the propagation of the triplet ground state. While the HPT is satisfied for ALSDA, the numerical propagation of the triplet state gets unstable in the case of ALSDA-SIC and violations of the HPT are observed.

As a major part of this thesis we attacked the challenge of calculating many-body observables within TDDFT. We introduced a simple projection ap-

proach to deduce state-to-state transition probabilities within TDDFT. The time-propagated Kohn-Sham Slater determinant is used as approximation of the full many-body wavefunction and is projected onto appropriate channel states. The channel states are either Kohn-Sham configuration state functions or exact eigenstates of the system. The projection method was first tested for the propagation of the singlet ground state. The overall behavior of the occupation probabilities obtained by this projection approach are in excellent agreement with exact results. After switch off of the laser-pulse the occupation probabilities, however, suffer oscillations which also pertain by projecting onto exact eigenstates of the Hamiltonian. Those oscillations, named "spurious cross channel correlations" are known from time-dependent Hartree Fock calculations for nuclear reactions. Averaging over those oscillations results, however, in excellent transition amplitudes. In the case of evolution from the triplet ground state the occupation probabilities are in good agreement with exact results as long as the HPT is satisfied.

Further we considered the propagation from an arbitrary coherent superposition of states in the absence of an external laser field. These systems, not subject to the HPT, show more complex dynamics and allow for distortions of the time-dependent density. To simplify the comparison of exact and TDDFT calculations we developed a time-dependent configuration interaction method on the basis of Kohn-Sham configuration states to solve the exact problem. ALSDA-SIC fails to reproduce the exact time-dependent density and therefore also transition probabilities obtained within TDDFT are wrong.

To study conceptional problems of the oversimplified TDDFT projection approach in the case of arbitrary initial states we have introduced one-dimensional model systems for which it is possible to construct an exact exchange correlation potential. This way errors of the exchange-correlation potential can be ruled out and the issue of determining state-to-state transition amplitudes within TDDFT becomes decoupled from the problem of finding good approximations of the effective Kohn-Sham potential. Even for those "exact" Kohn-Sham systems it was not possible to deduce reliable occupation probabilities. For more complex systems the time-dependent Kohn-Sham orbitals will in general be inadequate representatives for the many-body wavefunctions.

Having analyzed the deficiencies of the TDDFT projection approach we have tried to find improvements by combining TDDFT with other many-body approaches. We studied the performance of three different methods which, however, turned out to be inappropriate to improve on TDDFT results. The first method introduced relies on a functional integral representation of the time-evolution operator and is known under the names of functional integral

117

approach, mean-field method and stationary phase method. This functional integral approach connects final and initial states through a self-consistent density which acts as a source in the Hartree term. Unlike TDDFT or TDHF, this density is depending on initial and final states. The technical implementation of this method results in a series of TDDFT-like calculations. Unfortunately, converged results could only be generated in some special non-generic cases.

In a second attempt we introduced a Møller-Plesset like time-dependent perturbation theory in which not the pure Coulomb interaction but the difference of Coulomb interaction and the effective Kohn-Sham potential was treated as perturbation. The time-dependent Kohn-Sham system therefore acts as the unperturbed system. First order perturbation theory of the state-to-state transition amplitude turned out to be divergent. To circumvent the problem of renormalization of this divergent series we adopted a variational approach. The basis underlying the variational approach consists in an action-like functional, the stationary value of which yields the transition matrix element. This functionals should yield improved transition matrix elements if evaluated for an approximate wavefunction. Improvement of TDDFT transition amplitudes could, however, not been achieved. The cross-channel correlations are even enhanced in this case.

The projection approach defines the S-matrix as a functional of the time-dependent Kohn-Sham orbitals. A new functional to calculate the S-matrix has been proposed which directly depends on the time-dependent density. Within this new approach the S-matrix has a well-defined asymptotic limit and occupation probabilities of different states are free of cross-channel correlations. The functional was tested by means of the one-dimensional two-electron quantum dot. Accurate transition probabilities could be determined in the case of an arbitrary initial state. The implications of the application of this new functional to more complex systems which also explore the continuum of electronic states have to be studied. The promising results of our simple one-dimensional model are encouraging to attack those open problems in the near future.

Appendix A

The pseudo-spectral method

The aim of the pseudo-spectral method is to approximate a given function $f(x)$ defined in the interval $x \in [-1, 1]$ by the polynomial of degree N $f_N(x)$ [81]. Choosing the Legendre Polynomials $P_l(x)$, the exact function $f(x)$ is approximated by

$$f(x) \simeq f_N(x) = \sum_{l=0}^{N} a_l P_l(x) \, , \qquad (A.1)$$

with the expansion coefficients a_l

$$a_l = \frac{1}{\alpha_l} \int_{-1}^{1} f(x) P_l(x) dx \, . \qquad (A.2)$$

The key point of the pseudo-spectral method is to require the approximation to be exact on a set of points x_i, called collocation points

$$f(x_i) = f_N(x_i). \qquad (A.3)$$

These points x_i are chosen as the abscissas of (Legendre-Gauss-) Lobatto's Quadrature Formula.
The integral of a function $g(x)$, $x \in [-1, 1]$ over the whole of its specified range can be approximatively calculated [84] by

$$\int_{-1}^{1} g(x) dx = \sum_{i=0}^{N} w_i \, g(x_i) + R_{N+1} \, . \qquad (A.4)$$

The abscissas x_i for $i = 1, .., N - 1$ of this quadrature are related to the the $(N - 1)$ zeros of $P_N'(x)$ and we define $x_0 = -1$, $x_N = 1$. The corresponding weights are given by

$$w_i = \begin{cases} \frac{2}{N(N+1)[P_N(x_i)]^2} & i = 1, .., N - 1 \\ \frac{2}{N(N+1)} & i = 1, N \end{cases} \qquad (A.5)$$

119

The remainder R_{N+1} is proportional to the $2N$-th derivative of $g(x)$. Lobatto's quadrature therefore is exact for polynomials of degree $2N - 1$. The expansion coefficients a_l can be approximated by this quadrature rule through

$$a_l = \frac{1}{\alpha_l} \sum_{i=0}^{N} w_i \ f(x_i) P_l(x_i) \ . \tag{A.6}$$

The function $f(x)$ is therefore approximated by

$$f(x) \simeq \sum_{l=0}^{N} a_l P_l(x) = \sum_{i=0}^{N} f(x_i) \sum_{l=0}^{N} \frac{1}{\alpha_l} w_i \ P_l(x_i) P_l(x) = \sum_{i=0}^{N} f(x_i) g_i(x) \ , \tag{A.7}$$

where $g_i(x)$ is the so called cardinal function and is defined by

$$g_i(x) = \sum_{l=0}^{N} \frac{1}{\alpha_l} w_i \ P_l(x_i) P_l(x) \ . \tag{A.8}$$

The requirement of the approximation to be exact at x_i, $f(x_i) = f_N(x_i)$, implies that the cardinal functions have to satisfy $g_i(x_j) = \delta_{i,j}$ which explicitly reads

$$\sum_{l=0}^{N} \frac{1}{\alpha_l} w_i \ P_l(x_i) P_l(x_j) = \delta_{i,j} \ . \tag{A.9}$$

This equation is the completeness relation for the Legendre Polynomials on the discrete set of the collocation points $\{x_i\}$ and the condition of eq. (A.3) is fulfilled.

A.1 Generalized pseudo-spectral method to solve radial Schrödinger equation

In the following we consider a general radial Schrödinger equation

$$\frac{1}{2} \frac{d^2}{dr^2} \phi_l(r) + V_l(r) \phi_l(r) = E \phi_l(r) \ , \tag{A.10}$$

where the Potential $V_l = \frac{l(l+1)}{2r^2} + V_{ext} + 1/r$ includes the angular momentum part, and the wavefunction is $\Psi_l(\vec{x}) = \frac{\phi_l(r)}{r} Y_l^m(\Omega)$. In the following the angular momentum quantum number l will be omitted to simplify the notation. Since the potential $V(r)$ includes a repulsive Coulomb potential and the angular momentum part a typical problem with the numerical realization of

the Schrödinger equation lies in the choice of the grid. On the one hand the potential $V(x)$ exhibits a singularity at the origin $r = 0$, on the other hand it may be a long-range potential. The choice of an equidistant grid and an appropriate truncation of the r domain $[0, \infty)$ to some $[r_{min}, r_{max}]$ would result in a large number of grid points, which is computationally not favorable. To overcome this problem the domain $r \in [0, r_{max}]$ is mapped on the interval $x \in [-1, 1]$ and a pseudo-spectral method is applied, to create a non-equidistant grid. The mapping function is given by

$$r(x) = L\frac{1 + x}{1 - x + \alpha} \quad \text{where } \alpha = \frac{2L}{r_{max}} . \tag{A.11}$$

The grid points of the mapped domain x are chosen as the collocation points $\{x_i\}$ $i = 0, ..., N + 1$ of the pseudo-spectral method explained in section A. First we consider the mapping of the continuous Schrödinger equation. The radial wavefunction $\phi(r)$ is mapped on $\tilde{\phi}(x)$, the potential gets $\tilde{V}(x) = V(r(x))$. The mapped Schrödinger equation therefore reads

$$-\frac{1}{2}\left[-\frac{r''(x)}{r'(x)^3}\frac{d}{dx} + \frac{1}{r'(x)^2}\frac{d^2}{dx^2}\right]\tilde{\phi}(x) + \tilde{V}(x)\tilde{\phi}(x) = E\tilde{\phi}(x) . \tag{A.12}$$

For computational reasons it is convenient to symmetrize the Schrödinger equation by introducing the Ansatz $\tilde{\phi}(x) = \sqrt{r'(x)}f(x)$ [81, 83]. Eq. (A.12) with the mapping of eq. (A.11) then transforms to

$$-\frac{1}{2}\frac{1}{r'(x)}\frac{d^2}{dx^2}f(x) + \tilde{V}(x)r'(x)f(x) = Er'(x)f(x) . \tag{A.13}$$

In defining the function

$$A(x) = r'(x)f(x) = \sqrt{r'(x)}\tilde{\phi}(x) \tag{A.14}$$

we finally get the transformed Schrödinger equation

$$-\frac{1}{2}\frac{1}{r'(x)}\frac{d^2}{dx^2}\frac{1}{r'(x)}A(x) + \tilde{V}(x)A(x) = EA(x) . \tag{A.15}$$

The next step in the numerical realization of the eigenvalue problem is to discretize eq. (A.15) on the pseudo-spectral grid. According to eq. (A.7) and (A.8) the function $A(x)$ is approximated by the N-th order polynomial

$$A(x) \simeq \sum_{i=0}^{N} A(x_i)\, g_i(x), \tag{A.16}$$

121

where $A(x_i)$ is the vector representing the $A(x)$ at the the collocation points. Since the expansion of $A(x)$ is exact at the $(N-1)$ collocation points, the eigenvalue equation (A.15) evaluated at those points determines the exact values A_i. We arrive at the following linear matrix eigenvalue problem

$$-\frac{1}{2}\sum_{j=0}^{N}\frac{1}{r'(x_i)}\frac{d^2 g_j(x_i)}{dx^2}\frac{1}{r'(x_i)}A(x_j) + \sum_{j=0}^{N}\tilde{V}(x_i)A(x_j)\delta_{i,j} = E\sum_{j=0}^{N}A(x_j)\delta_{i,j}\ .$$

(A.17)

The derivatives of the cardinal functions $g_j(x)$ can be calculated. Introducing the matrix $d^{(2)}$ the derivatives get [81]

$$g_j''(x_i) = d_{i,j}^{(2)}\frac{P_N(x_i)}{P_N(x_j)}$$

(A.18)

with

$$d_{i,j}^{(2)} = -\frac{2}{(x_i - x_j)^2}\quad i \neq j,\ (i,j) \neq (0,N),\ (i,j) \neq (N,0)$$ (A.19)

$$d_{0,N}^{(2)} = d_{N,0}^{(2)} = \frac{N(N+1)-2}{4}$$ (A.20)

$$d_{j,j}^{(2)} = -\frac{N(N+1)}{3(1-x_j^2)}\quad j \neq N,\ j \neq 0$$ (A.21)

$$d_{0,0}^{(2)} = d_{N,N}^{(2)} = \frac{N(N+1)[N(N+1)-2]}{24}\ .$$ (A.22)

Defining the quantity

$$A_i := \frac{A(x_i)}{P_n(x_i)} = \frac{\sqrt{r'(x_i)}\tilde{\phi}(x_i)}{P_N(x_i)}.$$

(A.23)

the discretized radial Schrödinger equation finally becomes

$$\sum_{j=0}^{N}\left[-\frac{1}{2}\frac{1}{r'(x_i)}d_{i,j}^{(2)}\frac{1}{r'(x_j)} + \tilde{V}(x_i)\,\delta i,j\right]A_j = E\,A_i\ .$$

(A.24)

The discretized Schrödinger equation reduces to an eigenvalue problem of a symmetric real matrix for the quantities A_i. To include boundary conditions at x_0 or x_N the values of A_N and A_0 have to be specified and i in eq. (A.24) is restricted to $i = 1, ..., N - 1$. For Dirichlet boundary conditions we require $A_0 = A_N = 0$ and the sum in eq. (A.24) is truncated to the range $j = 1, 2, .., N - 1$.

Due to the special choice of the grid points, integrals over $\tilde{\phi}$ are especially easy to handle, using Lobatto's integral formula. The radial part of the

122

orthonormalization integral $\int d\Omega \int r^2 dr \Psi_{l,n}(\vec{r}) \Psi_{l',n'}(\vec{r})$ for example gets

$$\int_0^\infty dr \phi_{n,l}(r) \phi_{n',l'} = \int_{-1}^1 r'(x) \tilde{\phi}_{n,l}(x) \tilde{\phi}_{n',l'}(x) dx \simeq \frac{2}{N(N+1)} \sum_{i=0}^N A_i^{n,l} A_i^{n'l'} \ ,$$

$$(A.25)$$

where $A_i^{n,l} = \frac{\sqrt{r'(x_i)} \tilde{\phi}_{n,l}(x_i)}{P_N(x_i)}$. A general radial integral involving $\phi(r)$ and a function $f(r)$ is calculated by

$$\int_0^\infty dr \phi(r) f(r) = \int_{-1}^1 r'(x) \tilde{\phi}(x) f(r(x)) dx \simeq \sum_{i=0}^N w_i \sqrt{r'(x_i)} P_N(x_i) \, A_i \, f(r(x_i)) \ .$$

$$(A.26)$$

123

Appendix B

Spherical harmonics

B.1 Transformation of spherical coordinates from center of mass and relative coordinates to one-particle coordinates

The aim of this section is to review the coordinate transformation of spherical coordinates of the center-of mass and relative motion to single-particle spherical coordinates.

Following reference [148] we start out from the solid spherical harmonic of the center of mass system, which is defined through

$$\Upsilon_l^m(\vec{R}_{cm}) = R_{cm}^l Y_l^m(\Omega_{cm}), \tag{B.1}$$

where $\vec{R}_{cm} = \frac{\vec{r}_1 + \vec{r}_2}{2}$ and Y_l^m denotes the usual spherical harmonic. We want to express Υ_l^m as a function of $\vec{r}_1$ and $\vec{r}_2$. Defining

$$[Y_{l_1}(\Omega_1)Y_{l_2}(\Omega_2)]_{l,m} := \sum_{m_1,m_2} \langle l_1 l_2 m_1 m_2 | l m \rangle Y_{l_1}^{m_1}(\Omega_1) Y_{l_2}^{m_2}(\Omega_2) \tag{B.2}$$

and keeping in mind that Υ_l^m satisfies $\triangle_{cm}\Upsilon_l^m(R_{cm}, \Omega_{cm}) = 0$, and with fixed $\vec{r}_2$ $(\vec{r}_1)$ it also satisfies $\triangle_1 \Upsilon_l^m(R_{cm}, \Omega_{cm}) = 0$ $(\triangle_2 \Upsilon_l^m(R_{cm}, \Omega_{cm}) = 0)$, $\Upsilon_l^m(R_{cm}, \Omega_{cm})$ can be expanded in terms of $r_1^{l_1} r_2^{l_2} [Y_{l_1}(\Omega_1)Y_{l_2}(\Omega_2)]_{l,m}$. The expansion is given by

$$\Upsilon_l^m(R_{cm}, \Omega_{cm}) = \sum_{l_1, l_2 = 0}^{l} \delta_{l,l_1+l_2} G(l_1, l_2, l) r_1^{l_1} r_2^{l_2} [Y_{l_1}(\Omega_2)Y_{l_2}(\Omega_2)]_{l,m} , \tag{B.3}$$

where $G(l_1, l_2, l)$ are the expansion coefficients to be determined. The sum is restricted on l_1 and l_2 satisfying $l_1 + l_2 = l$, this is because $\Upsilon_l^m(R_{cm}, \Omega_{cm})$

is homogeneous of degree l in R_{cm}, and therefore also together in r_1 and r_2. Since the $G(l_1, l_2, l)$ are independent of Ω_1 and Ω_2, we choose $\theta_1 = \theta_2 = \phi_1 = \phi_2 = 0$ and therefore $\tan \theta_{cm} = 0$. Noting that $Y_l^m(0,0) = \delta_{m,0}\sqrt{\frac{2l+1}{4\pi}}$ eq. (B.3) becomes

$$R_{cm}^l \sqrt{\frac{2l+1}{4\pi}} = \sum_{l_1,l_2=0}^{l} \delta_{l,l_1+l_2} G(l_1, l_2, l) r_1^{l_1} r_2^{l_2} \langle l_1 l_2 00|l0\rangle \frac{\sqrt{(2l_1+1)(2l_2+1)}}{4\pi} .$$

(B.4)

In the special case of $\theta_1 = \theta_2 = \phi_1 = \phi_2 = 0$ we have $R_{cm} = \frac{r_1+r_2}{2}$ and with the explicit form of the Clebsch Gordon coefficients the expansion coefficients get

$$G(l_1, l_2, l) = \left(\frac{1}{2}\right)^l \sqrt{\frac{4\pi \cdot (2l+1)!}{(2l_2+1)!(2l_1+1)!}} .$$

(B.5)

Proceeding along similar lines we also get the expansion of the solid spherical harmonics as function of the relative coordinate $\vec{r} = \vec{r}_1 - \vec{r}_2$

$$\Upsilon_l^m(r, \Omega_{rel}) = \sum_{l_1,l_2} \delta_{l,l_1+l_2} r_1^{l_1} r_2^{l_2} g(l_1, l_2, l)[Y_{l_1}(\Omega_1), Y_{l_2}(\Omega_2)]_{l,m}$$

(B.6)

with

$$g(l_1, l_2, l) = (-1)^{l-l_1} \sqrt{\frac{4\pi \cdot (2l+1)!}{(2l_1+1)!(2l_2+1)!}} .$$

(B.7)

125

Appendix C

Matrix elements in CI calculation

C.1 Coulomb matrix elements

We want to calculate the coulomb matrix elements between Kohn-Sham configuration states. For spin-singlet states, the symmetric coordinate part of the configuration state functions is defined as [156]

$$
|n_1 l_1 n_2 l_2, L0\rangle := \begin{cases} \frac{1}{\sqrt{2}} \sum_m [\langle l_1 m \, l_2 -m | L0 \rangle \, |n_1 l_1 m\rangle_1 \otimes |n_2 l_2 -m\rangle_2 & n_1 \neq n_2 \\ \quad + \langle l_2 -m \, l_1 \, m | L0 \rangle \, |n_2 l_2 -m\rangle_1 \otimes |n_1 l_1 m\rangle_2] & \text{or } l_1 \neq l_2 \\[2mm] \sum_m \langle l_1 l_1 m \, -m | L0 \rangle \, |n_1 l_1 m\rangle_1 \otimes |n_1 l_2 -m\rangle_2 & n_1 = n_2 \\ & \text{and } l_1 = l_2 \,, \end{cases} \tag{C.1}
$$

where $|langler|nlm\rangle = \frac{\phi_n^l}{r} Y_l^m(\Omega)$ denotes the Kohn-Sham orbital. In the case of spin-triplet states, the coordinate part of the Kohn-Sham configuration state functions has to be antisymmetric with respect to particle exchange and reads

$$
|n_1 l_1 n_2 l_2, L0\rangle := \begin{cases} \frac{1}{\sqrt{2}} \sum_m [\langle l_1 m \, l_2 -m | L0 \rangle \, |n_1 l_1 m\rangle_1 \otimes |n_2 l_2 -m\rangle_2 & n_1 \neq n_2 \\ \quad + \langle l_2 -m \, l_1 \, m | L0 \rangle \, |n_2 l_2 -m\rangle_1 \otimes |n_1 l_1 m\rangle_2] & \text{or } l_1 \neq l_2 \\[2mm] 0 & n_1 = n_2 \text{ and } l_1 = l_2 \end{cases} \tag{C.2}
$$

Only different configurations are allowed in the spin-triplet case. Coulomb matrix elements between configuration state functions

$$
\left\langle n_1 l_1 n_2 l_2, L0 \left| \frac{1}{|\vec{r}_1 - \vec{r}_2|} \right| n_3 l_3 n_4 l_4, L'0 \right\rangle.
$$

126

therefore involve the basic coulomb-matrix elements

$$\left\langle n_1 l_1 m_1 n_2 l_2 - m_1 \left| \frac{1}{|\vec{r}_1 - \vec{r}_2|} \right| n_3 l_3 m_3 n_4 l_4 - m_3 \right\rangle.$$

Using the identity

$$\frac{1}{|\vec{r}_1 - \vec{r}_2|} = \sum_{l=0}^{\infty} \sum_{m=-l}^{l} \frac{4\pi}{2l+1} \frac{r_<^l}{r_>^{l+1}} Y_l^m(\Omega_1) Y_l^{m*}(\Omega_2) \qquad (C.3)$$

with $r_< = \min(r_1, r_2)$ and $r_> = \max(r_1, r_2)$ one arrives at

$$\left\langle n_1 l_1 m_1 n_2 l_2 - m_1 \left| \frac{1}{|\vec{r}_1 - \vec{r}_2|} \right| n_3 l_3 m_3 n_4 l_4 - m_3 \right\rangle =$$

$$\sum_{l=l_{min}}^{l_{max}} \sum_{m=-l}^{l} (-1)^m F_l(n_1 l_1 n_2 l_2 n_3 l_3 n_4 l_4) \sqrt{(2l_1+1)(2l_2+1)(2l_3+1)(2l_4+1)} \cdot$$

$$\begin{pmatrix} l_1 & l_3 & l \\ 0 & 0 & 0 \end{pmatrix} \begin{pmatrix} l_1 & l_3 & l \\ -m_1 & m_3 & m \end{pmatrix} \begin{pmatrix} l_2 & l_4 & l \\ 0 & 0 & 0 \end{pmatrix} \begin{pmatrix} l_2 & l_4 & l \\ m_1 & -m_3 & -m \end{pmatrix} \text{(C.4)}$$

with $l_{min} = \max(|l_1 - l_3|, |l_2 - l_4|)$ and $l_{max} = \min(l_1 + l_3, l_2 + l_4)$ and

$$\begin{pmatrix} l_1 & l_2 & l \\ m_1 & m_2 & m \end{pmatrix} = (-1)^{l_1 + l_2 - m} \frac{1}{\sqrt{2l+1}} \langle l_1 m_1 l_2 m_2 | l - m \rangle \qquad (C.5)$$

denotes a Wigner-3j-symbol. Due to the properties of the Wigner-3j-symbols reduce the number of addend, only addenda for which $l_1 + l_3 + l$ =even, $l_2 + l_4 + l$ =even, $m_1 = m_3 + m$ are unequal to zero. The purely radial integrals are given by

$$F_l(n_1 l_1 n_2 l_2 n_3 l_3 n_4 l_4) = \iint dr_1 dr_2 \phi_{n_1}^{l_1}(r_1) \phi_{n_2}^{l_2}(r_2) \phi_{n_3}^{l_3}(r_1) \phi_{n_4}^{l_4}(r_2) \frac{r_<^l}{r_>^{l+1}} . \qquad (C.6)$$

In principle eq. (C.6) are easy to solve by means of the pseudo-spectral method. One splits the integral into

$$\int_0^{r_{max}} dr_1 \int_0^{r_{max}} dr_2 \frac{r_<^l}{r_>^{l+1}} \ldots = \int_0^{r_{max}} dr_1 \int_0^{r_1} dr_2 \frac{r_1^l}{r_2^{l+1}} \ldots + \int_0^{r_{max}} dr_1 \int_{r_1}^{r_{max}} dr_2 \frac{r_2^l}{r_1^{l+1}} \ldots$$

$$\text{(C.7)}$$

In the pseudo-spectral method one therefore has to calculate two double sums. Calculating matrix elements of a big number of configurations and taking all the angular momentum quantum numbers l into account is a lengthy task. We therefore propose a numerical method to calculate the integrals of

127

eq. (C.6) in more efficient way. Our numerically faster algorithm tries to split the double sum into a product of single sums. The term coupling both sums is $\frac{r_<^l}{r_>^{l+1}}$. In the numerical realization we discretize space into set of points $\{r_i, i = 1, ..., N\}$ in the radial direction. Therefore $\frac{r_<^l}{r_>^{l+1}}$ can be seen as a set of real symmetric matrices $A(l)$:

$$A_{i,j}(l) = \begin{cases} \frac{r_i^l}{r_j^{l+1}} & i \le j \\ \frac{r_j^l}{r_i^{l+1}} & i > j \end{cases} \qquad (C.8)$$

Diagonalizing these matrices

$$A_{i,j}(l) = \sum_{k=1}^{N} a_k(l) v_i^k(l) v_j^k(l) \qquad (C.9)$$

the double sum can be reduced to N single sums, suitable to be numerically parallelized. We noticed that with increasing k the eigenvalues $a_k(l)$ get smaller and smaller. The sum in eq. (C.9) therefore can be truncated at a value $n < N$, further increasing the efficiency of the program. The total Coulomb matrix elements of the symmetric (spin singlet) or antisymmetric (triplet) configuration states can then be easily constructed. In the case of mutually different configurations $(n_1, l_1) \ne (n_2, l_2)$ and $(n_3, l_3) \ne (n_4, l_4)$ the matrix elements only unequal to zero if $l1 + l2 + l3 + l4 - L - L' =$ even and yields

$$\left\langle n_1 l_1 n_2 l_2, L0 \left| \frac{1}{|\vec{r}_1 - \vec{r}_2|} \right| n_3 l_3 n_4 l_4, L'0 \right\rangle =$$

$$\sum_{m,m'} \langle l_1 l_2 m \, -m | L0 \rangle \langle l_3 l_4 m' \, -m' | L'0 \rangle \left\langle n_1 l_1 m n_2 l_2 \, -m \left| \frac{1}{|\vec{r}_1 - \vec{r}_2|} \right| n_3 l_3 m' n_4 l_4 \, -m' \right\rangle \pm$$

$$\langle l_2 l_1 \, -mm | L0 \rangle \langle l_3 l_4 m' \, -m' | L'0 \rangle \left\langle n_2 l_2 \, -m n_1 l_1 m \left| \frac{1}{|\vec{r}_1 - \vec{r}_2|} \right| n_3 l_3 m' n_4 l_4 \, -m' \right\rangle \qquad (C.10)$$

where the exchange term comes with a $+$ sign in the spin-singlet case and is subtracted in the spin-triplet case. In the case of only one pair of equal configurations (only for singlet) $(n_1, l_1) = (n_2, l_2)$ or $(n_3, l_3) = (n_4, l_4)$ the result of eq. (C.10) has according to the normalization of eq. (C.1) be multiplied by a factor $1/\sqrt{2}$, in the case that $(n_1, l_1) = (n_2, l_2)$ and $(n_3, l_3) = (n_4, l_4)$ by a factor $1/2$. In both cases the exchange term becomes equal to the direct term.

C.2 Matrix elements of one-particle observables

The matrix-elements of single-particle operators $\hat{O}$ between Kohn-Sham configuration state functions are basically one-particle matrix elements. They are equal to zero if both configuration state-functions have not at least one common configuration. Assuming that $(n_1, l_1) \neq (n_2, l_2)$ and $(n_1, l_1) \neq (n_4, l_4)$ we only get matrix-elements different from zero if $l_2 + l_3 + L - L' =$ even and get

$$\left\langle n_1 l_1 n_2 l_2, L0 \left| \sum_{i=2,3} \hat{O}_i \right| n_1 l_1 n_4 l_4, L'0 \right\rangle =$$

$$\sum_m \langle n_2 l_2 - m | \hat{O} | n_3 l_3 - m \rangle \langle l_1 m l_2 - m | L0 \rangle \langle l_1 m l_3 - m | L'0 \rangle \ . \quad (C.11)$$

Further selection rules depend on the one-particle operator in play. In the spin-singlet case of one pair of equal configurations $(n_1, l_1) = (n_2, l_2)$ and $(n_1, l_1) \neq (n_4, l_4)$ the result of eq. (C.11) has to be multiplied by $\sqrt{2}$, due to the normalization of the symmetrized configuration state functions. In the case of $(n_1, l_1) = (n_2, l_2) = (n_4, l_4)$ the factor becomes 2.

The dipole matrix element between two Kohn-Sham orbitals is calculated as follows:

$$\langle n_1 l_1 m_1 | z | n_2 l_2 m_2 \rangle = (-1)^{m_1} \sqrt{(2l_1 + 1)(2l_2 + 1)} \begin{pmatrix} l_1 & l_2 & 1 \\ -m_1 & m_1 & 0 \end{pmatrix} \cdot$$

$$\begin{pmatrix} l_1 & l_2 & 1 \\ 0 & 0 & 0 \end{pmatrix} \int dr \ r \ \phi_{n_1}^{l_1 *}(r) \ \phi_{n_2}^{l_2}(r) \quad (C.12)$$

Selection rules for the dipole-matrix element therefore are $|l_1 - l_2| = 1$. Matrix-elements of the spherical-symmetric exchange correlation potential are straight- forward to calculate and not given explicitly here.

Appendix D

CI analysis of exact states

In the following we present some results of the expansion of some exact eigenstates of the two-electron parabolic quantum dot in the basis of configuration-state functions of Kohn-Sham orbitals introduced in chapter 8. We show two cases of weak ($\omega = 1$) and strong ($\omega = 0.01$) correlated systems. The following tables show the overlap of exact-wavefunctions with products of Kohn-Sham orbitals $|n_i l_i m_i s_i n_j l_j m_j s_j\rangle$, the basic ingredient to calculate the overlap with configuration state-functions. We performed the 6-dimensional integrals partly analytically (angular momentum part). The results stand in perfect agreement with a configuration interaction calculation in the basis of Kohn-Sham configuration-state functions.

The tables are organized as follows. In the first column the quantum numbers of the considered product wavefunction $|n_i l_i m_i s_i n_j l_j m_j s_j\rangle$ are listed. The second column shows the overlap integral c_i of this wavefunction with the exact wave-function $|\Phi\rangle = |n_{cm} l_{cm} n_{rel} l_{rel}\rangle$. Since we are considering spin singlet states, each product wavefunction with at least one different pair of quantum numbers possesses a symmetric partner of exchanged quantum numbers which has the same overlap with $|\Phi\rangle$. This is accounted for through the multiplicity a_i. The third column gives the weight of the configuration which is defined by $\mu_i = \sum_i a_i \cdot c_i^2$ where the sum extends over all states belonging to this configuration. The fourth column shows the sum of weights over all configurations considered so far. The last column gives the energy of the configuration within LSDA-SIC which will be defined in the following. A rigorous extension of DFT to higher excited states leaves the Kohn-Sham regime (see the review article [157] and references therein). Speaking of excitation energies in DFT one has to specify the approximation for calculating them. We are solving the ground-state DFT problem, finding the occupied ground-state Kohn-Sham orbital Φ_0 and vacant (virtual) excited Kohn-Sham spin-orbitals $\Phi_{i,\sigma}$ (i stands for configuration $n_i l_i$) with

spin-density $n_{i,\sigma} = |\Phi_{i,\sigma}|^2$. We define the energy of a certain configuration $n_1 l_1 n_2 l_2$ of total density $n = n_{1,\uparrow} + n_{2,\downarrow}$ through the energy functional

$$E[n_{1,\uparrow}, n_{2,\downarrow}] = \int dr^3 \left(-\frac{1}{2}\vec{\nabla}^2 + \frac{\omega^2}{2}\vec{r}^2 \right) n(\vec{r}) + J[n] + E_{xc}^{SIC}[n_{1,\uparrow}, n_{2,\downarrow}] , \quad (D.1)$$

where J and E_{xc}^{SIC} are given by eq. (3.7) and (3.8).

Table D.1: $n_{cm}l_{cm}n_{rel}l_{rel}$: $0s0s$, $\omega = 1$, $E_{exact} = 3.731$

$n_1 l_1 m_1 n_2 l_2 m_2$	c_i	a_i	weight	$\sum a_i |c_i|^2$	energy
0 s 0 0 s 0	0.99295	1	0.98595	0.98595	3.7195
1 p 0 1 p 0	-0.06096	1			
1 p 1 1 p -1	-0.06096	2	0.01115	0.99710	5.5446
2 s 0 0 s 0	-0.00019	2	$3.6 \cdot 10^{-8}$	0.99710	5.5776

Table D.2: $n_{cm}l_{cm}n_{rel}l_{rel}$: $1p0s$, $\omega = 1$, $E_{exact} = 4.731$

$n_1 l_1 m_1 n_2 l_2 m_2$	c_i	a_i	weight	$\sum a_i |c_i|^2$	energy
0 s 0 1 p 0	0.70040	2	0.98112	0.98112	4.6051
1 p 0 2 d 0	-0.05006	2			
1 p 1 2 d -1	0.04335	4	0.01253	0.99365	6.4911
1 p 0 2 s 0	0.03482	2	0.00243	0.99608	6.4992
0 s 0 3 p 0	-0.02153	2	0.00092	0.99700	6.5211

Table D.3: $n_{cm}l_{cm}n_{rel}l_{rel}$: $2s0s$, $\omega = 1$, $E_{exact} = 5.731$

$n_1 l_1 m_1 n_2 l_2 m_2$	c_i	a_i	weight	$\sum a_i |c_i|^2$	energy
0 s 0 2 s 0	0.49409	2	0.48824	0.48824	5.5776
1 p 0 1 p 0	-0.40092	1			
1 p 1 1 p -1	-0.40092	2	0.48222	0.97046	5.5446
2 d 0 2 d 0	0.05049	1			
2 d 1 2 d -1	0.05049	2			
2 d 2 2 d -2	0.05049	2	0.01275	0.98321	7.4560
0 s 0 0 s 0	-0.07328	1	0.00537	0.98858	3.7195
1 p 0 3 p 0	-0.02645	2			
1 p 1 3 p -1	-0.02645	4	0.00429	0.99287	7.4661
2 s 0 2 s 0	0.05016	1	0.00252	0.99539	7.4933
4 s 0 0 s 0	-0.02967	2	0.00167	0.99706	7.5033

Table D.4: $n_{cm}l_{cm}n_{rel}l_{rel}$: $2d0s$, $\omega = 1$, $E_{exact} = 5.731$

$n_1 l_1 m_1 n_2 l_2 m_2$	c_i	a_i	weight	$\sum a_i |c_i|^2$	energy
1 p 0 1 p 0	0.57181	1			
1 p 1 1 p -1	0.28591	2	0.49046	0.49046	5.5446
0 s 0 2 d 0	0.49368	2	0.48744	0.97790	5.5241
1 p 0 3 f 0	-0.04137	2			
1 p 1 3 f -1	0.03378	4	0.00798	0.98588	7.4459
2 s 0 2 d 0	0.04947	2	0.0049	0.99078	7.4494

132

Table D.5: $n_{cm}l_{cm}n_{rel}l_{rel}$: $0s0s$, $\omega = 0.01$, $E_{exact} = 0.079205$

$n_1 l_1 m_1 n_2 l_2 m_2$	c_i	a_i	weight	$\sum a_i|c_i|^2$	energy
0 s 0 0 s 0	0.82964	1	0.68830	0.68830	0.08079
1 p 0 1 p 0	-0.29460	1			
1 p 1 1 p -1	-0.29460	2	0.26037	0.94867	0.09193
1 p 0 3 p 0	-0.07192	2			
1 p 1 3 p -1	-0.07192	4	0.03103	0.9797	0.10788
2 s 0 2 s 0	-0.09203	1	0.00847	0.98817	0.10909
2 d 0 2 d 0	0.03211	1			
2 d 1 2 d -1	0.03211	2			
2 d 2 2 d -2	0.03211	2	0.00516	0.99333	0.10632
2 d 0 4 d 0	0.01165	2			
2 d 1 4 d -1	0.01165	4			
2 d 2 2 d -2	0.01165	4	0.00136	0.99469	0.12355
0 s 0 4 s 0	-0.01819	2	0.00066	0.99535	0.11067
0 s 0 2 s 0	0.01189	2	0.00028	0.99563	0.09484
3 p 0 3 p 0	-0.00838	1			
3 p 1 3 p -1	-0.00838	2	0.00021	0.99584	0.12308

Table D.6: $n_{cm}l_{cm}n_{rel}l_{rel}$: $1p0s$, $\omega = 0.01$, $E_{exact} = 0.08921$

$n_1 l_1 m_1 n_2 l_2 m_2$	c_i	a_i	weight	$\sum a_i|c_i|^2$	energy
0 s 0 1 p 0	0.537408	2	0.57761	0.57761	0.08568
1 p 0 2 d 0	-0.23906	2			
1 p 1 2 d -1	0.20703	4	0.28575	0.86336	0.10646
2 s 0 1 p 0	0.166333	2	0.05533	0.91869	0.09956
3 p 0 2 d 0	-0.074606	2			
3 p 1 2 d -1	0.0646107	4	0.02783	0.94652	0.11488
0 s 0 3 p 0	-0.112845	2	0.02547	0.97199	0.08681
3 f 0 2 d 0	0.030975	2			
3 f 1 2 d -1	-0.029204	4			
3 f 2 2 d -2	0.023088	4	0.00746	0.97945	0.11418
1 p 0 4 d 0	-0.036774	2			
1 p 1 4 d -1	0.031847	4	0.00676	0.98621	0.11602
2 s 0 3 p 0	-0.044932	2	0.00404	0.99025	0.11564
3 p 0 4 d 0	-0.006019	2			
3 p 1 4 d -1	-0.005213	2	0.00013	0.99038	0.13139

Table D.7: $n_{cm}l_{cm}n_{rel}l_{rel}$: $2d0s$, $\omega = 0.01$, $E_{exact} = 0.09921$

$n_1 l_1 m_1 n_2 l_2 m_2$	c_i	a_i	weight	$\sum a_i|c_i|^2$	energy
1 p 0 1 p 0	0.440042	1			
1 p 1 1 p -1	0.220021	2	0.29045	0.29045	0.09193
0 s 0 2 d 0	+0.333194	2	0.22204	0.51249	0.09188
1 p 0 3 f 0	-0.193443	2			
1 p 1 3 f -1	0.157945	4	0.17463	0.68712	0.10646
2 s 0 2 d 0	0.226296	2	0.10242	0.78954	0.10582
2 d 0 2 d 0	-0.170619	1			
2 d 1 2 d -1	0.085310	2			
2 d 2 2 d -2	0.170619	2	0.10189	0.89143	0.10632
0 s 0 4 d 0	-0.149903	2	0.04494	0.93637	0.10904
3 p 0 3 f 0	-0.074242	2			
3 p 1 3 f -1	0.060619	4	0.02572	0.96209	0.12242
2 d 0 4 d 0	-0.036183	2			
2 d 1 4 d -1	0.018092	4			
2 d 2 4 d -2	0.036183	4	0.00916	0.97125	0.12355
4 s 0 2 d 0	0.056297	2	0.00633	0.97758	0.12315
4 g 0 2 d 0	0.029041	2			
4 g 1 2 d -1	-0.026511	4			
4 g 2 2 d -2	0.018746	4	0.00591	0.98349	0.12224
5 p 0 3 f 0	-0.024457	2			
5 p 1 3 f -1	0.019969	4	0.00279	0.98628	0.12242
2 s 0 4 d 0	-0.035131	2	0.00247	0.98875	0.12333
4 g 0 4 d 0	0.010567	2			
4 g 1 4 d -1	-0.009647	4			
4 g 2 4 d -2	-0.000782	4	0.00078	0.98953	0.13968
1 p 0 3 p 0	0.014367	2			
1 p 1 3 p -1	0.007183	4	0.00062	0.99015	0.10788
3 p 0 3 p 0	-0.018949	1			
3 p 1 3 p -1	-0.009474	2	0.00054	0.99069	0.12308
4 s 0 4 d 0	-0.014405	2	0.00042	0.99111	0.14006

Appendix E

The different quantum numbers of the harmonic oscillator

In the following we are considering the problem of a single electron in a three-dimensional harmonic potential well. The Schrödinger equation

$$\left\{ -\frac{\vec{\nabla}^2}{2m} + \frac{m\omega^2}{2}\vec{r}^2 \right\} \Psi(\vec{r}) = E\Psi(\vec{r}) \tag{E.1}$$

can be separated either in kartesian coordinates or in spherical coordinates. This gives rise to two different sets of eigenfunctions pertaining to the energy level $E_n = \omega\left(n + \frac{3}{2}\right)$ characterized either through the kartesian quantum numbers $|n_x, n_y, n_z\rangle$ with $n_1 + n_2 + n_3 = n$ or states due to a separation in spherical coordinates of well defined angular momentum $|n, l, m\rangle$. The question is how those states are interrelated. We have to find a unitary transformation within subspace of energy E_n to connect those two representations. In the case of separation into kartesian coordinates the quantum numbers n_1, n_2, n_3 denote the numbers of oscillator quanta in x, y and z direction, i.e.

$$a_i^\dagger a_i |n_1, n_2, n_3\rangle = n_i |n_1, n_2, n_3\rangle \quad i = 1, .., 3, \tag{E.2}$$

where $a_i := \frac{\sqrt{m\omega}\hat{x}_i + i\hat{p}_i}{\sqrt{2m\omega}}$ $(a_i^\dagger = \frac{\sqrt{m\omega}\hat{x}_i - i\hat{p}_i}{\sqrt{2m\omega}})$ denotes the anihilation (creation) operator in i-direction and $H|n_1, n_2, n_3\rangle = \omega\left(a_1^\dagger a_1 + a_2^\dagger a_2 + a_3^\dagger a_3 + \frac{3}{2}\right)|n_1, n_2, n_3\rangle = E_n|n_1, n_2, n_3\rangle$ The separation in spherical coordinates leads to eigenstates of angular momentum l and angular momentum projection m:

$$H|n, l, m\rangle = E_n|n, l, m\rangle \tag{E.3}$$
$$L^2|n, l, m\rangle = l(l+1)|n, l, m\rangle \tag{E.4}$$
$$L_3|n, l, m\rangle = m|n, l, m\rangle . \tag{E.5}$$

According to Moshinsky [148] the state $|n, l, m\rangle$ can be constructed from the vacuum state by application of the cartesian creation operators through

$$|n, l, m\rangle = A_{l,n}(\vec{a}^\dagger \cdot \vec{a}^\dagger)^{\frac{n-l}{2}} \Upsilon_{l,m}(\vec{a^\dagger})|0\rangle , \qquad (E.6)$$

with the notation $(\vec{a}^\dagger \cdot \vec{a}^\dagger) := (\sum_{i=1}^3 a_i^\dagger a_i)$. $A_{l,n}$ is a normalization constant independent of m given by

$$A_{l,n} = \sqrt{\frac{4\pi}{(n+l+1)!!(n-l)!!}} . \qquad (E.7)$$

$\Upsilon_{l,m}(\vec{r})$ denotes the solid spherical harmonic

$$\Upsilon_{l,m}(\vec{r}) = r^l Y_l^m(\theta, \phi) . \qquad (E.8)$$

$\Upsilon_{l,m}$ as a function of $a_i^\dagger$ has to be understood as an expansion of operators a_i. In spherical coordinates we have

$$\Upsilon_{l,m}(\vec{r}) = r^l (-1)^m \sqrt{\frac{2l+1}{4\pi}} \sqrt{\frac{(l-m)!}{(l+m)!}} \ e^{im\phi} P_l^m(cos\theta) . \qquad (E.9)$$

Using the explicit expansion of P_l^m and turning into cartesian coordinates we get

$$\Upsilon_{l,m} = (\vec{r})(-1)^m \sqrt{\frac{2l+1}{4\pi}} \sqrt{\frac{(l-m)!}{(l+m)!}} 2^{-l} \cdot (x+iy)^m \cdot$$

$$\sum_{k=0}^{\left[\frac{l-m}{2}\right]} (-1)^k \frac{(2l-2k)!}{(l-k)!k!(l-m-2k)!} z^{l-m-2k} r^{2k} . \qquad (E.10)$$

We therefore get explicitly

$$|n, l, m\rangle = (-1)^m \sqrt{\frac{2l+1}{(n+l+1)!!(n-l)!!}} \sqrt{\frac{(l-m)!}{(l+m)!}} 2^{-l}(a_1^\dagger + ia_2^\dagger)^m \cdot$$

$$\sum_{k=0}^{\left[\frac{l-m}{2}\right]} \frac{(-1)^k(2l-2k)!}{(l-k)!k!(l-m-2k)!}(a_3^\dagger)^{l-m-2k}(\vec{a}^\dagger \cdot \vec{a}^\dagger)^{k+\frac{n-l}{2}}|0\rangle \quad (E.11)$$

136

Bibliography

[1] P. Lambropoulos, P. Maragakis, J. Zhang, Physics Rep. **305**, 203 (1998).

[2] D.N. Fittinghoff, P.R. Bolton, B. Chang, K.C. Kulander, Phys. Rev. Lett. **69**, 2642 (1992).

[3] A.D. Bandrauk, H. Yu, Phys. Rev. A **59** 539 (1999).

[4] D.G. Lappas, R. van Leeuwen, J. Phys. B: At. Mol. Opt. Phys. **31**, L249 (1998).

[5] E. Runge, E. K. U. Gross, Phys. Rev. Lett. **52**, 997 (1984).

[6] M. Petersilka, E.K.U. Gross, Laser Physics **9**, 105 (1999).

[7] N.T. Maitra, K. Burke, H. Appel, E.K.U. Gross, R. van Leeuwen, Rev. Mod. Quant. Chem.,*A Celebration of the Contributions of R.G. Parr* (2001).

[8] K. Burke, E.K.U. Gross, it A Guided Tour of Time-dependent Density Functional Theory, Procedings of Merensee Summer School, (Springer, 1997).

[9] R. van Leeuwen, Phys. Rev. Lett. **80**, 1280 (1998).

[10] R. van Leeuwen, Phys. Rev. Lett. **82**, 3863 (1999).

[11] P. Hohenberg, W. Kohn, Phys. Rev. **136**, B864 (1964).

[12] W. Kohn, L.J. Sham, Phys. Rev. **140**, A1133 (1965).

[13] W. Kohn, Rev. Mod. Phys. **71**, 1253 (1998).

[14] R. G. Parr, W. Yang, *Density-Functional Theory of Atoms and Molecules*, (Oxford University Press, 1989)

[15] T. Kato, Commun. Pure Appl. Math. **10**, 151 (1957).

[16] J.C. Kimball, Phys. Rev. A **7**, 1648 (1973).

[17] A.K. Rajagopal, J.C. Kimball, M. Banerjee, Phys. Rev. B **18**, 2339 (1978).

[18] K. Burke, J.C. Angulo, J.P. Perdew, Phys. Rev. A **50**, 297 (1994).

[19] K. Husimi, Proc. Phys. Math. Soc. Japan **22**, 264 (1940).

[20] R. McWeeny, Rev. Mod. Phys. **32**, 335 (1960).

[21] O. Gunnarsson, B.I. Lundqvist, J.W. Wilkins, Phys. Rev. B **10**, 1319 (1974).

[22] O. Gunnarsson, B. I. Lundqvist, Phys. Rev. B **13**, 4274 (1976).

[23] O.Gunnarsson, M. Jonson, B.I. Lundqvist, Phys. Rev. B **20**, 3136 (1979).

[24] Y. Wang, J.P. Perdew, Phys. Rev. B **44**, 13298 (1991).

[25] J.P. Perdew, Y. Wang, Phys. Rev. B **45**, 13244 (1992).

[26] J.P. Perdew, Y. Wang, Phys. Rev. B **46**, 12947 (1992).

[27] A.D. Becke, J. Chem. Phys. **88**, 1053 (1987).

[28] M. Slamet, V. Sahni, Phys. Rev. A **51**, 2815 (1995).

[29] P. Gori-Giorgi, F. Sacchetti, G. B. Bachelet, Phys. Rev. B **61**, 7353 (2000).

[30] P. Gori-Giorgi, J.P. Perdew, Phys. Rev. B **66**, 165118 (2002).

[31] R. Colle, O. Salvetti, Theor. Chim. Acta **37**, 329 (1975).

[32] C. Lee, W. Yang, R.G. Parr, Phys. Rev. B **37**, 785 (1988).

[33] Y. Imamura, G.E. Scuseria, J. Chem. Phys. **116**, 6458 (2002).

[34] Y. Imamura, G.E. Scuseria, J. Chem. Phys. **118**, 2464 (2003).

[35] R. Singh, L. Massa, V. Sahni, Phys. Rev. A **60**, 4135 (1999).

[36] M. Taut, Phys. Rev. A **53**, 3143 (1996).

[37] R.J. Magyar, W. Terilla, K. Burke, J. Chem. Phys. **119**, 696 (2003).

[38] N.R. Kestner, O. Sinanoglu, Phys. Rev. **128**, 2687 (1962).

[39] M. Taut, Phys. Rev. A **48**, 3561 (1993).

[40] P. M. Laufer, J. B. Krieger, Phys. Rev. A **33**, 1480 (1986).

[41] M. Taut, A. Ernst, H. Eschrig, J.Phys. B: At. Mol. Opt. Phys. **31**, 2689 (1998).

[42] C. Yannouleas, U. Landman, Phys. Rev. Lett. **85**, 1726 (2000).

[43] D.P. O'Neill, P.M.W. Gill, Phys. Rev. A **68**,22505 (2003).

[44] Z. Qian, V.Sahni, Phys. Rev. A **57**, 2527 (1998)

[45] J.-L. Zhu, Z.-Q. Li, J.-Z. Yu, K. Ohno, Y. Kawazoe, Phys. Rev. B **55**, 15819 (1997).

[46] J. Ciosloski, K. Pernal, J. Chem. Phys. **113**, 8434 (2000).

[47] U. Schwengelbeck, Phys. Lett. A **253**, 168 (1999).

[48] I. D'Amico, G. Vignale, Phys. Rev. B **59**, 7876 (1999).

[49] D.A. Telnov, S.-I Chu, Phys. Rev. A **63**, 12514 (2000).

[50] P. Hessler, J. Park, K. Burke, Phys. Rev. Lett. **82**,378 (1999).

[51] P. Hessler, N. T. Maitra, K. Burke, J.Chem.Phys. **117**, 72 (2002).

[52] A. K. Dhara, S. V. Lawande, Phys. Rev. A **30**,560 (1984).

[53] R. P. Feynman, A. R. Hibbs, *Quantum Mechanics and Path Integrals*, (M cGraw-Hill Book Company, 1965) p. 64

[54] A. Samanta, S. K. Ghosh, Phys. Rev. A **42**, 1178 (1990).

[55] D.V. Kulakovski, A.M. Popov, Laser Physics **10**, 967 (2000).

[56] W. Que, Phys. Rev. B **45**, 11036 (1992).

[57] P. Bonche, S.E. Koonin, J.W. Negele Phys. Rev. C **13** 1226 (1976).

[58] J.J. Griffin, P.C. Lichtner, M. Dworzecka, Phys. Rev. C **21** 1351 (1980).

[59] J. Hubbard, Phys. Rev. Lett. **3**, 77 (1959).

[60] S. Levit, Phys. Rev. C **21**, 1594 (1980).

[61] S. Levit, J.W. Negele, Z. Paltiel, Phys. Rev. C **21**, 1603 (1980).

[62] S. Levit, J.W. Negele, Z. Paltiel, Phys. Rev. C **22**, 1979 (1980).

[63] Y. Alhassid, S.E. Koonin, Phys. Rev. C **23**, 1590 (1981).

[64] K.R. Sandhya Devi, S.E. Koonin, Phys. Rev. Lett. **47**, 27 (1981).

[65] Y. Alhassid, B. Müller, S. E. Koonin, Phys. Rev. C **23**, 487 (1981).

[66] T. Troudet, S.E. Koonin, Phys Rev. C **28**, 1465 (1983).

[67] J. W. Negele, Rev. Mod. Phys. **54**, 913 (1982).

[68] J.P. Blaizot, H. Orland, Phys. Rev. C **24**, 1740 (1981).

[69] Y.N. Demkov, *Variational principles in the theory of collisions* (Pergamon Press, Oxford 1963)

[70] J.P. Blaizot, G. Ripka, Phys. Lett. B **105**, 1 (1981).

[71] R. Balian, M. Veneroni, Annals of Phys. **281**, 65 (2000).

[72] B. Gazdy, D.A. Micha, Phys. Rev. A **33**, 4446 (1986).

[73] D.A. Micha, B. Gazdy, Phys. Rev. A **36**, 539 (1987).

[74] B. Gazdy, D.A. Micha, Phys. Rev. A **36**, 546 (1987).

[75] A. Messiah, *Quantum Mechanics Volume II*, (North Holland Publishing Company, Amsterdam, 1961)p. 722 ff

[76] L.V.Keldysh, Sov. Phys. JETP **20**, 1018 (1965).

[77] V. Peuckert, J.Phys.C:Solid State Phys. **9**, 809 (1976).

[78] V. Peuckert, J.Phys.C:Solid State Phys. **11**, 4945 (1978).

[79] R. van Leeuwen, Int. J. Mod. Phys. B **15**, 1969 (2001).

[80] L.D. Landau, E.M. Lifschitz, *Lehrbuch der theoretischen Physik, Band 10 Physikalische Kinetic*, (Akademie Verlag, Berlin 1983)

[81] J.Wang, S.-I Chu,C.Laughlin, Phys. Rev. A **50**, 3208 (1994).

[82] S.-I Chu, Chem. Phys. Lett. **167**, 155 (1990).

[83] G.Yao, S.-I Chu, Chem. Phys. Lett. **204**, 381 (1993).

[84] M. Abramowitz, I.A. Stegun, *Handbook of MathematicalFunctions*, (Dover Publications, 1965)

[85] B. Fornberg, *A practical guide to pseudospectral methods*, (Cambridge University Press,1996)

[86] X. M. Tong, S. I. Chu, Chem. Phys. **217**, 119 (1997).

[87] D.A.Telnov, S.-I Chu, Phys. Rev. A **59**, 2864 (1999).

[88] J. P. Perdew, A. Zunger, Phys. Rev. B **23**, 5048 (1982).

[89] J. D. Talman, W. F. Shadwick, Phys. Rev. A **14**, 36 (1976).

[90] J. B. Krieger, Y. Li, G. J. Iafrate, Phys. Rev. A **45**, 101 (1992).

[91] J. B. Krieger, Y. Li, G. J. Iafrate, Phys. Rev. A **46**, 5453 (1992).

[92] S. Kümmel, J. P. Perdew, Phys. Rev. Lett. **90**,043004 (2003).

[93] S. Kümmel, J. P. Perdew, Phys. Rev. B **68**,035103 (2003).

[94] E. Engler, R. M. Dreizler, J. Comp. Chem. **2031** (1999).

[95] J. P. Perdew, M. R. Norman, Phys. Rev. B **26**,5445 (1982).

[96] M. R. Norman, D. D. Koelling Phys. Rev. B **30**,5530 (1984).

[97] J. B. Krieger, Y. Li, G. J. Iafrate, Phys. Rev. A **47**, 165 (1993).

[98] J. Chen, J. B. Krieger, Y. Li, G. J. Iafrate, Phys. Rev. A **54**, 3939 (1996).

[99] X.-M. Tong, S.-I Chu, Phys. Rev. A **55**, 3406 (1997).

[100] X.-M. Tong, S.-I Chu, Phys. Rev. A **57**, 452 (1998).

[101] T.F. Jiang, X.-M. Tong, S.-I Chu, Phys. Rev. A **63**, 045317 (2001).

[102] Xi Chu, S.-I Chu, Phys. Rev. A **63**, 023411 (2001).

[103] C. A. Ullrich, U. J. Gossmann, E. K. U. Gross, Phys. Rev. Lett. **74**, 872 (1995).

[104] W. Kohn, PHys. Rev. **123**, 1242 (1961).

[105] G. Vignale, Phys. Rev. Lett. **74**, 3233 (1995).

[106] J. F. Dobson, Phys. Rev. Lett. **73**, 2244 (1994).

[107] W. C. Henneberger, Phys. Rev. Lett. **21**, 838 (1968).

[108] H.A. Fertig, W. Kohn Phys. Rev. A **62**, 052511 (2000).

[109] A. Görling, Phys. Rev. A **47**, 2783 (1993).

[110] A. Görling, Phys. Rev. Lett. **85**,4229 (2000).

[111] Á. Nagy, J. Phys. B **32**,2841 (1999).

[112] J.F. Janak, A.R. Williams, Phys. Rev. B **23**,6301 (1981).

[113] F.W. Kutzler, G. S. Painter, Phys. Rev. Lett. **59**, 1285 (1987).

[114] N.T. Maitra, K. Burke, Phys. Rev. A **63**, 042501 (2001).

[115] N.T. Maitra, K. Burke, C. Woodward Phys. Rev. Lett. **89**, 023002 (2002).

[116] A. Holas, R. Balawender, Phys. Rev. A **65**, 034502 (2002).

[117] E.K.U. Gross, W. Kohn, Phys. Rev. Lett. **55**, 2850 (1985)

[118] J.F. Dobson, M.J. Bünner, E.K.U. Gross, Phys. Rev. Lett. **79**, 1905 (1997).

[119] R. Nifosì, S. Conti, M.P. Tosi, Phys. Rev. B **58**,12758 (1998).

[120] Z. Qian, G. Vignale, Phys. Rev. B **65**, 235121 (2002).

[121] L.J. Sham, Phys. Rev. B **32**, 3876 (1985).

[122] C. Møller, M.S. Plesset, Phys. Rev. **46**, 618 (1934).

[123] K. F. Freed, Phys. Rev. **173**, 1 (1968).

[124] A. Görling, M. Levy, Phys. Rev. B **47**, 13105 (1993).

[125] A. Görling, M. Levy, Phys. Rev. B **50**, 196 (1994).

[126] R. van Leeuwen, Phys. Rev. Lett. **76**, 3610 (1996).

[127] A. Görling, Phys. Rev. A **55**, 2630 (1997).

[128] A. Görling, Phys. Rev. A **57**, 3433 (1998).

[129] P. Bour, J. Comp. Chem. **21**, 8 (2000).

[130] M. Seidl, J.P. Perdew, S. Kurth, Phys. Rev. Lett. **84**, 5070 (2000).

[131] A. Facco Bonetti, E. Engel, R.N. Schmid, R.M. Dreizler, Phys. Rev. Lett. **11**,2241 (2001).

[132] Y.M. Niquet, M. Fuchs, X. Gonze, Phys. Rev. Lett. **90**, 219301 (2003).

[133] A. Facco Bonetti, E. Engel, R.N. Schmid, R.M. Dreizler, Phys. Rev. Lett. **90**, 219302 (2003).

[134] I. Grabowski, S. Hirata,S. Ivanov, R.J. Bartlett, J. Chem. Phys. **116**, 4415 (2002).

[135] S. Ivanov, K. Burke, M. Levy, J. Chem. Phys. **110**, 10262 (1999).

[136] S. Ivanov, M. Levy, J. Chem. Phys. **116**, 6926 (2002).

[137] S. Ivanov, S. Hirata, I. Grabowski, R.J. Bartlett, J. Chem. Phys. **118**, 461 (2003).

[138] R.J. Bartlett, I. Grabowski, S. Hirata, S. Ivanov, J. Chem. Phys. **122**, 034104 (2005).

[139] N. E. Dahlen, U. von Barth, Phys. Rev. B **69**, 195102 (2004).

[140] C.J. Umrigar, X. Gonze, Phys. Rev. A **50**, 3827 (1994).

[141] M. Warken, Chem. Phys. Lett. **237**, 256 (1995).

[142] R. Pollet, A. Savin, T. Leininger, H. Stoll, J. Chem. Phys. **116**, 1250 (2002).

[143] T. Hupp, B. Engels, A. Görling, J. Chem. Phys. **119**, 11591 (2003).

[144] O. Sugino, Y. Miyamoto, Phys. Rev. B **59**, 2579 (1999).

[145] M. Suzuki, J. Phys. Soc. Jpn. **61**, L3015 (1992).

[146] A. Castro, M.A.L. Marques, A. Rubio, J. Chem. Phys. **121**, 3425 (2004).

[147] N. Watanabe, M. Tsukada, Phys. Rev. E **65**, 036705 (2002).

[148] M. Moshinsky, *The Harmonic Oszillator in Modern Physics: From Atoms to Q uarks*, (Gordon and Breach Science Publishers, 1969)p. 25

[149] D.M. Brink, G.R. Satchler, *Angular Momentum*, (Clarendon Press, Oxford, 1993)

[150] I. Lindgren, J. Morrison, *Atomic Many-Body Theory*, (Springer-Verlag, Berlin, 1982)

[151] S. H. Vosko, L.Wilk, M. Nusair, Can. J. Phys. **58**, 1200 (1980).

[152] R. van Leeuwen, N.E. Dahlen, Phys. Rev. A **64**, 023405 (2001).

[153] T. Brabec, J. Zanghellini, M. Kitzler, A. Scrinzi, J. Phys. B: At. Mol. Opt. Phys. **37**, 763 (2004).

[154] L. Fritsche, Phys. Rev. B **33**,3976 (1986).

[155] C. Froese Fischer, T. Brage, P. Jönsson *Computational Atomic Structure: An MCHF Approach*, (Institute for Physics Publishing, Bristol, 1997).

[156] R.D. Cowan *The theory of atomic structure and spectra*, (University of California press, Berkeley, 1981)

[157] R. Singh, B.M. Deb, Physics Reports **311**, 47 (1999).

[158] Simone Peter, *Diplomarbeit (Master Thesis)*, (Vienna University of Technology, 2004)

Acknowledgments

Curriculum Vitae

Dipl.Ing. Nina Rohringer
Institute for Theoretical Physics
Vienna University of Technology
Wiedner Hauptstraße 8-10/136
A-1040 Vienna, Austria
phone: +43 1 58801-13633, fax: +43 1 58801-13699
mobile phone: +43 699 10720890
nina@concord.itp.tuwien.ac.at

PERSONAL DATA

Name: Nina Renate Gabriele Rohringer

Date and place of birth: April, 25th 1977 in Vienna, Austria

Nationality: Austrian

Marital status: single

Private address: Grenzstraße 141/2, 2231 Straßhof, Austria

EDUCATION

2001 - present PhD in physics at the Institute for Theoretical Physics at the Vienna University of Technology
Title: A quantitative test of time-dependent density functional theory: two-electron systems in an external laser field; Advisor: Joachim Burgdörfer

12 2000 Master degree (Dipl. Ing.) with distinction

1999/2000 Master thesis at Swiss Federal Institute of Technology Lausanne, Switzerland
Title: Semiclassical Aspects of the Quantum Hall effect
Advisors: Joachim Burgdörfer, Nicolas Macris

1997/1998 Erasmus exchange student at the Swiss Federal Institute of Technology, Lausanne, Switzerland

1995-2000 Physics student at Vienna University of Technology

TEACHING EXPERIENCE

2002,2003 Lecturer in the exercise classes 'Quantum Mechanics' at Vienna University of Technology

1997/1998 Teaching assistant in Mathematics (Analysis) at the Swiss Federal Institute of Technology, Lausanne, Switzerland

EMPLOYMENT, INTERNSHIPS

02/2001 - present: University assistant at Vienna University of Technology

07/08 1998 Internship at Plasma Physics Research Center at ETH Lausanne

08 1997 Internship at Hewlett&Packard Vienna, Medical Support Departement

09 1996 Internship at OMV AG, Refinery Schwechat

08 1996 Internship at Schmalbach-Lubeca Ges.m.b.H., Administration

PUBLICATIONS

N. Rohringer, J. Burgdörfer and N. Macris, *Bargmann representation for Landau levels in two dimensions*, J. Phys. A: Math. Gen. 36, 4173(2003).

S. Rotter, B. Weingartner, N. Rohringer and J. Burgdörfer *Ballistic quantum transport at high energies and high magnetic fields* Phys. Rev. B 68, 165302 (2003).

J. Burgdörfer, N. Rohringer, P.S. Krstic and C.O. Reinhold *Nonadiabatic processes near barriers* in 'Nonadiabatic transition in quantum systems' edited by V.I. Osherov, L.I. Ponomarev, Chernogolovka, Russia p. 205 (2004). 2004 Institute of Chemical Physics RAS ISBN 5-901675-48-7

C. Deiss, N. Rohringer, J. Burgdörfer *Cluster-laser interaction: fast production of hot electrons by short laser pulses* accepted for publication in Nucl. Instr. and Meth. B (2005)

S. Peter, N. Rohringer, J. Burgdörfer *Combination of TDDFT and configuration-interaction methods: a test for two electrons in one-dimensional model potentials* in preparation

N. Rohringer, J. Burgdörfer *A quantitative test of TDDFT: parabolic two-electron quantum-dot in laser fields* in preparation

SCHOLARSHIPS/AWARDS

2000-present PhD grant within the special research program *Advanced Light Sources (ADLIS)* of the Austrian Science Fund (FWF)

1999/2000 Scholarship of the Swiss Federal commission of scholarships for foreigners

1997/1998 Erasmus scholarship of the European Union (exchange program)

1997 - 2000: Achievement scholarships of the Vienna University of Technology

LANGUAGES

German: mother language

English: fluently spoken and written

French: fluently spoken and written

Spanish: fluently spoken

Italian: basic knowledge

COMPUTATIONAL SKILLS

Programming languages: Fortran, LabView

Operating systems: Linux, Unix, Windows

Software: Mathematica, Matlab, Microsoft Office, LaTex, Gnuplot etc.

EXTRACURRICULAR INTERESTS

Languages, literature, theatre, music, singing, hiking, sports